M. Shrivastava

Vertical Hydrodynamic Forces on a Flat Bottom Body Oscillating Vertically, Close to Seabed

TU Delft

Vertical Hydrodynamic Force on Flat Bottom Body Oscillating Vertically, Close to Seabed

Master of Science Thesis

By

Manish Shrivastava

Offshore and Dredging Engineering

Faculty of Mechanical, Maritime and Materials Engineering

Delft University of Technology

October 2015

Committee

Prof. Dr. Ir. R.H.M. Huijsmans

Dr. Ir. A. Akkerman

Dr. Ir. S.A. Miedema

Ir. O.A.J. Peters

TU Delft

ABSTRACT

World's demand for energy has increased significantly in the last few years, and it is expected to continue growing. As a result offshore industry is expanding to explorations in deeper water and more remote areas. Consequently, the size of offshore structures, which are the possible future cargos for HTV involved in Heavy Marine Transport (HMT), is growing. These HTV use float-on/off operation to load and unload the cargo. Currently HMT is limited to sailing to and from sheltered areas. Here, the environmental loadings caused by waves, wind and current are low. In order to realize full potential of HMT, Dockwise is researching the possibility to perform loading and discharge operations in a harsher environment at open sea. This requires understanding of Hydrodynamic behavior of HTV and Cargo during most critical stage of loading/unloading operation (float-on or float-off). This occurs when the gap between cargo and HTV deck is very small. In this pursuit, Dockwise conducted experiments to understand an analogous problem of a cylinder oscillating close to towing tank bed, which have shown vertical forces on cargo model are non-linear (w.r.t. motion) and have very large troughs. These non-linear forces are not calculated by potential software; however the linear part of the vertical hydrodynamic force is calculated by potential software reasonably.

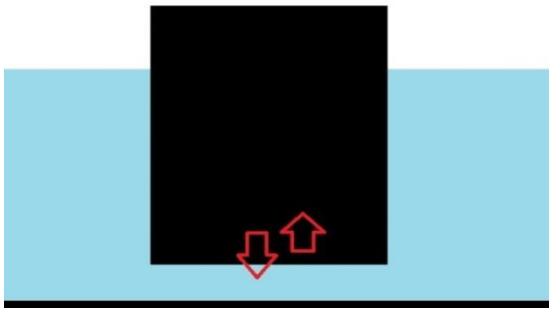

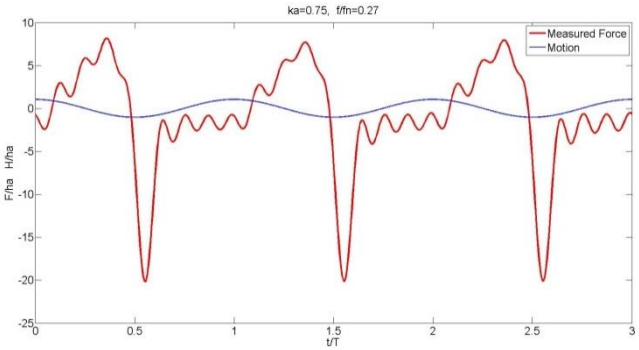

Objective of thesis has been to model the non-linear forces and come up with a general expression for vertical force on a flat bottom model oscillating vertically, close to seabed.

To better understand the flow in the gap, model was simulated in the cfd software COMFLOW under a range of oscillation frequencies and amplitudes. Vertical forces calculated by COMFLOW were in close agreement with experiment results and were not significantly affected by viscosity.

To be able to perform calculations in within reasonable time an approach was sought to adapt potential software results to include non-linear effects during small gap. To this effect

a simplified mathematical model was considered in which flow in gap was assumed to be uniform. Analysis of this model indicated that the non-linear peaks in force are caused by high inertial accelerations imparted to the water inside the gap. Further it was found that at the small gap, the lift force becomes important, which is not modeled in potential software in order to keep equations linear.

For a general flat bottom model vertical forces on bottom can be written as

$$F = F_{AQWA} - s_1 \rho A^2 \left(\frac{1}{h_0} - \frac{1}{h} \right) h_{tt} + s_2 \frac{\rho A^2}{h^2} h_t^2$$

Here s1 and s2 are shape coefficients, value of which will depend upon the profile of the bottom area.

Above adaptation has been found to well represent observations in COMFLOW simulations and experiment for cylindrical, triangular, square and rectangular bottom models.

Contents

ABBREVIATION AND DEFINITIONS

HTV - Heavy Transport Vessel

HMT- Heavy Marine Transport

Float-on: Float-on refers to offshore operation in which a floating cargo is loaded on the HTV, by means of first ballasting and then de-ballasting of HTV.

Float-off: Float- of is reverse of float-on operation, cargo is unloaded by ballasting the HTV.

1 Introduction

A structure can be loaded on an HTV in harbour by performing float-on operation and it can be unloaded offshore from HTV using float-off operation. Similarly, a structure can be loaded on-board HTV for dry docking by float-on operation, can be unloaded after dry-docking by float-off operation. During float-on/off operation, the most critical stage occurs when cargo is floating buoyant with a very small gap between cargo bottom and deck of HTV. To understand the dynamic behaviour of cargo deck at this stage, it is important to understand first the hydrodynamic flow behaviour and vertical hydrodynamic forces when there is very small gap between cargo and deck. Knowledge of vertical hydrodynamic force at small gap will be needed to estimate workability of HTV for float on/off operations.

In order to analyse vertical hydrodynamic loading during float-on/off operation from HTV Dockwise Vanguard, Dockwise has performed towing tank experiments on models. In such experimental study in order to simplify the problem of hydrodynamic interaction between cargo and deck of Vanguard, an analogous set up was used in which model was oscillated close to seabed. Experiment was supposed to help in understanding problems in estimating hydrodynamic forces when a relatively small gap exists between bottom of cargo and deck of Vanguard.

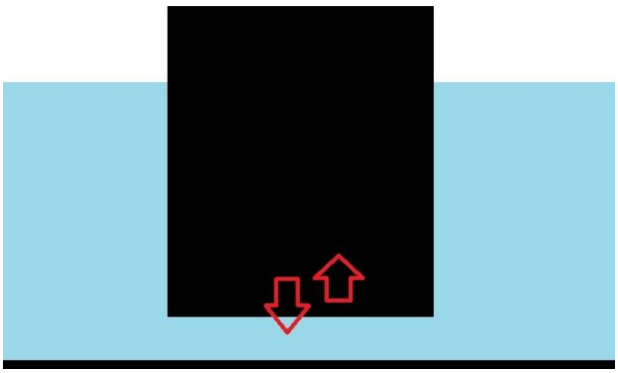

Figure 1: Model Oscillating Close to Seabed

The measured forces in the experiment were found to have nonlinear peaks. Normal industrial practice to estimate hydrodynamic loads is to use linear potential software, because it is fast and accurate for deep water problems. While comparing Dockwise experiment results with potential software results, it has been found that potential software are inaccurate in estimating vertical hydrodynamic forces when a model is oscillated very close to seabed (small gap size compared to horizontal extent of the model bottom).

Problem of hydrodynamic forces on a model oscillating in close proximity of the horizontal boundary or seabed can also be extended to several applications in maritime and offshore industry such as vertical forces on a barge in shallow water or in a channel etc.

Present work is a part of study (not complete study) aimed to improve workability of Dockwise Vanguard and other HTV for float-on/off operations in deep water.

In this chapter, a general introduction to heavy marine transport will be given, industry requirements and operability effects will be treated. Chapter will be concluded by defining objectives of present work and document structure.

1.1 Heavy Marine Transport Industry

Heavy Marine Transport is need of the hour to expand boundaries of deep-water oil and gas explorations. Heavy transport vessels with capability for foat-on/off operation are well suited to step into task of heavy marine transport. In this section it will be explained why.

The world's demand for energy has increased significantly in the last few years and is expected to continue growing. As oil and gas is major source of energy and shallow water reserves are depleting at faster rate, industry is moving into exploration of reserves in deeper waters and more remote sea areas where fabrication, supply etc. is very expensive and difficult. One of the ways for cutting cost is to complete welding fabrication, and all the processes on-shore and transport it to site (offshore fabrication, welding etc are very expensive). To maintain competitiveness with shore based oil producers, deep-water offshore oil and gas producers need to increase production rates which means larger structures will be needed. Size and weight of structures which need to be deployed and hence transported to the site, is increasing.

Structures required for deep-water oil exploration can be divided into three categories: self-propelled structures, structures which can be towed and structures which need to be transported. For the structures which need to be transported, there are two options. Transporting in modules which can be installed on site and assembling several modules on site or transporting complete structure. But offshore assembling will require mobilization of several vessels, waiting time for weather window to assemble and special operations. Offshore assembling has proven to be much more time consuming, hazardous to the extent of losing complete modules sometime. Also module concept is limited to few structures, such as topside. Transporting complete structures is more preferred. It reduces loss of time, as there is no need for hook-up and commissioning. In offshore, loading and

unloading of structures are normally done by cranes. But structures heavier than 20,000 tonnes are beyond capacity of most powerful cranes of present day.

Industry is looking for the means to perform transfer of fully commissioned heavy structures and floaters directly into deep-water which would eliminate the need for offshore hook up and hazardous operations involved.

This introduces the need for heavy marine transport which uses float-on and float-off method to load and unload cargo (not cranes with its limits of lifting capacity). Vessels which can perform heavy marine transport are called Heavy Transport Vessel (HTV). Ideally HTV can be designed to carry very heavy loads and transfer them using float-on/off. Heavy marine transport has capacity to expand the limits of offshore transport and production infrastructure size.

Figure 2: Heavy Marine Transport

Besides advantages for oil and gas industry, heavy marine transport can also help shipbuilding industry and will make it possible to construct the ship hull economically in the east and transport it to west to fit in vital machinery and systems.

Dockwise Vanguard has been a successful example in direction of HMT, because of vessel design to perform transport operations and float-on/off operations with much larger cargo sizes.

1.1.1 Dockwise Vanguard

Dockwise is an oil & gas service company providing logistical management of large and heavy structures. Key services performed by Dockwise are Heavy Marine Transport, Offshore Transport & Installation. Dockwise operates the largest fleet of specialized vessels in the world: a versatile fleet of 25 semi-submersible, heavy transport vessels of different concepts and designs. Dockwise Vanguard an HTV, is the latest in the fleet of Dockwise vessels.

Dockwise Vanguard (Figure 3) is a semi-submersible HTV, has a bowless design and can accommodate intact superstructures as entire length of the vessel can be used to keep cargo. Keeping in view the future and the position of the Dockwise at the premium end of the heavy marine transport industry, Dockwise Vanguard was built with aim to create its own market by redefining the limits of exceptional heavy marine transport. Dockwise Vanguard uses float-on/off operation to load and unload cargo. Study of vertical hydrodynamic forces at small gap in this thesis work is being considered with aim to improve workability of Dockwise Vanguard for float-on/off operations.

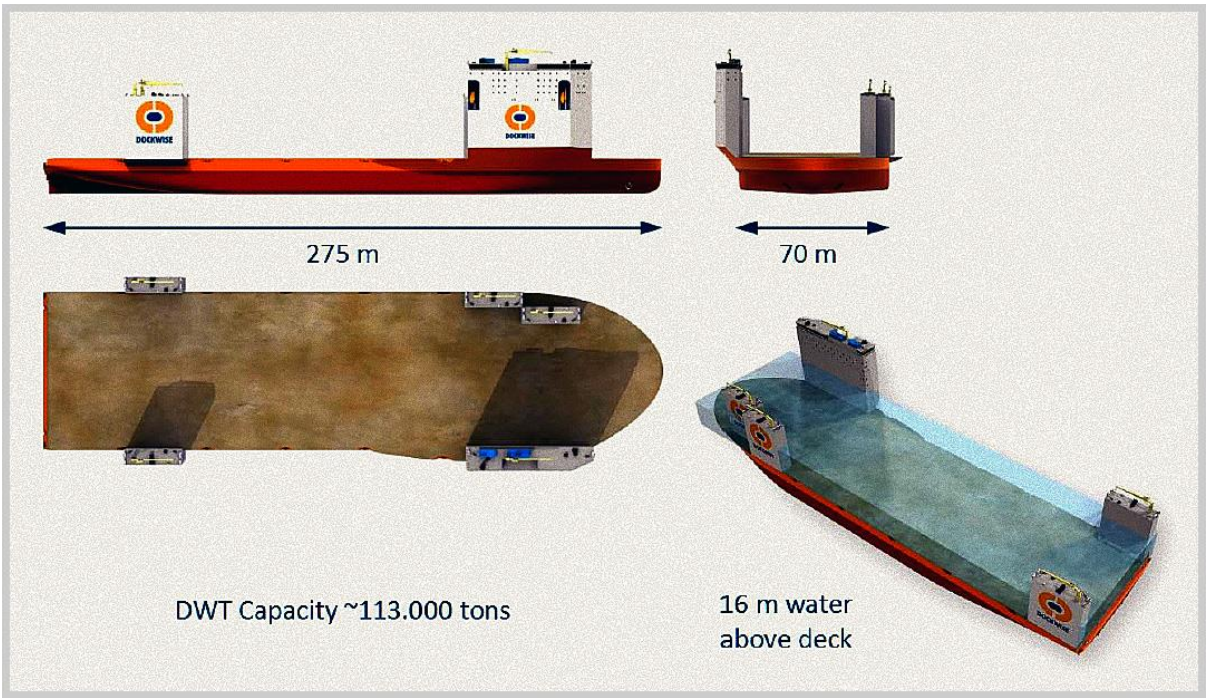

Figure 3: Dockwise Vanguard

The vessel has been specifically built to enable oil and gas majors and EPIC contractors consider design and transport opportunities for mega offshore units, which were until now considered unthinkable.

1.2 On Station Dry Docking by Float-On

Offshore dry-docking of structures is another very important market where HTV with float-on/off facility can be used [3].

Structures engaged in oil fields need to be operated, transported and maintained round the year, in all weather conditions. This has necessitated availability of on-site docking facilities. Exploration at deep water requires floating rigs and storage structures of very high storage capacity (to deal with uncertainties in weather, shuttle tanker can't arrive in bad weather). These structures need offshore Hull maintenance, on site docking, on site survey of underwater parts.

In deep water a variety of floating rig and support structure are used, for example: FPSO, semi-submersible, other new floating concepts. At present 224 FPSOs are operating in deep waters around the world and numbers are increasing fast. Majority of them are engaged in exploration contracts which require them to be on the site for 20-30 years. But like normal tanker ship hull, hull of these structures also need dry docking after every five years to meet requirements of classification society. Dry docking means stopping production, hull needs to be brought to shore for dry docking and then taken back to the site. A typical dry-docking period of a FPSO can be up to 50-60 days. That means a loss of $100 million of order for oil production company. Towing to and back from location of dry-dock will cost extra time. In comparison, HTV with float-on/off operation facility provides a competitive solution for dry-docking FPSO in deep-water production sites. On-site dry-docking operation will require FPSO or semi-submersible to be docked on the hull of HTV, without disconnecting production risers and mooring turret.

Figure 4: Offshore Dry-Docking of FPSO

1.3 Float-on/off Operation Stages

Float-on operation to load an FPSO or any structure, on deck of a HTV, consists of stages of controlled ballasting and de-ballasting. Complete operation will theoretically require seven stages of operation which are being described below in sequence.

I. First stage is to bring HTV at the site and start ballasting.

II. Second stage is to ballast HTV so that there is enough water depth above deck to bring floating cargo on top of it.

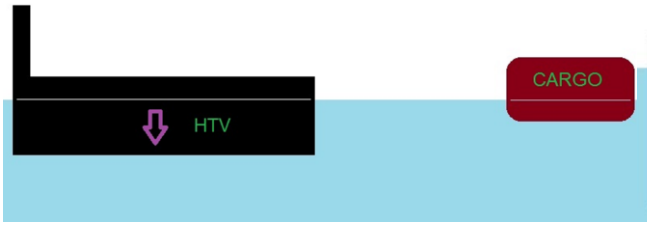

Figure 5 : Float-On, Stage 1

Figure 6: Float-On, Stage 2

III. In third stage cargo is pulled on top of HTV with help of tugs.

IV. HTV de-ballasting is started, HTV starts moving upwards.

Figure 7: Float-on Stage 3

Figure 8: Float-On stage 4

V. De-ballasting continues. Clearence between the cargo and HTV deck becomes very small. Cargo is just floating above deck of HTV. Now afterwards cargo will land on HTV as HTV keeps moving up.

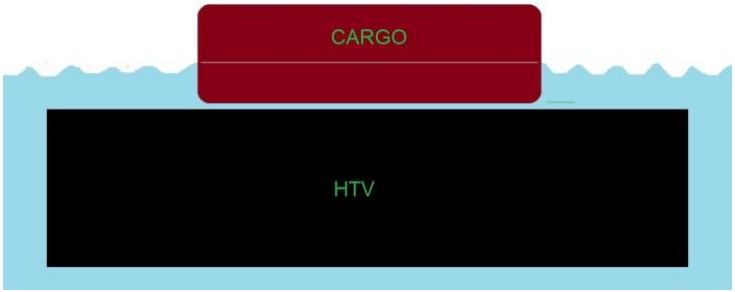

Figure 9: Float-On Stage 5

VI. De-ballasting continues cargo lands up on deck of HTV and moves upwards with HTV.

VII. HTV deck emerges from water and HTV-cargo lashings are secured on HTV deck.

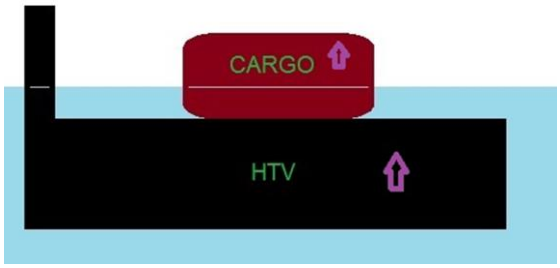

Figure 10: Float-On Stage 6

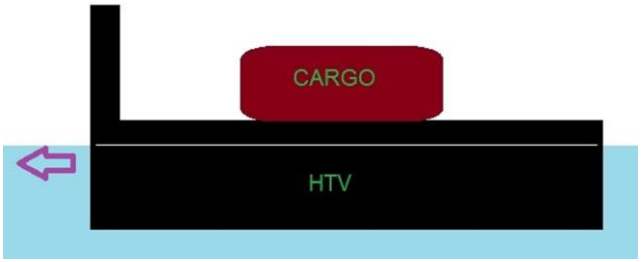

Figure 11: Float-On Stage 7

Now HTV can move or stay on site. Float-off operation has a sequence reverse of float-on.

1.4 Operability for Float-on/off Operation

In general workability of loading and discharging the cargo from HTV (Dockwise Vanguard) will depend on type of cargo and the weather conditions. Until now weather condition for float on/off operation was mainly being decided based on past operation experience.

Here we will discuss a particular example of available weather window for float-on operation in offshore Brazil, based on operational experience [3]. This will help us understand relative effect of improving workability on total expense of operation.

To float-on/off an FPSO from HTV in offshore Brazil, weather window required for operation depends on the time taken in loading the FPSO, which in turn will depend on many other factors such as ballasting capacity of HTV, i.e. how fast HTV can dock the FPSO and how fast it can undock.

The table 1 down below gives expected weather window for various significant wave heights in offshore Brazil. To explain, weather window of 1.5 days with significant wave height of 1m, will be available on average after 30 days. In comparison weather window of 1.5 days with Hs of 2m will be available on average after one day waiting period.

Table 1 Expected Waiting for Weather Window in Offshore Brazil

Hs	Expected waiting for weather window (most favourable month) in days		
Weather window (days)	1.0	1.5	2.0
0.5 m	43.83	43.83	43.83
1.0 m	25.98	30.12	35.17
1.5 m	3.78	5.15	7.22
2.0 m	0.61	0.92	1.38

One can see from the table above that for offshore dry-docking to be relatively more competitive, HTV must be able to do the float on/off operation with a relatively higher significant wave height in order to reduce the number of waiting days.

A better understanding of hydrodynamic interaction when a very small gap exists during operation will lead to better estimation of weather conditions in which operation can be performed. Which means that any improvement in estimation of maximum weather condition (in which HTV can perform float-on/off operation) will improve workability and will have tremendous financial repercussions on total cost of operation.

1.5 Challenges in Float-on/off Operation

Today float-on/off operations are limited to loading cargo in sheltered locations and unloading again at sheltered locations. Sheltered locations have very benign sea conditions, so dynamic forces during operation are also expected to be comparatively smaller. But as cargo size is increasing, there are not many sheltered locations which have logistics and draft to perform float-on/off operations.

When cargo is discharged in sheltered location, it still has to be carried over to remote deep sea location. This reduces the relative advantage of float-on/off operation. Because of that, capability of Dockwise Vanguard and other HTV (Heavy Transport Vessel) which

perform float-on/off operations to load or unload cargo, has been so far not been extended to deep water [5].

The option of offshore dry-docking is also not being used at present as it will require float-on/off operation in deep water under harsher conditions.

Full capacity of HTV with float-on/off operation can only be utilized when operation can be performed in offshore deep-water location under most of sea conditions. To know the highest sea condition when operation can be performed, it is essential to know the factors which are most critical during operation and determine interactive forces.

Most critical situation during operations (both float-on and float-off), occurs when very small gap exists between deck of HTV and cargo bottom as shown in figure 9. There are two major Hydrodynamic challenges at this stage:

(1) **Controlling horizontal relative movement of HTV and cargo**

Controlling horizontal movement is crucial to avoid damage of tow lines, mooring lines or loosing cargo. Tests and model simulation measurements were conducted by Dockwise to estimate this movement. The horizontal stability during operation can be achieved by using tugs and shore tension winches [8]. This topic is not part of present work and will not treated any further.

(2) **Estimating Vertical movement and hydrodynamic interaction force**

During the operation it is very important to know the vertical interactive load on the cargo and HTV deck, as it will have effect on HTV deck loading and forces on cargo bottom hull. Any excessive load may bring relatively large stresses on deck girders or may damage deck cribbing, cargo bottom.

Avoiding collision or any unwanted loading between cargo bottom and HTV deck may require accurate knowledge of forces between deck and cargo at this stage. Also it may give idea about expected loads on cribbing and grillage, which support cargo on deck.

To get on time knowledge about vertical hydrodynamic forces during offshore float-on/off operation, an accurate, fast and economical method is sought.

As a first step to understand vertical hydrodynamic forces during separation, Dockwise conducted tests on flat bottom models in MARIN towing tank in which model was oscillated close to seabed with a fixed oscillation amplitude and frequency. Results have shown high non-linear peaks in the measured force which are not present in potential software results.

1.6 Objective of Present Work and Document Structure

Goal of present work is to analyse the vertical hydrodynamic interaction forces between a flat bottom model and seabed when the gap between model and seabed is relatively small, in particular the non-linear hydrodynamic forces which are difficult to capture by linear potential software. Second goal is to find a way to adapt results of linear potential software to use it analyse forces when relatively small gap exist between model and boundary.

To understand and analyse the interaction forces on such a model, first a study of Dockwise test results for cylindrical model has been done, and results have been compared with potential software results (chapter 2). In second stage cylindrical models have been simulated in COMFLOW, while experiment results availed by Dockwise has been used for verification of COMFLOW results for cylindrical model (Chapter 3). In third stage an attempt has been made to come up with simplified analytical solution for vertical hydrodynamic forces on cylindrical model and barge model by simplifying the flow inside the gap to uniform flow (Chapter 4). In last stage a general solution for a random bottom surface area model has been attempted based on analytical solutions for cylindrical and barge models. Applicability of such general solution to estimate dynamic forces acting on the models of general shape has been verified with triangular, square bottom models (Chapter 5). A summary of conclusions and recommendations has been given in Chapter 6 and 7. Appendices at end of document give detailed results and support the topics in main discussion.

1.7 Approach by Other Authors

Problem of estimation of vertical hydrodynamic force on models with small gap from seabed has been studied by some other authors.

Y. Drobyshevski [7] attempted to solve the problem of hydrodynamic analysis of vertical sided structures with flat bottom oscillating close to seabed. Drobyshevski assumed that problem of flow inside the gap can be described as two dimensional flow problem, and solved potential function equations analytically to obtain potential function for flow in the gap. Results were found to be accurate for small gaps sizes. But the equations presented were not simple to apply.

Onno J Peters [5] investigated the problem by implementing multi-domain potential theory. In his study, he split the control volume into two domains I and II (figure-12), and normal 3D potential theory was applied to domain I with the additional boundary conditions at the boundary of domain D. Inside gap domain 2D potential theory solution was used. The

potential functions for two domains need to satisfy boundary conditions at the boundary between two domains (normal velocity and pressures should be equal). Further development of method is in progress.

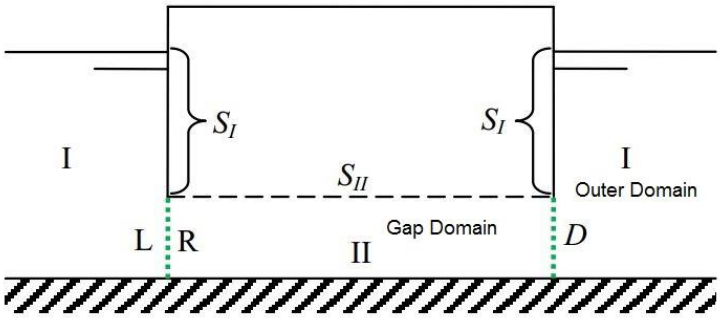

Figure 12: Multi Domain Potential Approach

Molin [1] considered the theoretical prediction of the hydrodynamic loads acting upon flat footings in forced vertical motion very close to the sea-floor. He tackled problem by using potential function to describe flow in the gap and the method of matched asymptotic expansions and obtained analytical expressions of the vertical hydrodynamic loads for 2D and 3D plates (circular in the latter case), when the gap is small as compared to their horizontal extents. Molins results have been found satisfactory for circular disk when compared with experiments. His work has shown that effect of viscosity on the force is secondary. A comment on work of Molin will be made in section 5.4, during review of present work.

Brenen [2] solved analytically the force on bottom of a flat plate moving vertically close to seabed. He considered flow as uniform inside the gap. Brenens work will be referred in chapter 4.

2 Dockwise Experiments and AQWA results

The simplest approach to analyse vertical hydrodynamic forces is modelling in potential diffraction software, as it is cheap and takes very less time to obtain results. But linear potential software are based on several assumptions which may not hold in all for all cases. This makes experiment validation necessary. In this chapter experiments conducted by Dockwise to study vertical dynamic forces, when there is very small gap between seabed and model, has been discussed. Further Dockwise results have been compared with linear potential software results result in order to find out applicability of such results for close gap hydrodynamic interactions.

2.1 Experiment Setup

In 2008, Dockwise conducted a series of tests on cargo models (with different bottom shape but same area), at varying frequencies and varying vertical motion amplitudes. Experiment set up for cylindrical model has been shown in figure 13.

During experiment, cargo was oscillated sinusoidally with known amplitude and frequency and hydromechanical forces acting on model was measured. MARIN towing tank has boundary located quite far away, so there is weak reason to believe that reflections from boundary will affect the force measured. For the purpose of thesis, Dockwise has availed data for model tests.

Figure 13: Dockwise Cylindrical Model

2.2 Axis System and Notations

In this section notations for cylindrical model and axis system will be explained. This axis system will be applied to cylindrical model in coming chapters, while for other models there will be slight change in notation of dimensions as model geometries change.

Let us assume that, m is mass of model; T is time period of oscillation of model; ω is angular frequency of oscillation for model; f is the oscillation frequency; d is draft of the model bottom; R is radius of the model bottom; h is scalar denoting the size of gap between model bottom and seabed at time t; z is the vertical distance of an arbitrary point in the fluid domain from the seabed. h_0 is the mean gap size between bottom of model

and seabed; h_a is amplitude of oscillation of cargo model. In polar coordinates horizontal dimension: $x = r\cos\theta$, $y = r\sin\theta$. Suppose model starts oscillating at t=0 at which position of model bottom is: $h = h_0 + h_a$.

Then, $$h = h_0 + h_a \mathrm{Cos}\left(\omega.t\right) \quad \text{.....(1)}$$

Oscillation of model bottom from mean draft has been defined as H;

$$H = h - h_0 = h_a \mathrm{Cos}\left(\omega\, t\right) \quad \text{.....(2)}$$

In figure 14, horizontal view of cargo model in towing tank has been shown.

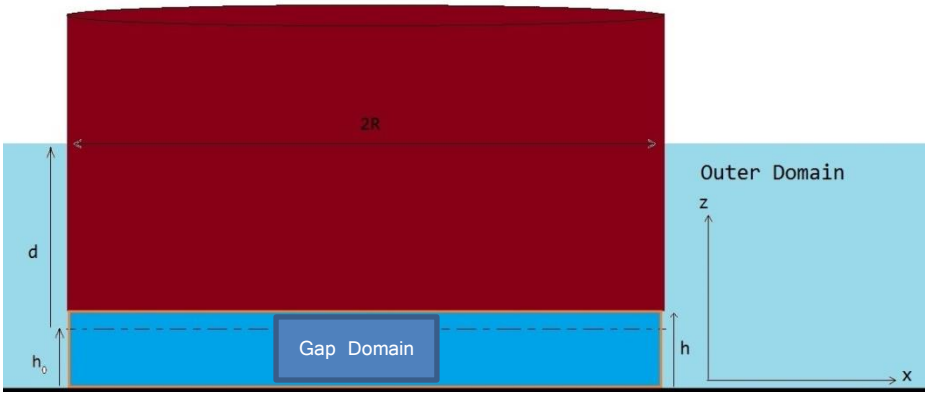

Figure 14: Axis System for Cylindrical Model

Force acting in upward direction will be taken as positive.

Fluid domain between model bottom and seabed, shown in dark sky, will be referred as gap domain, while fluid domain outside shown in light sky will be referred as outer domain.

Ratio of oscillation amplitude and gap height has been referred as k_a

$$k_a = \frac{h_a}{h_0}$$

Natural heave frequency of the model will be denoted as f_n, this has been used to non-dimensionalize the oscillation frequency in plots.

$$f_n = \frac{1}{2\pi}\sqrt{\frac{g}{d}}$$

2.2.1 Force Definition

Hydromechanical force acting on cargo model has three parts: static force at mid draft, varying hydrostatic force, dynamic force.

Static Force: Vertical buoyancy force acting on model bottom at mean draft d which has been balanced by weight of the model or force applied by set-up on the model in experiment.

$$\text{Static Force} = \rho g d \cdot \pi R^2 = mg + \text{Downward Applied Force}$$

Rest out of balance force is measured during experiment.

Varying Hydrostatic Force: Hydrostatic force has been defined as residual buoyancy force acting on model when gap between model bottom and seabed is h.

$$F = \rho g(h_0 - h)\,\pi R^2 = -\pi\rho g\, HR^2$$

Dynamic Force

Dynamic Force = Total Hydromech. Force -Static Force - Varying Hydrostatic Force

$$F_{Hydrodynamic} = F_{Hydromech,\,total} - \pi\rho g(d - H)R^2 \quad .....(3)$$

2.2.2 Parameters Used in the Experiments with Cylindrical Model

Dosckwise experiments were performed at three frequencies of oscillation

$$f = 0.225,\ 0.338,\ 0.45 \text{ Hz}, \quad f / f_n = 0.135,\ 0.20,\ 0.27$$

Model was oscillated with three oscillation amplitudes for each of three frequencies.

$$h_a = 5,\ 10,\ 15 \text{ mm}, \quad k_a = 0.25,\ 0.50,\ 0.75$$

Mean gap height $h_0 = 2$ cm

Radius of cylinder $R = 40$ cm

Mean draft of cylinder $d = 9$ cm

Water Depth $d + h_0 = 11$ cm

$f_n = 1.66$ Hz

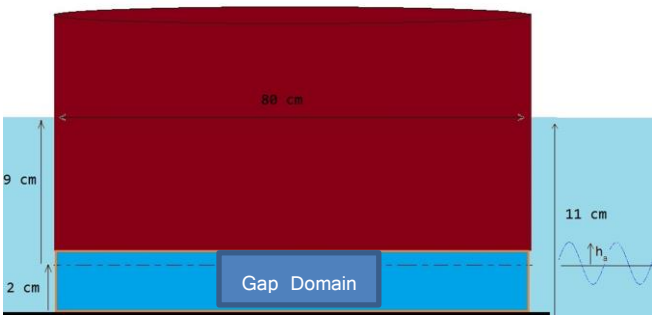

Figure 15: Cylindrical model dimensions

Average gap height is much smaller compared to dia. of the cylinder ($2R / h_0 = 40$).

The table 2 below gives the nine experiment cases, which will be referred throughout later.

Table 2: Dockwise Experiment Cases with Cylindrical Model

Case	Frequency (Hz)	Amplitude(mm)	Normalized Frequency (f/fn)	Amplitude Ratio (Ka=ha/h0)
1	0.225	5	0.135	0.25
2	0.225	10	0.135	0.50
3	0.225	15	0.135	0.75
4	0.338	5	0.20	0.25
5	0.338	10	0.20	0.50
6	0.338	15	0.20	0.75
7	0.450	5	0.27	0.25
8	0.450	10	0.27	0.50
9	0.450	15	0.27	0.75

In next sections results for 2008 experiments with cylindrical shape cargo model will be discussed to check qualitatively the varying force w.r.t. time.

2.3 Linear Theory and Analysis of Results from Dockwise Experiments

A function y is said to be linear function of x if it can be written as y = ax + b. In that case if a and b are known, in that case y can be found for any case by just changing x.

In hydromechanics linear theory we assume that a sinusoidal forces acting on model result in a sinusoidal motion and vice-versa, such that

$$F_{amp}\cos(\omega t + \phi) = f(a_m, b, \omega)\, h_a \cos(\omega t + \phi)$$

Where F_{amp} is amplitude of resulting force (sum of all forces) on object. In above case, for a given force condition, motions can be found out and vice versa, by substituting the values in above equation.

During Dockwise experiment, time, position of model bottom and hydromechanical force acting on model bottom in vertical direction was measured. Since no waves were sent to model in experiment, there would be no diffraction and wave excitation force. Total hydromechanical force acting vertically on model should be equal to sum of radiation force $(-ah_{tt} - bh_t)$ and hydrostatic buoyancy $(-cH)$. If sinusoidal motion has to result in sinusoidal force then equation below should be valid for experiment results.

$$-a_m h_{tt} - bh_t - cH = F_{Measured} \quad \text{.....(4)}$$

Here a_m is heave added mass coefficient and b is heave damping coefficient, h_t and h_{tt} are first and second derivative of h w.r.t. time, and hydrostatic spring coefficient c equals $\rho g(\pi R^2)$, $F_{measured}$ is measured force and is known. These values a_m and b can be found from equation 4.

It will be found later, Dockwise experiment cases in which models were oscillated very close to seabed, when analyzed don't fit into equation 4.

To discuss qualitatively experiment results, in this section first results at one arbitrary frequency (in experiment) and arbitrary oscillation amplitude will be discussed.

First a random case 8 will be discussed, which has a high oscillation frequency for the frequencies oscillated ($f / f_n = 0.27$), and high oscillation amplitude ($k_a = 0.5$). In plot below, vertical force on the bottom of cargo model as measured during experiment has been plotted on y axis; force has been normalized w.r.t. oscillation amplitude h_a. Oscillation of cargo model about mean position (H) also has been plotted on y axis; has been normalized w.r.t. oscillation amplitude h_a, time has been plotted on x axis; has been normalized with time period T.

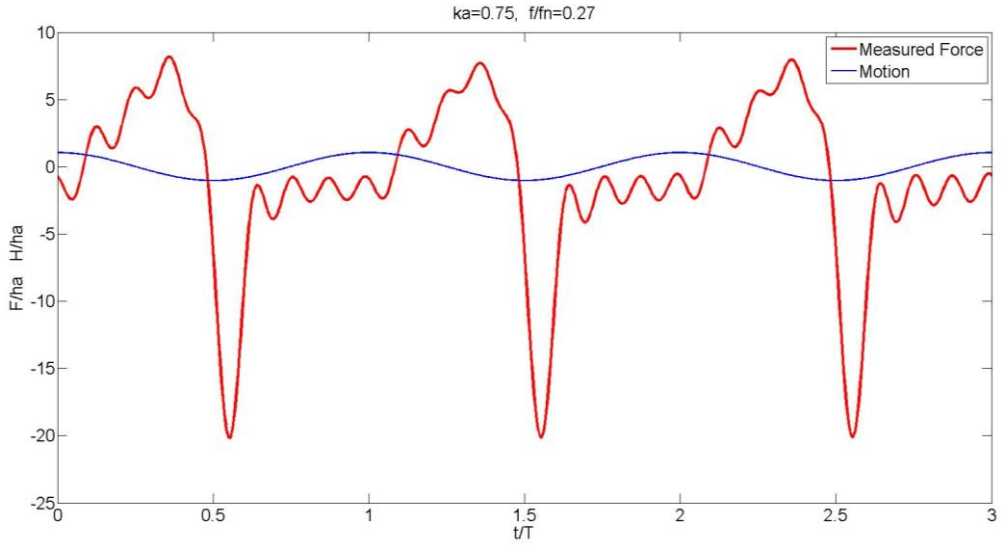

Figure 16: Experiment Vertical Force for Case 8

It can be seen from plot above, when model is simulated at very small gap height relative to radius, then there is no linear relation between force and sinusoidal motion, hence it is not possible to find a solution for linear equation 4. Vertical force on cylinder oscillating close to seabed is non-linear.

Negative peaks are higher than calculated with linear potential software for deep water. The phenomenon of very high non-linear negative peaks which tends to suck the model towards the seabed is called sticking effect [5] (or suction effect). And the phenomena of high positive peak (higher than force on a model oscillating in deep water) which is pushing the cylinder upwards is called cushioning effect.

Also it can be observed in figure 16 that negative (downward) force peaks are higher than positive (upward) force peaks. Comparing the experiment results it was found that the phenomena of high peaks and troughs become more visible at high oscillation amplitudes.

Before going forward it will be useful to check frequencies present in the measured vertical force data.

Fourier Analysis of Data Measured in Experiments: A Fourier analysis of Hydrodynamic force signals was conducted to investigate frequencies present in the experimental force data. In the plot below, frequencies present in case 7 and 9 are plotted, as these cases correspond to lowest and highest oscillation amplitude in the experiment respectively for oscillation frequency f/fn=0.27.

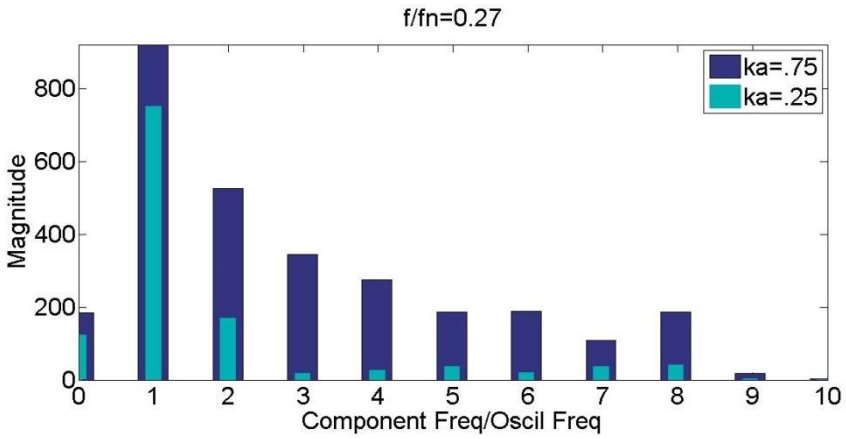

Figure 17: Comparison of Component Frequencies for Measured Force, Case 7 and 9

From Fourier plot, it can be observed that at lower oscillation amplitude first frequency is ω is relatively more dominant while at higher oscillation amplitude, there are other higher dominant frequency components.

2.4 Potential Theory

Potential software are a radiation/diffraction program developed for the analysis of interaction of surface waves with offshore structures. It is based on a three-dimensional source distribution technique for the solution of linearized velocity potential problem.

In potential theory, fluid is assumed to be inviscid, homogeneous, irrotational and incompressible. Velocity potential ϕ is a scalar function of the coordinates and of the time, such that derivative of ϕ in any direction with respect to coordinates in that direction gives velocity at that point in fluid in that direction, for example

$$\frac{\partial \phi}{\partial x} = u$$

Knowledge of velocity potential inside the complete fluid domain is sufficient for calculation of pressure at any point in domain.

$$p = -\frac{d\phi}{dt} + \rho(u^2 + v^2 + w^2) - \rho gh$$

To linearize above equation, the velocity term is neglected in above equation.

$$p = -\frac{d\phi}{dt} - \rho gh$$

For the computations, the mean wetted part of the hull of the model is approximated by a number of rectangular plane elements, representing a distribution of source singularities, each of which contributes to the velocity potential describing the flow. Linear equations are solved by satisfying boundary conditions, which gives source strength of panels. Using this source strengths velocity potential at any point in domain can be calculated.

For present work, Ansys AQWA was used for calculating added mass and damping for given structures geometry, water depth. Same geometry was used to perform simulations as used in Dockwise experiments (Figure 15). When gap size between model and seabed was varied from infinity to very small (compared to radius of cylinder), then an exponential variation in added mass and damping was obtained for small values of gap size, which can be seen in the plots below.

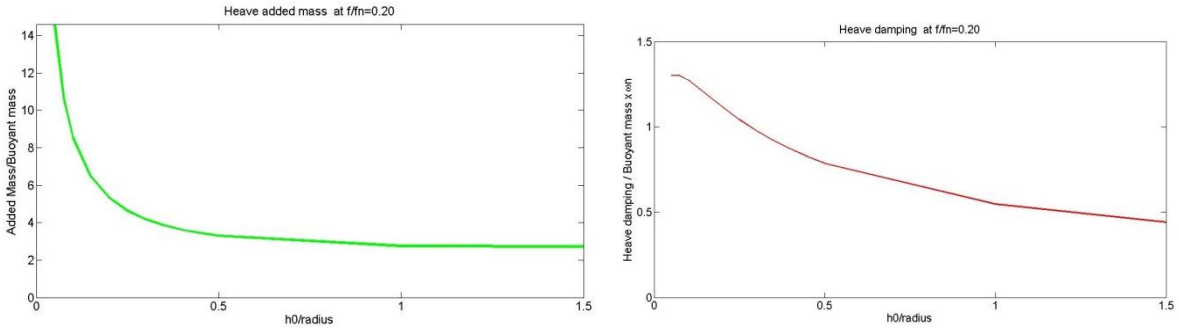

Figure 18: Added Mass and Damping Obtained From AQWA With Varying Gap Size

2.5 Dynamic Force comparison AQWA and Experiment

In order to check the correctness of AQWA results at small gap, it is important to compare it with experiment results. Since statically varying forces are usually same in both experiment and AQWA, it would be useful to only focus on dynamic parts.

Added mass and damping obtained from AQWA can be used to find vertical dynamic force on model by substitution into equation below

$$-a_m\, h_{tt} - bh_t = F_{AQWA}$$

These forces are being compared in the plots below for two cases, one with low amplitude in the experiment and one with highest amplitude in the experiment.

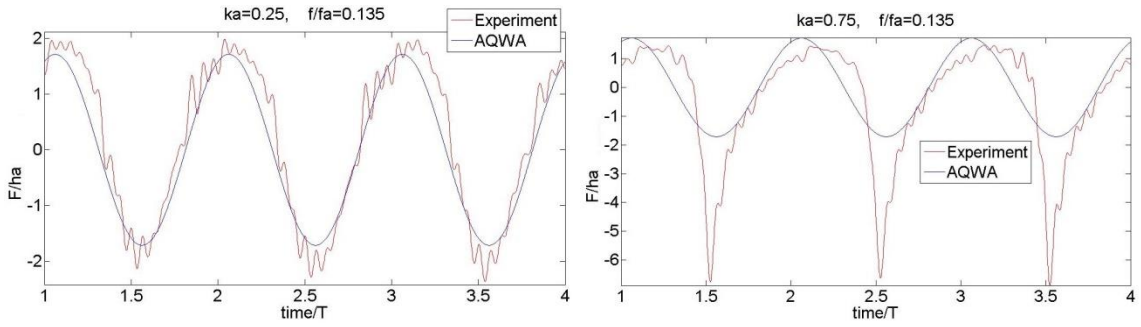

Figure 19 : Comparison Dynamic Force between AQWA and Experiment

It can be seen from plots above that AQWA is not able to give a reasonable estimate of vertical dynamic forces for the experiment case with high oscillation amplitude; difference between AQWA and experiment results is smaller when oscillation amplitudes is small.

A comparison of AQWA results and Experiment results for all nine cases in table 2 has been shown in appendix I.

Experiment is expensive, limited to few cases, measurements in experiments give information about only few parameters (e.g. force). Experiments are difficult to be used for real time calculation. Potential diffraction software is not able to give correct estimate of dynamic forces for close gap. This creates a need for other methods such as CFD simulation to understand the physical phenomena which is governing flow inside gap and causing non-linear effects. With CFD it is possible to look into flow velocities, pressure distribution and several other parameters inside the fluid domain.

3 CFD-COMFLOW Simulation of Model

CFD methods are based on solving Navier-Stokes equations, which if accurately solved give pressure for each point in fluid domain; these pressures are then integrated over the area of surface to give force. In this section, it will be checked whether dynamic forces observed in close gap oscillation experiments can be captured by CFD or not. CFD can be extended to analyse geometries and more cases.

In first section of this chapter an introduction to COMFLOW has been given. In the later sections COMFLOW set-up under which simulations were performed to determine hydrodynamics loads on cylinder, have been explained. In last sections effect of viscosity on simulated forces will be discussed and then COMFLOW results will be compared with AQWA results and experiment results.

3.1 Introduction to COMFLOW

COMFLOW is CFD program based on volume of fluid method. A run of COMFLOW consists of the definition of the geometry (using GEODEF), and the run of the fluid solver (COMFLOW).

Mathematical Model

Navier-Stokes equations: Fluid motion in a three dimensional (arbitrary) domain can be described by the Navier-Stokes equations. For water motion, where water is considered as an incompressible and viscous fluid, the Navier-Stokes equations can be simplified to:

Conservation of mass

$$\nabla \cdot \mathbf{u} = 0,$$

Conservation of momentum

$$\frac{\partial \mathbf{u}}{\partial t} + \mathbf{u}\cdot\nabla\mathbf{u} = -\frac{1}{\rho}\nabla p + \frac{\mu}{\rho}\nabla\cdot\nabla\mathbf{u} + \mathbf{F}.$$

In this equation, p is the pressure, μ is the dynamic viscosity, ρ denotes density, and **F** stands for external forces (gravity for example).

Calculation of forces: The fluid in a flow domain induces a force on an object in the domain. COMFLOW calculates pressure at each point in domain. The force is calculated as the integral of the pressure along the boundary of the object *S*.

$$\mathbf{F} = \int_S p\mathbf{n}ds.$$

3.2 Simulation of Cylindrical Model in COMFLOW

In this section simulation set-up of case 8 (for f/fn = 0.27 and ka = 0.5) and most important inputs for simulation have been discussed. For complete input please refer to Appendix II. The set-up has been used to simulate other eight cases also.

Geometry: Only one quarter of cylinder geometry and domain was simulated and symmetry boundary was applied, to reduce the computation time. Geometry of the CFD cylindrical model is same as used in experiment by Dockwise. Radius of cylinder is 40 cm, draft 9 cm, water depth 11 cm, height of cylinder above waterline is 5 cm. A square outer domain is chosen (20m x 20m). Domain boundary is located at 10 m from the center of cylinder.

It was found that as boundary is moved outward, the pressure at edge of gap domain and inside the gap domain converges at boundary distance of 10 m. In the first plot below edge pressure has been plotted against time for different boundary distances from center of cylinder, (generating absorbing boundary condition has been applied on boundary in x and y directions). Pressure inside gap at a radius r=0.5 R is shown in second plot below.

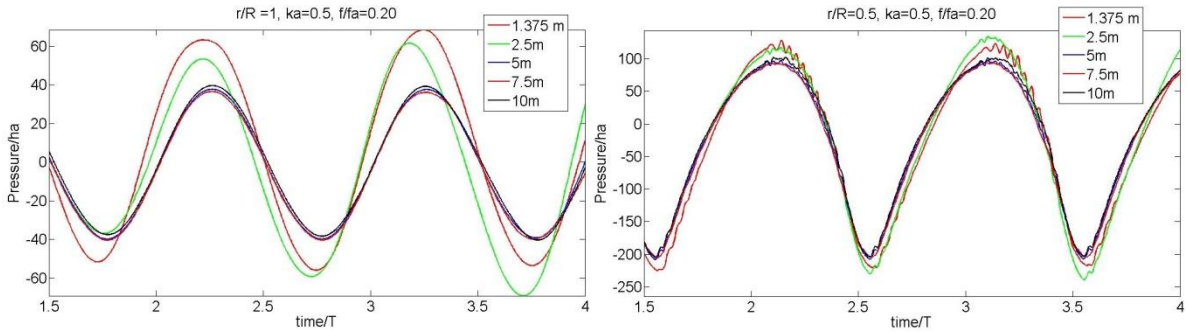

Figure 20: Effect on Pressure at Edge and Inside Gap with Different Boundary Distances

By putting pressure points close to boundary, it was observed that reflections from boundary are very weak, when boundary is kept at 10 m. It is good to avoid any reflection from far field as we wish to focus mainly on effect of vicinity of seabed on vertical force. Geometry of domain and cylinder has been shown in the figure below.

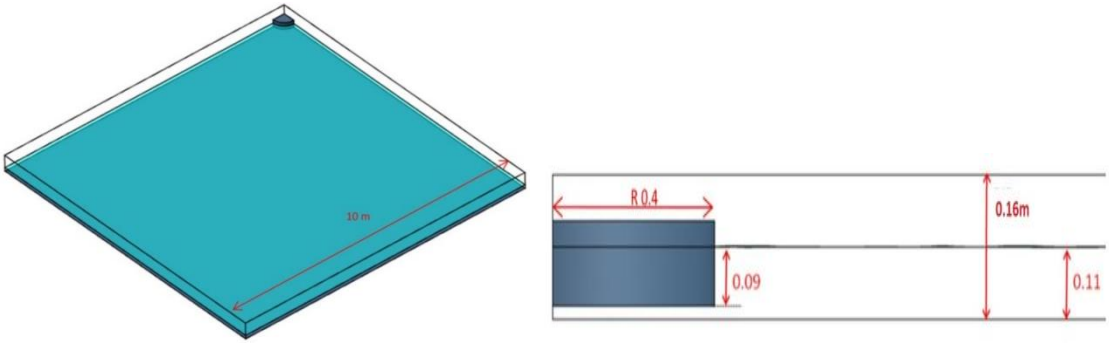

Figure 21: Domain and Geometry

Mesh: A uniform relatively dense mesh grid was used inside the gap while in outer domain a stretched grid was used along x, y and z axis. Reason for using such distribution is to capture the flow in the gap with relatively dense grid, while reduce the computation time by stretching the grids in outer zone. Main focus is to study the flow behavior inside gap domain. Grid distribution along three axes is being explained below.

X axis (60 grids): 25 grids were taken inside the gap of 0.40 m; grid density 0.016 m per grid. 35 grids were taken in outer domain of 9.6 m with smallest panel close to cylinder being 0.016m, rest stretched by a factor of 1.14 outward from center.

Y axis (60 grids): In same fashion as grid in X axis direction.

Z axis (32 grids): 15 grids were taken in gap of 30 mm, (2mm per grid), 17 in outer domain of 0.13 m (stretch ratio 1.08).

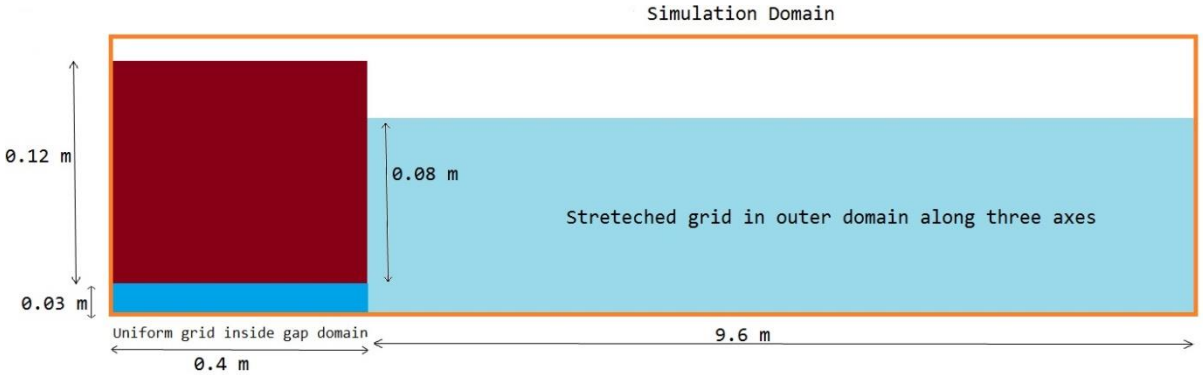

Figure 22: Mesh Plan Showing Quarter Domain

Grid study: To perform grid study a coarse grid was chosen to start with, as refined grids are very time consuming computationally.

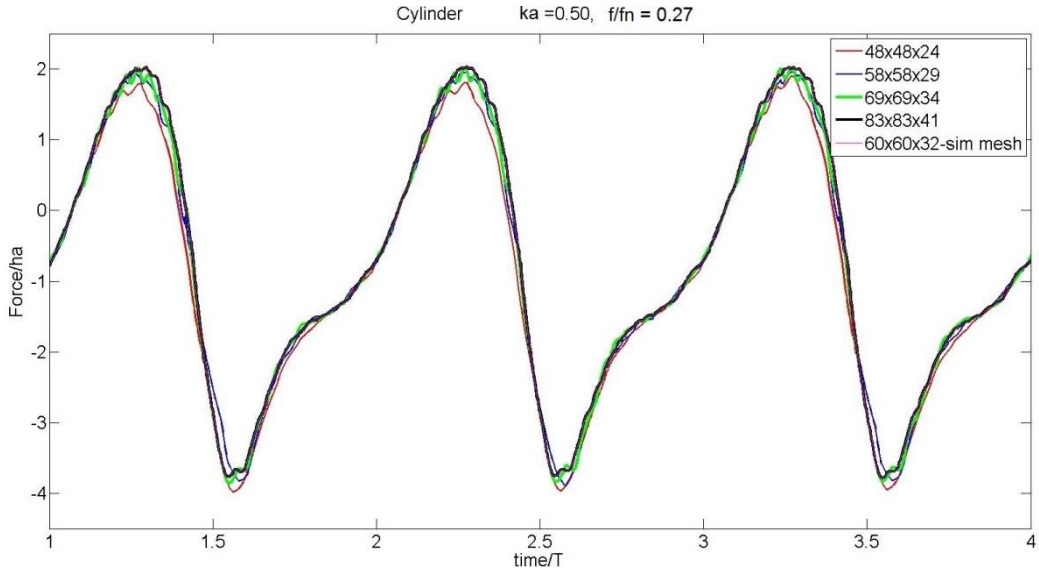

Figure 23:

In figure 23 simulated forces for various grid densities has been shown. Grid refinement was increased by increasing grid number with a factor of 1.2 both inside the gap and outside to keep it uniform. A close view of peak and trough for different grid is being shown below in Figure 24.

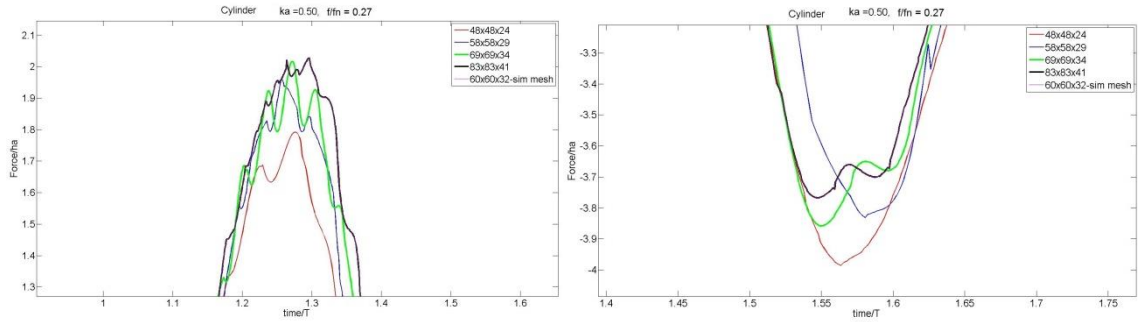

Figure 24: Grid Study, Highlighted View of Peaks and Troughs

Convergence of grids is apparent from the plots above as difference between calculated force values gets smaller with each refinement step.

Boundary Conditions: *Symmetry BC* was applied along x and y axis. COMFLOW calculates the results for quarter of cylinder, which is mirrored to obtain solution for complete domain. *GABC* (Generating and Absorbing Boundary Condition) was applied at domain boundaries along x and y direction to avoid any reflection. GABC has a property prevent wave reflection from the domain boundaries. *No-slip* boundary condition is automatically applied by COMFLOW at solid walls (seabed and model).

A study of boundary conditions at 10 m boundary (Figure 25), showed little difference in calculated vertical force for various boundary conditions. Since it was known that in Dockwise experiment towing tank walls were located far away so it seemed safer to use gabc to avoid any far field reflection.

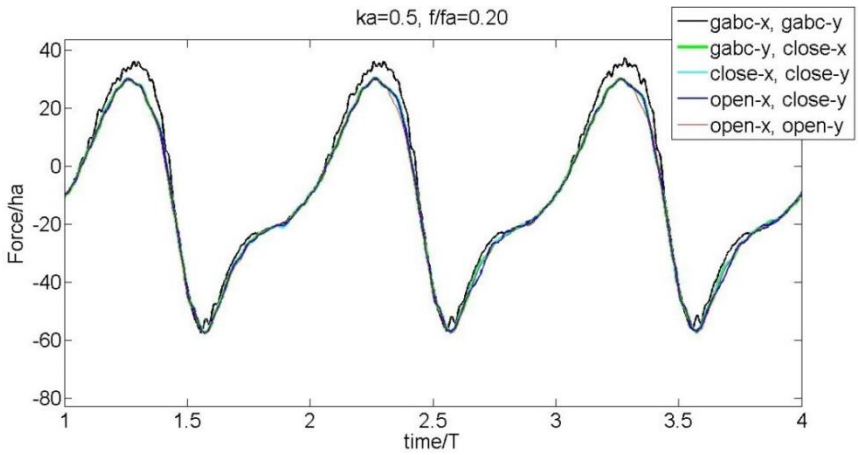

Figure 25: Relative Effect of Various Boundary Conditions

Motion: Sinusoidal motion was applied to model (equation 1), amplitude of motion and frequency is mentioned in title of each plot. COMFLOW gives specified motion from start of simulation itself.

Time Step: Input options were chosen to let COMFLOW adjust time step to keep CFL number range between 0.2-0.5 during simulation.

Viscous Effect: Comflow is not good for viscous simulations. Viscous and turbulence modeling was switched off in simulation, this means simulations are essentially solutions of Euler equations.

3.3 Results and Analysis

The resulting force and time plot of COMFLOW simulation of case 8 is shown below. Varying hydrostatic force has been removed from the force result in COMFLOW, the plotted force is only dynamic force.

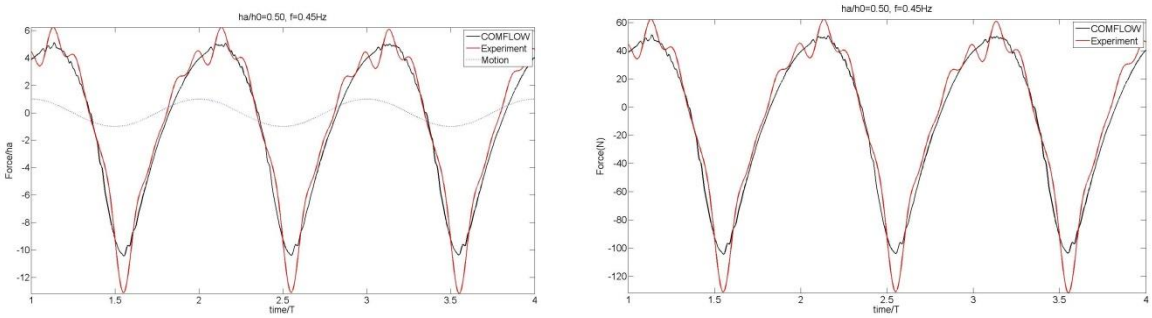

Figure 26: Comparison of COMFLOW Result with Experiment

In the plot on right side of figure 26, it can be seen that while dynamic forces vary from -131 N to 61 N in experiment, it varies from -101 N to 54 N in simulation. The visual comparison of plot lines shows that COMFLOW has been able to calculate dynamic force in agreement with dynamic force in experiment.

A comparison COMFLOW results and experiment results for eight remaining frequencies and oscillation amplitudes in table 2 has been shown in appendix I.

A comparison of this COMFLOW result with experimental result shows: (1) positive peak has same estimate in both experiment and COMFLOW, (2) phenomena of non-linearity of force w.r.t. motion is observed in both experiment and COMFLOW, (3) negative peaks are of higher magnitude compared to positive peaks in experiment and COMFLOW.

We can suspect an error in experiment measurements or there can be some error in COMFLOW set-up. In the plot below, Fourier analysis of hydromechanical force on cylinder bottom for case 7 (with smaller non-linear effect) and case 8 has been shown.

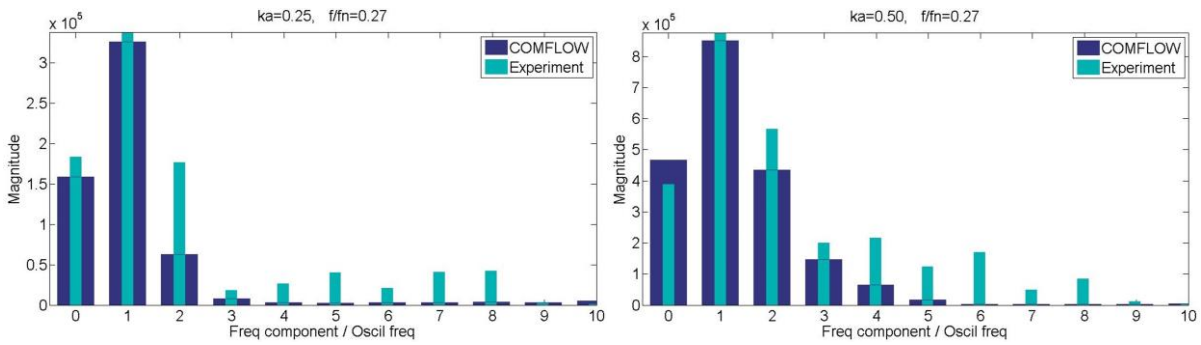

Figure 27: Fourier analysis of COMFLOW and Experiment Results for Case 7 and 8

It can be seen that at small oscillation amplitudes (for the same oscillation frequency) higher frequencies are negligible in COMFLOW while in experiment it is there. At small oscillation amplitude force is expected to be linear but data from experiment has higher frequency components also. The higher frequencies (3rd and high) observed in experiment can be due to vibration in set up of experiment. It can be assumed that COMFLOW results are more reliable than experiment results. Henceforth COMFLOW results will be used in chapter 4 and 5 for validation of analytical expressions (not the experiment results). Experiment results are only available for nine cylinder cases so using COMFLOW is only option.

3.4 Effect of Viscosity

It is important to see effect of viscosity on simulated force. If effect of viscosity is small, then there is possibility that Foude modelling of model to full scale will give good estimation of forces on full scale. In the figure below vertical varying force (varying static force and dynamic force) has been plotted for both viscous and inviscid simulations.

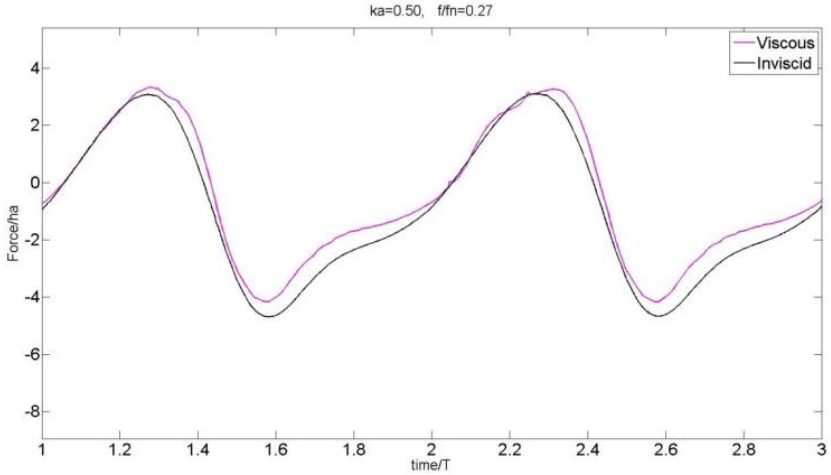

Figure 28: Effect of Viscocity on Simulated Forces, Case 8

It can be seen from plot above that viscosity has relatively small effect on simulated forces compared to magnitude of peaks observed. It was found that COMFLOW results are not much stable for viscous simulation for the cases studied.

3.5 Comparison of COMFLOW Results with AQWA

If we compare the results of AQWA and COMFLOW (given in appendix I) then we see that at Oscillation amplitudes ¼ (ka=0.25) of gap height, AQWA solutions are much closer to COMFLOW results. While at oscillation amplitude 1/8 and 1/16 (Ka=0.125, 0.0625) of gap height, matching is almost perfect. It can be assumed that at oscillation amplitudes ¼ of gap height, or smaller, AQWA can be used to determine heave forces, for the range of frequency used in experiment. While at oscillation amplitude higher than 1/4, i.e. ½, or ¾ the potential software results are not able to account for large negative peaks.

Linear part of the COMFLOW force can be obtained by using Fourier transform to obtain magnitudes corresponding to all frequencies, then retaining only first frequency (which is equal to oscillation frequency) and performing inverse Fourier for that frequency only.

A comparison of linear part of COMFLOW force and AQWA force has shown good resemblance. In the plot below linear component of COMFLOW dynamic force and AQWA force has been shown for case 8.

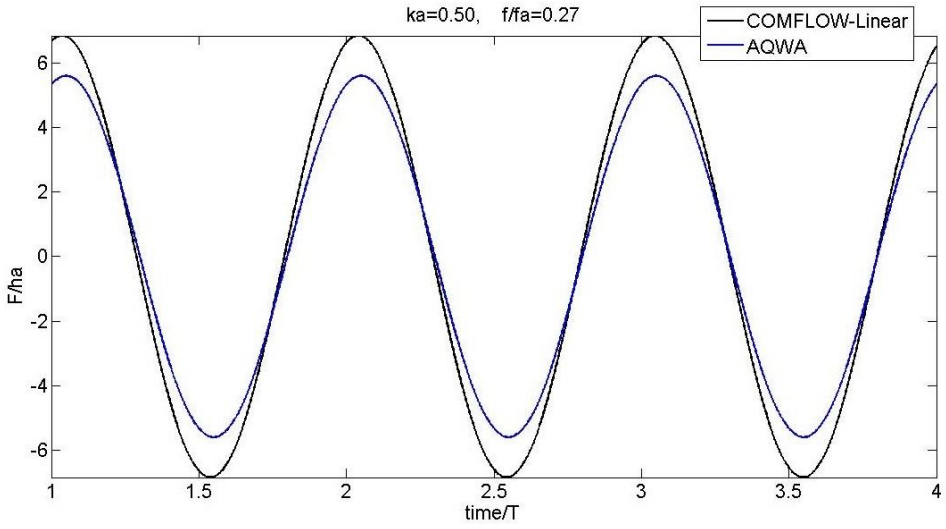

Figure 29: Comparison of Linear Component Forces COMFLOW and AQWA

From plot above, it can be observed that AQWA is able to calculate the linear part of forces while non-linear part which is observed only in simulation at higher oscillation amplitudes leads to difference between AQWA and COMFLOW results.

A comparison of linear and nonlinear components contribution to total dynamic force (COMFLOW) is given below.

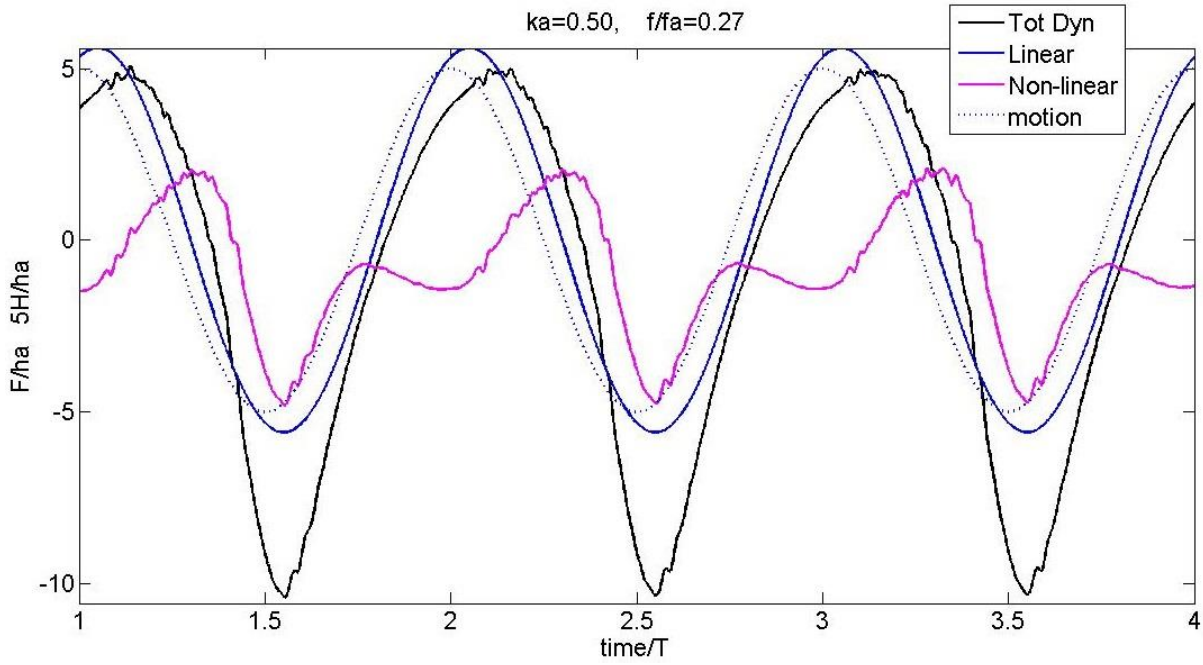

Figure 30: Linear and Nonlinear parts in COMFLOW Simulation, Case 8

In above plot it can be seen that asymmetry in total dynamic force is caused by asymmetry in non-linear component which leads to oval shape of total dynamic force. Nonlinear force is asymmetric in two ways (1) positive and negative parts are not similar, moving from mid position towards seabed and moving away from mid position results in different force magnitudes; (2) It is not symmetric in a time period on left and right of T/2. This means for the same position about mid, non-linear force is different when model is moving upwards and downwards.

4 Analytical Method for Cylinder and Barge

Discussion in present section is aimed to look for simplified analytical approach which can estimate dynamic forces observed in experiment and COMFLOW simulations.

To develop a method to analyze vertical forces, flow characteristic in the gap domain and outer domain needs to be considered. Below we will discuss logical development of a simplified flow model for flow inside the gap between model and seabed, which can be solved analytically and can give good estimate of dynamic forces on cylinder bottom.

Why Model Flow Inside Gap Domain?

Force on bottom of model originates from pressure at the bottom. To explain, consider a simple case when a cylinder model is static, at this time pressure inside the gap will be same as pressure at the edge of the cylinder as there is no flow inside. This no flow means pressure at all points inside gap are in equilibrium with pressure at the boundary of gap domain, net force on fluid pockets in the gap is zero.

Now if model starts oscillating vertically, there will be a flow inside the gap, and outside the gap induced by oscillation of cylinder. This flow outside will create a linear and non-linear effect of its own in pressure outside, but non-linear effect due to flow outside is difficult to model analytically. But if force due to flow in outer domain is linear then non-linear force due to flow inside gap if it can be modelled will give total non-linear force.

For the case of cylinder it has been found that pressures in outer domain and at the boundary between gap domain and outer domain (at edge) are sinusoidal (section 4.4). Hence If non-linear force due to flow inside the gap can be modelled, it will give total non-linear force.

Also if flow outside is causing non-linear pressures at the boundary (which will act on bottom as pressure inside gap has to be in equilibrium at the edge and hence it will transfer to bottom of model) and these non-linear pressures are known then non-linear force only due to flow inside the gap can be found out by analytically modelling flow inside the gap. That is case with barge oscillating close to seabed (section 4.8 and 4.9). And then next step can be that is it possible to find curve fit to model non-linear forces due to flow outside the gap in the same form equations as that of non-linear force due to flow inside gap.

For now, we need to question, how to model flow inside the gap so as to capture non-linear force due to gap.

Modeling Flow inside Gap

Any fluid domain physics can be captured relatively accurately by Navier Stokes equation. But computational time involved in simplest of CFD methods adopted, makes it impossible for engineers to use it, as they need on spot workable estimate of forces and motions, while performing operation.

A way ahead is Euler's equation, in which viscosity is neglected. It is suitable for the flows where viscosity is of minor influence. (We have seen in section 3.4 that viscosity is of minor influence during close gap flow). Simulation results analyzed in chapter 3 were essentially solution of Euler's equation. Euler method has been found to be able to capture non-linear force as we saw in Chapter 3. But computational time is still huge.

A further simplification can be made when it is found that rotation is not of that much effect in the inviscid fluid domain. That means curl of velocity vector is zero. Such flow is called potential flow. But potential flow solutions are linearized in software and simple analytical potential solutions are also quite difficult to derive.

Here author will look to simplify flow even further by considering a uniform flow in horizontal and vertical direction inside gap domain. Investigation will be made whether such model can capture the non-linear dynamic forces observed in COMFLOW simulation and experiments. Approach was first used by Brenen [2] to find out hydrodynamic forces on circular disk.

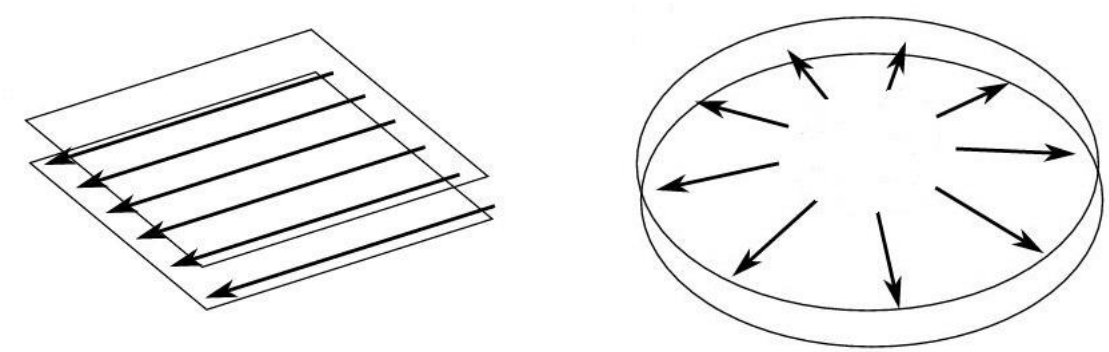

Figure 31: Stream Lines in Uniform Flow Inside the Gap

4.1 Analytical Derivation of Pressure inside Gap for Cylinder

In this section an attempt is being made to come up with analytical solution for vertical force on cylinder bottom, using flow model discussed before. It is useful to start with cylinder model, as because of the symmetrical geometry of cylinder bottom, flow in radial direction is expected to be symmetric inside gap, analytical derivation of forces is relatively easier. Also verification of cylindrical model is possible because of availability of experimental results which were discussed in chapter 2.

In present section, flow in gap domain between cylinder bottom and seabed is being considered as uniform inside gap, flow outside the gap in outer domain has not been modeled.

Figure 32, down below shows horizontal view of a model of cylinder oscillating close to seabed such that, pressure at a point at variable distance r from center is p. Author has assumed flow between cylinder and seabed is uniform inside the gap. Which will mean radial velocities will be same across the vertical plane section at any radius r $(r \leq R)$, and vertical velocities will be same at any height z (0<z<h) inside gap domain. Edge pressure at radius R is p_e. Assuming uniform flow will mean, radial velocity at all points 1,2,3,4,5 (figure 32) at a radius r but varying vertical positions in flow has been assumed to be same.

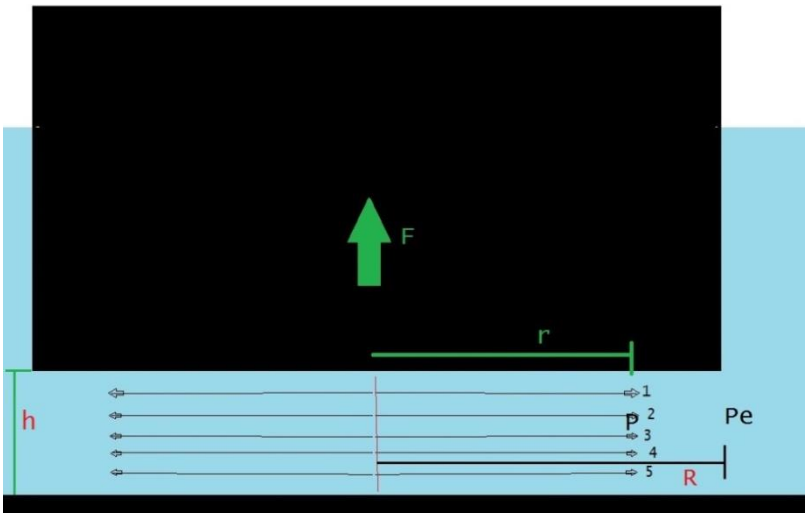

Figure 32: Horizontal View of flow Model between Cylinder and Seabed

4.1.1 Analytical Mass conservation Equations

We decide to give a sinusoidal motion, in same fashion as represented by equation 1.

Figure 33 below shows, a box of radius r and height h between cylinder bottom and seabed. Movement of cylinder between time t to t+dt is dh, while radial velocity at radius r, at time t is u_r.

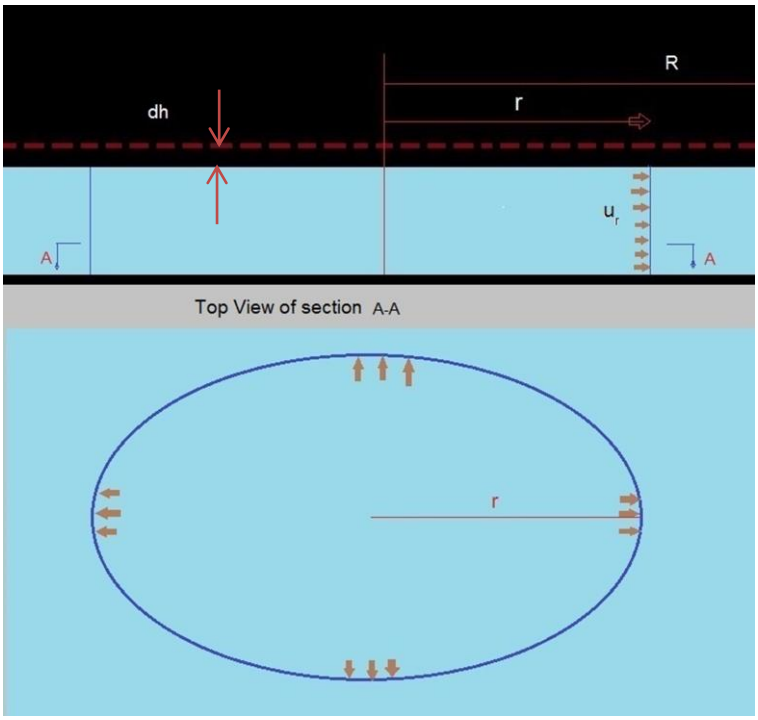

Figure 33: Cylinder; Front and Top View of Box of Radius r Height h

The volume of water being squeezed out of cylindrical box of radius r and height h in time dt will equal the volume of water rushing out of boundary of the cylinder at radius r in time dt.

$$u_r\,(2\pi rh)\,dt = -\pi r^2 \frac{\partial h}{\partial t}\,dt \quad \text{.....(5)}$$

Since h is only function of time and is independent of radius, it can be written

$$\frac{\partial h}{\partial t} = \frac{dh}{dt}$$

Cancelling dt from both sides in equation 5, and rearranging the terms will lead to

$$u_r = -\frac{r}{2}\,h_t \quad \text{.....(6)}$$

In similar way now flow in the vertical direction inside the gap will be considered. Let us consider conservation of mass in a box of radius r and height z from seabed.

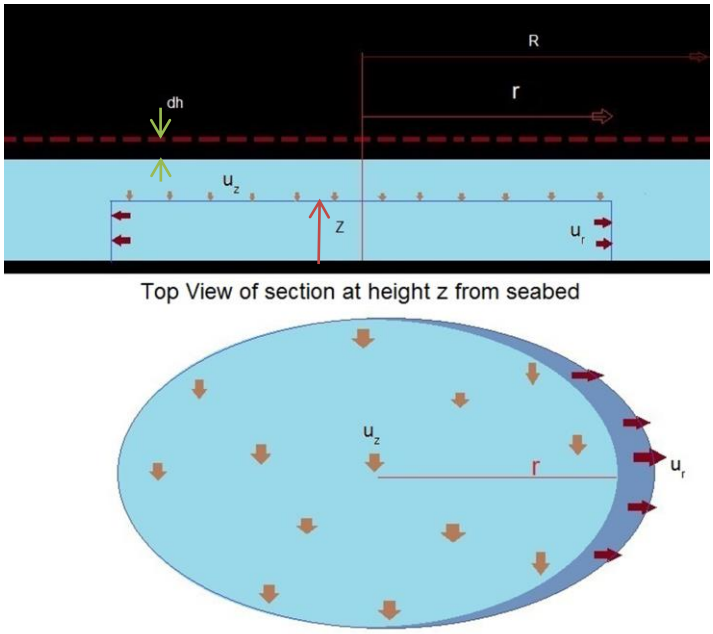

Figure 34: Cylinder; Front and Top View of Box of Radius r Height z

We assume that vertical velocity u_z is constant across the area at height z. The Volume of water flowing vertically into cylinder of radius r and height z in time dt will equal the volume of water rushing out horizontally from boundary at radius r.

$$u_r \left(2\pi rz\right) dt = -u_z \left(\pi r^2\right) dt$$

Substituting u_r from equation 6, will give

$$u_z = \frac{z}{h} h_t \quad \text{.....(7)}$$

4.1.2 Comparison Analytical Velocity with COMFLOW Results

Before proceeding further, it will be useful to compare assumptions of uniform flow and equations for velocity in radial direction derived in previous subsection with that of observations in COMFLOW (for case 8). It has been observed from COMFLOW simulation that close to center of gap, flow is near to uniform up to certain radius for various cases, while at the edge where flow inside gap domain meets outer domain, velocities are erratic. Boundary layer is present on the bottom of model and on seabed in the simulation result

(no slip was applied), leading to a different velocity at the seabed and bottom of model, but effect doesn't extend to the inviscid core. The plot below shows radial velocity field during outward flow.

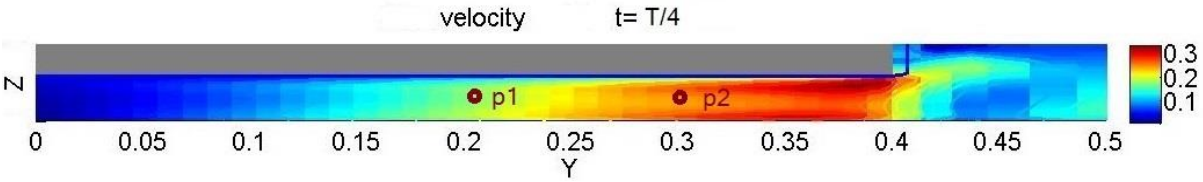

Figure 35: Radial Velocity Field inside the Gap, Case 8

A time plot of velocity at point P1 located at r=0.5R in figure 35 has been shown in the figure below. One can observe in plot that analytical velocity is much closer to COMFLOW velocity in this case, however a slight difference occurs during upward motion of cylinder.

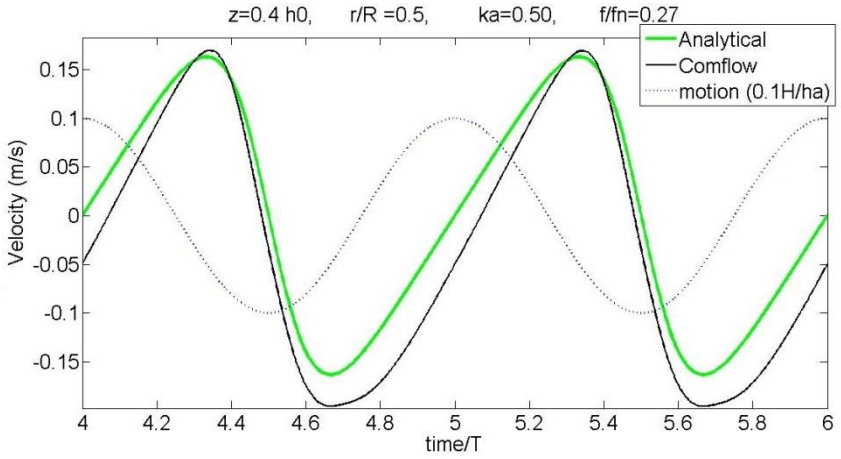

Figure 36: Time Plot of Radial Velocity at Point Close to Centre

A time plot of velocity at point P2 located at r=0.75R in figure 35 has been shown in the figure below. One can observe in plot that COMFLOW velocity is very different from velocity calculated by equation 6 at this point.

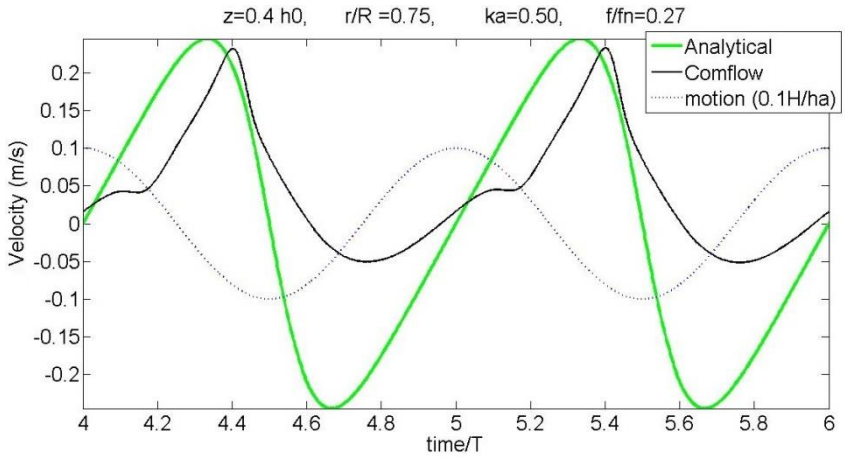

Figure 37: Time Plot of Radial Velocity at a Point Close to Edge

For the case 8, it has been observed in COMFLOW that velocities can be assumed to follow expression for radial velocity in equation 6 up to radius 0.65 R. The radius up to which flow linearity is observed in COMFLOW simulations differs for different oscillation amplitudes. Erratic flow close to edge seems to be due to flow separation causing velocities to differ and vary close to edge of gap domain.

Regarding uniformity of the flow velocity across a vertical section (i.e. whether radial velocities are uniform at a points 1,2,3,4 and 5 in figure 32 or not) a pattern has been observed that velocities are more uniform when cylinder is moving down and flow is in outward direction; more irregularity has been observed when cylinder is moving upwards and flow is in inward direction.

A view of the flow field for case 8, at time t=4T+T/4, when cylinder is at mid position, while flow is in outwards direction has been shown below. In the color map, vorticity has been plotted. The vectors arrows in radial and vertical direction show radial and vertical velocities respectively (vertical arrows are barely visible because magnitude is very small).

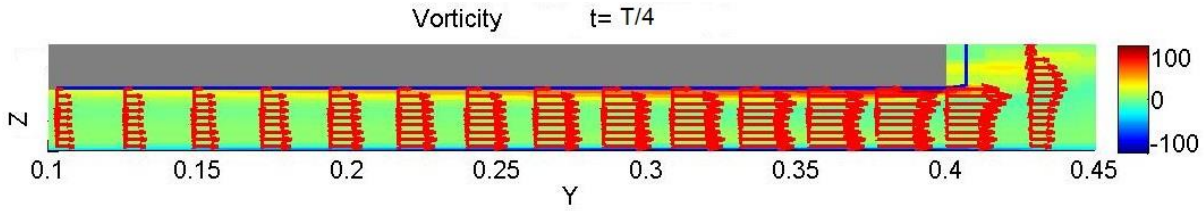

Figure 38: Outward Flow, Case 8

Figure below shows the flow field inside the gap at time t=4T+3T/4, when cylinder is at mid position while flow is in inward direction. Color map shows vorticity.

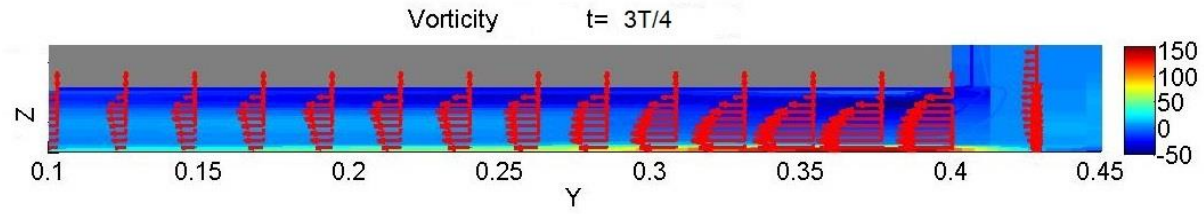

Figure 39: Inward Flow, Case 8

In the plot below, a time plot of velocity at four moving points in the stream at different fixed distance from bottom of moving cylinder has been shown.

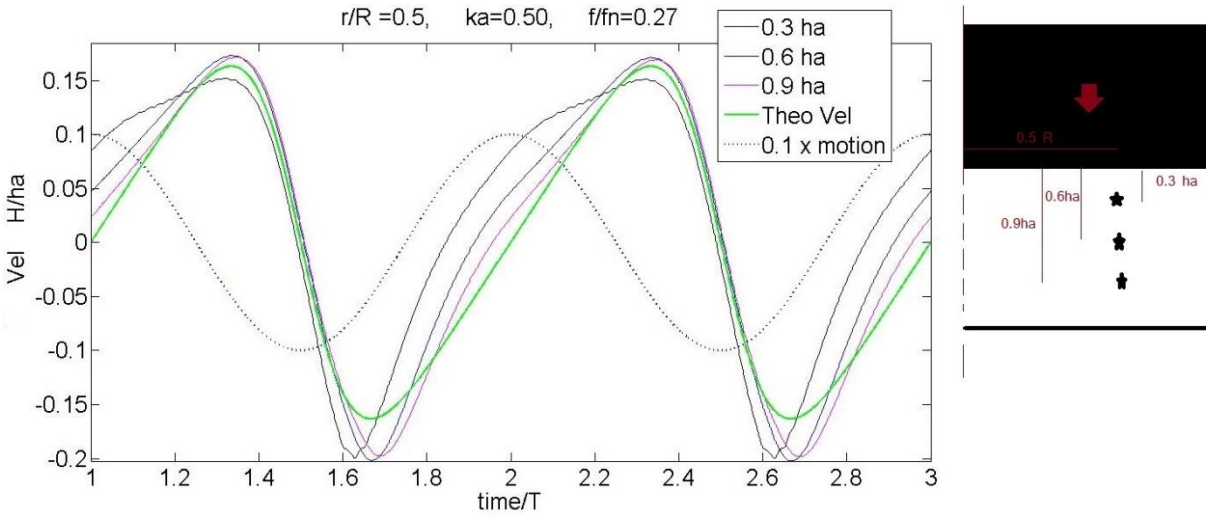

Figure 40: Radial Velocity at Several Points in a Vertical Section at r=0.5 R

In plot above, it can be seen again that larger deviation in radial velocity occurs at all points during upward motion (compared to theoretical velocity) and velocities are different at points despite points being in same vertical line.

The colour map in figure 39 shows that during inward velocity there is vortex formation at the entrance of flow into the gap, this vortex formation seems to be caused by separation of flow at entrance. Physical argument for disparity in velocities across the vertical section seems to be that vortices formed during inward flow at the entrance of gap, block the flow into the gap.

Deviations in velocities across the vertical section has been found to be higher when flow is in inward direction and decelerating (3T/4-T). Obvious reason is inertia is also opposing the flow.

During comparison of theoretical velocity with velocities observed in simulation for other cases, it has been observed that deviations from theoretical velocity becomes larger at higher oscillation amplitudes, while at smaller oscillation amplitudes deviation from theoretical velocity is very less. At higher oscillation amplitudes lower resemblance can be expected because of higher velocities causing more turbulence and higher Reynolds number.

Despite slight non-resemblance, overall radial velocity in equation 6 seems to be good estimate of flow velocities inside the gap. In next section, we will substitute u_r and u_z from equation 6 and 7 into Navier-Stokes continuity equation and find out whether these values are indeed solution of continuity equation. In the second stage these values will be substituted into momentum conservation equation, to determine pressure.

4.1.3 Pressure Equation for Cylinder

Navier Stokes continuity equation for uniform flow in polar form can be written as

$$\frac{1}{r}\frac{\partial(r\,u_r)}{\partial r} + \frac{\partial u_z}{\partial z} = 0$$

By substitution, it can be found that u_r and u_z derived before in section 4.1.1, do satisfy continuity equation above.

Navier Stokes momentum equation for uniform flow in polar form can be written as

Momentum equation in r direction

$$\rho\left(\frac{\partial u_r}{\partial t} + u_r\frac{\partial u_r}{\partial r} + u_z\frac{\partial u_r}{\partial z}\right) = -\frac{\partial p}{\partial r} \text{.....(8)}$$

Momentum equation in z direction can be written as

$$\rho\left(\frac{\partial u_z}{\partial t} + u_r\frac{\partial u_z}{\partial r} + u_z\frac{\partial u_z}{\partial z}\right) = -\frac{\partial p}{\partial z} + \rho g \text{.....(9)}$$

There will be no θ Component no angular flow exists in uniform flow model assumed in section 4.1.1.

In order to find equation for pressure from equation 8 and 9, values of u_r and u_z are substituted from equation 6 and 7, giving equation for pressure derivatives along radial and z directions.

Substituting u_r and u_z from equation 6 and 7 into equation 8 gives

$$\frac{\partial p}{\partial r} = \rho\left(\frac{r}{2h}h_{tt} - \frac{r}{4h^2}h_t^2\right) \text{.....(10)}$$

Substituting u_r and u_z in equation 9,

$$\frac{\partial p}{\partial z} = -\rho\left(\frac{z}{2h}h_{tt} + \frac{z}{4h^2}h_t^2 - g\right) \text{.....(11)}$$

Since p is a function of z and r,

$$dp = \frac{\partial p}{\partial r}dr + \frac{\partial p}{\partial z}dz$$

Substituting $\frac{\partial p}{\partial r}$ and $\frac{\partial p}{\partial z}$ from equation 10 and 11 respectively,

$$dp = \rho\left(\frac{r}{2h}h_{tt} - \frac{r}{4h^2}h_t^2\right)dr - \rho\left(\frac{z}{2h}h_{tt} + \frac{z}{4h^2}h_t^2 - g\right)dz$$

$$dp = \rho\left(\frac{r}{2h}h_{tt} - \frac{r}{4h^2}h_t^2\right)dr - \rho\left(\frac{z}{2h}h_{tt} + \frac{z}{4h^2}h_t^2 - g\right)dz \quad .....(12)$$

Let us denote pressure at radius r and height z as $p_{r,z}$ and pressure at radius R at height h as $P_{e,R,h}$. Integrating equation 12 from radius R to r and height h to z gives

$$\int_{p_{e,R,h}}^{p_{r,z}} dp = \rho\left(\frac{h_{tt}}{2h} - \frac{h_t^2}{4h^2}\right)\int_R^r r\,dr - \rho\left(\frac{h_{tt}}{2h} - \frac{h_t^2}{4h^2}\right)\int_h^z z dz + \int_h^z \rho g dz$$

$$p_{r,z} = p_{e,R,h} + \rho\left(\frac{h_{tt}}{2h} - \frac{h_t^2}{4h^2}\right)\left(\frac{r^2 - R^2}{2}\right) - \rho\left(\frac{h_{tt}}{2h} - \frac{h_t^2}{4h^2}\right)\left(\frac{z^2 - h^2}{2}\right) + \rho g(z - h)$$

I II III IV

The fourth term on right hand side is hydrostatic pressure variation. Second and third terms describe dynamic pressure in the fluid inside gap domain due to fluid motions inside the gap. The third term on right hand side can be disregarded if $h << R$. The relative effect of third term on total pressure will be insignificant in comparison to second term.

$$\rho\left(\frac{h_{tt}}{2h} - \frac{h_t^2}{4h^2}\right)\left(\frac{r^2 - R^2}{2}\right) >> \rho\left(\frac{h_{tt}}{2h} - \frac{h_t^2}{4h^2}\right)\left(\frac{z^2 - h^2}{2}\right)$$

A comparison of COMFLOW calculation of dynamic pressures (not including varying static pressure) at various points in the a vertical line between seabed (z=0) to height $z = h_0 - h_a$, has been shown below.

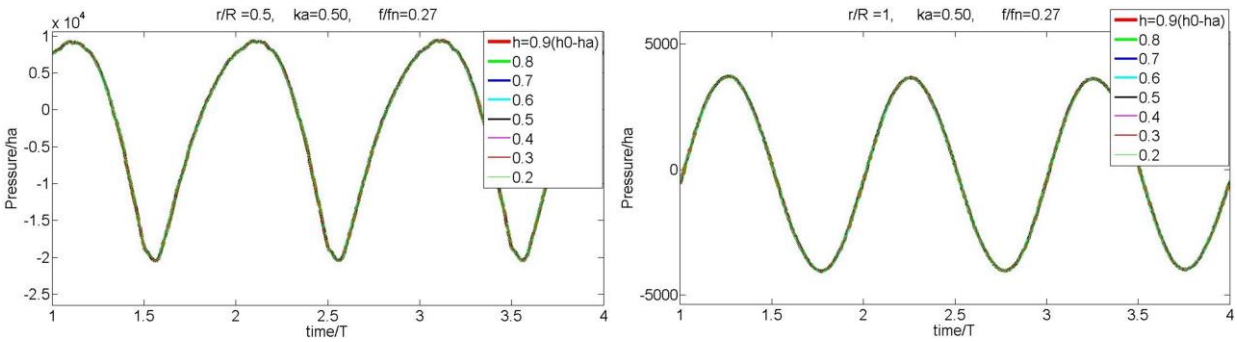

Figure 41: Pressure Variation along Vertical Section in COMFLOW Simulation

We can observe from plots above that vertical variation of pressures are very small and can be neglected in comparison with total dynamic pressure.

After removing third term, we can write pressure equation now as,

$$p_{r,z} = \left[p_{e,R,h} - \rho g(z - h)\right] + \rho\left(\frac{h_{tt}}{2h} - \frac{h_t^2}{4h^2}\right)\left(\frac{r^2 - R^2}{2}\right)$$

Pressure at the bottom of the cylinder $p_{r,h}$ determines vertical force acting on cylinder. Substituting z=h

$$p_{r,h} = p_{e,R,h} + \rho\left(\frac{h_{tt}}{2h} - \frac{h_t^2}{4h^2}\right)\left(\frac{r^2 - R^2}{2}\right)$$

To reduce the write up, from now onwards pressure at arbitrary radius r and height h, $p_{r,h}$ will be denoted just p and $p_{e,R,h}$ will be denoted as p_e.

$$p = p_e + \left[\frac{\rho}{2h} h_{tt} - \frac{\rho}{4h^2} h_t^2\right]\left(\frac{r^2 - R^2}{2}\right) \quad \text{.....(13)}$$

This pressure p is function of edge pressure p_e, gap height h, radius r and time t.

4.2 Validation of Pressure Expression

To validate this expression in equation 13, by using pressure measured from CFD results, above equation 13 is rearranged. Dynamic pressure inside gap only due to flow inside the gap domain can be written as

$$p - p_e = \left[\frac{\rho}{2h} h_{tt} - \frac{\rho}{4h^2} h_t^2\right]\left(\frac{r^2 - R^2}{2}\right) \quad \text{.....(14)}$$

Terms on left hand side can be obtained from CFD data while terms on right can be plotted by calculating h_t and h_{tt} corresponding to oscillation frequency and amplitude in the simulation. The pressure difference $p - p_e$ is dynamic pressure due to flow inside the gap domain.

Let us consider the case 8 simulated in chapter 3.2. In the first plot below pressure difference (or dynamic pressure at the centre due to flow in gap domain) $p - p_e$ at centre of gap (r=0) calculated from equation 14 has been plotted against the dynamic pressure obtained from COMFLOW. In the second plot pressure difference $p - p_e$ at $r = 20$ cm ($r / R = 0.5$) inside the gap has been plotted against the dynamic pressure obtained from COMFLOW.

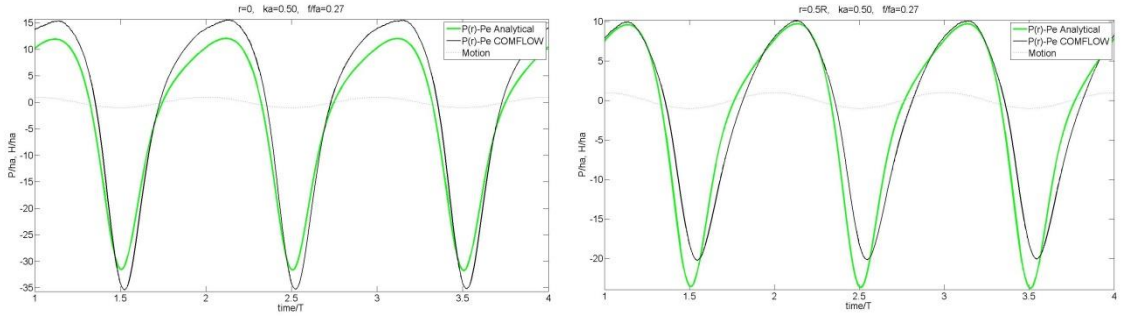

Figure 42: Comparison of Dynamic Pressures between COMFLOW and Analytical Model

As one can see from the plots above, the pressure obtained from equation 14 gives good estimate of dynamic pressure due to gap.

4.3 Dynamic Force Due to Flow Inside Gap

Integrating the pressure from equation 13, for full gap domain radius will give total force on the bottom of cylinder.

$$F = \int_0^R p\, 2\pi\, r\, dr = \pi R^2 p_e - \frac{\rho\pi R^4}{8h} h_{tt} + \frac{\rho\pi R^4}{16h^2} h_t^2 \quad \text{.....(15)}$$

$$F = Ap_e - \left(\frac{1}{8\pi}\right)\frac{\rho A^2}{h} h_{tt} + \left(\frac{1}{16\pi}\right)\frac{\rho A^2}{h^2} h_t^2 \quad \text{.....(16)}$$

This force F is total hydromechanical force acting on cylinder bottom as cylinder oscillates. In equation 16, the first term right side Ap_e is sum of force due to hydrostatic pressure and dynamic force due to flow in outer domain.

Second term has form of inertia force, which increases with decrease in distance from seabed. (We saw in section 2.4 and figure 18 that dynamic added mass increases in the vicinity of cylinder, it is due to higher accelerations imparted to the fluid as body moves closer to the seabed.) The higher negative peaks observed in simulation and experiments can be ascribed to the fact that h being in denominator of inertia term (which has same phase as motion), becomes very small when model is at lowermost position during motion. The reason behind very high negative peaks may be due to very small value of h when cylinder is closer to seabed during oscillation. High accelerations are caused by cylinder motion at this point as it is more closer to seabed but in linear potential software inertia is calculated for mid draft only.

Third term has form of lift force and acts always in upward direction. Magnitude of this term will only be appreciable when cylinder bottom is very close to seabed. Magnitude of radial velocity is highest at the edge (equation 6), means minimum lift pressure at the

edge, while inside magnitude of velocities are smaller so higher lift pressure inside compared to edge, hence lift force tends to push cylinder up during both upwards and downward movement. Lift term with h_t^2 coefficient has a frequency of 2ω, this term becomes more significant at oscillation amplitudes, hence higher frequencies are more observed in Fourier analysis of cases with higher amplitude as observed in section 2.3, figure 17.

Total dynamic force after removing static force and varying static force can be written as

$$F\ (\text{total dynamic}) = A(p_e - \rho g d + \rho g H) - \left(\frac{1}{8\pi}\right)\frac{\rho A^2}{h} h_{tt} + \left(\frac{1}{16\pi}\right)\frac{\rho A^2}{h^2} h_t^2 \quad \text{.....(17)}$$

To validate above equation, COMFLOW simulation results was used to compare dynamic forces in simulation with dynamic force obtained from above expression. Here Pe can be found from COMFLOW simulation. Substitution gives following plot for total dynamic force.

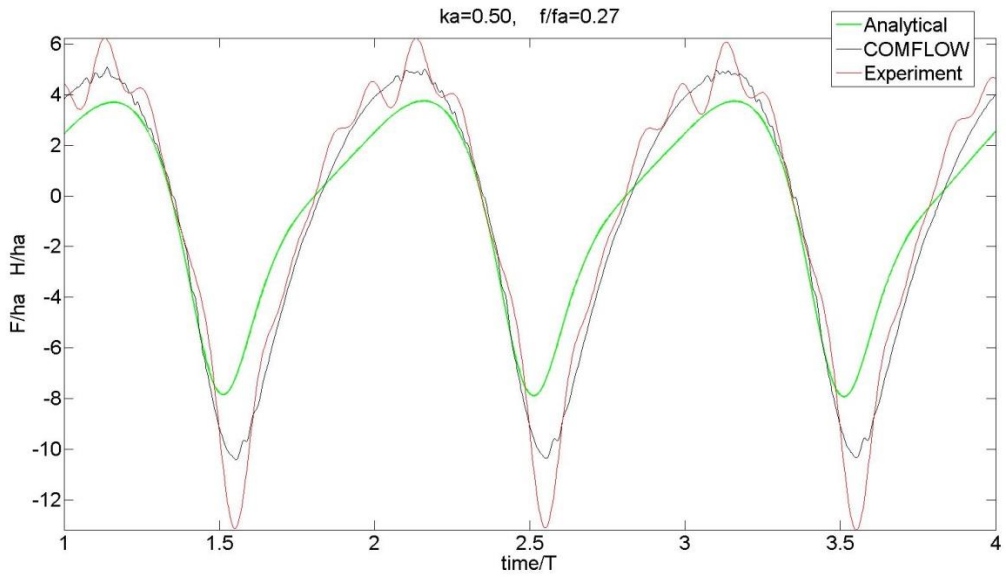

Figure 43: Comparison of COMFLOW and Analytical Dynamic Force

From plot above it can be seen that equation 17 gives good approximation of dynamic forces obtained from COMFLOW. A plot of dynamic force comparison between analytical equation 17 and COMFLOW for other cases has been shown in appendix III.

Dynamic force only due to small fluid motions inside gap (excluding effect of outer domain on edge pressure) can be written as

$$F_{d,gap} = -\left(\frac{1}{8\pi}\right)\frac{\rho A^2}{h} h_{tt} + \left(\frac{1}{16\pi}\right)\frac{\rho A^2}{h^2} h_t^2 \quad \text{.....(18)}$$

While dynamic force due to Fluid motions in outer domain can be written as

$$F_{d,\,outer} = A(p_e - \rho gd + \rho gH)$$

Above expression is useful for studies relating to domain splitting as the entire dynamic force can be split into dynamic force due to flow inside gap (equation 18) and dynamic force due to flow outside the domain.

4.4 Edge pressure and Effect of outer Domain

If we were to consider pressure derivation in equation 13, the flow inside gap domain doesn't contribute to edge pressure (as r-R=0). Any non-linearity in edge pressure mostly will come through flow in outer domain.

Fourier analysis of edge pressure has shown that, only one frequency is present in edge pressure calculated by COMFLOW. A time variation of edge pressure can be seen in the plot below.

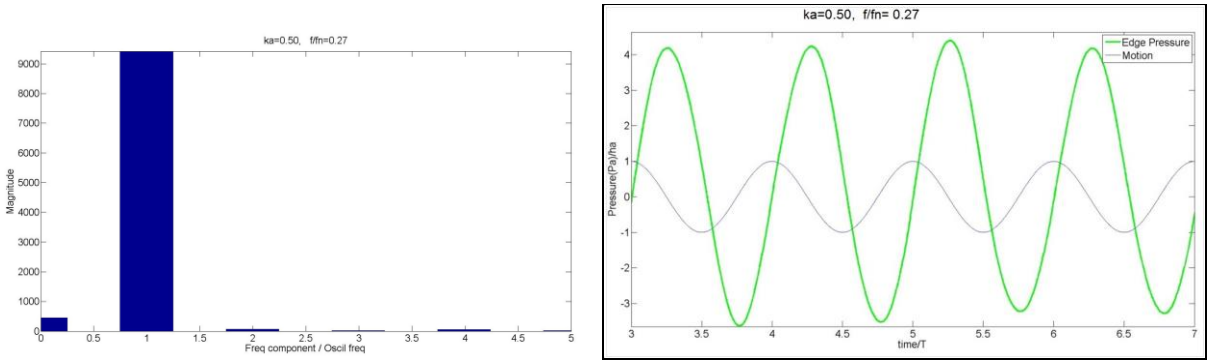

Figure 44: Fourier Analysis of Pe and Time Plot

For cylinder, edge pressure has been found to be linear w.r.t. motion for all nine cases, when these were simulated in COMFLOW. Simulation results show that edge pressure vary almost sinusoidaly. An intuitive reason would be the sudden drop in velocity at edge outside the gap, as it is observed in COMFLOW (figure-45 below), causing lift pressures (corresponding to h_t^2) to be very small. Flux from the gap can be considered acting like a source in the uniform flow. The spreading of flux from such source doesn't result in non-linear inertia dynamic effects.

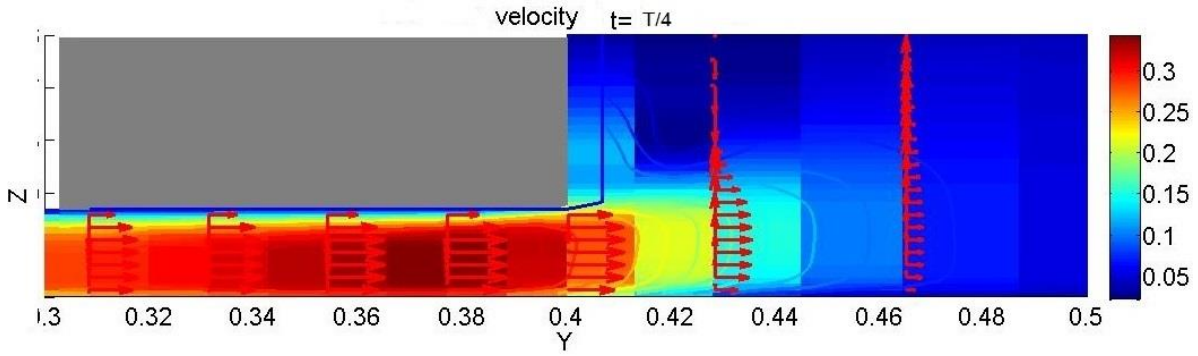

Figure 45: Velocity Field Outside Edge, Case 8

Important conclusion which can drawn is Pe is linear in case of cylinder and hence we can conclude that outer domain doesn't contribute to non-linear effect on vertical force in simulation, and Pe should be able to be calculated by potential software. If we consider gap as radiation source, it can be modelled as

$$p_e = p_h - k1\, h_{tt} - k2\, h_t \text{ .....(19)}$$

A plot of coefficients k1 and k2 obtained by curve fitting for COMFLOW simulation results for nine cases in table 2, is shown below.

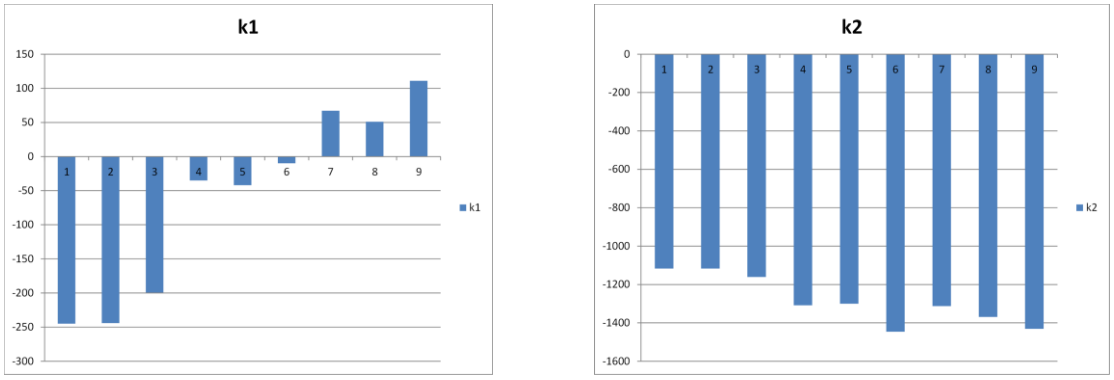

Figure 46: Coefficients k1 and k2 for Cylinder Edge Pressure for Case 1-9

Edge pressure may not be linear in all cases and will depend upon geometry of bottom area and location of point on the area edge. For example edge pressure is not linear in case of a barge with rectangular bottom (we will see in later sections), that means flow in outer domain also contributes to non-linearity in simulated dynamic force in that case.

4.5 Non-linear Part of Heave Force and Modified AQWA results

It has been said earlier that linear potential software doesn't calculate the non-linear components in dynamic force. But, in section 3.5 we saw that AQWA gives good results for linear part of dynamic force. It is useful to separate the nonlinear parts of vertical

dynamic force expressed in the equation 17 and check whether this part added to linear force obtained from AQWA can give total dynamic force observed in COMFLOW.

After Taylor expansion of second part of force equation 17 and retaining only linear part, linear part of dynamic force can be expressed as

$$F_{linear,dyn} = A(p_e - \rho gd + \rho gH) - \left(\frac{1}{8\pi}\right)\frac{\rho A^2}{h_0} h_{tt} \quad \text{.....(20)}$$

In equation above first part which is dynamic force due to flow in outer domain has been considered linear as found in COMFLOW simulations (discussed in previous section).

By subtracting the linear part from total dynamic force expression, non-linear part can be written as

$$F_{non-linear} = \left(\frac{1}{8\pi}\right)\rho A^2 \left(\frac{1}{h_0} - \frac{1}{h}\right) h_{tt} + \left(\frac{1}{16\pi}\right)\frac{\rho A^2}{h^2} h_t^2 \quad \text{.....(21)}$$

Expression for modifying AQWA results to include non-linear effect for vertical force on a cylindrical model can be written as

$$F(\text{modified AQWA}) = F_{AQWA} + F_{non-linear}$$

$$F(\text{modified AQWA}) = F_{AQWA} + \left(\frac{1}{8\pi}\right)\rho A^2 \left(\frac{1}{h_0} - \frac{1}{h}\right) h_{tt} + \left(\frac{1}{16\pi}\right)\frac{\rho A^2}{h^2} h_t^2 \quad \text{.....(22)}$$

A comparison of modified AQWA dynamic force with dynamic force calculated by COMFLOW for case 8 has been shown in the plot below.

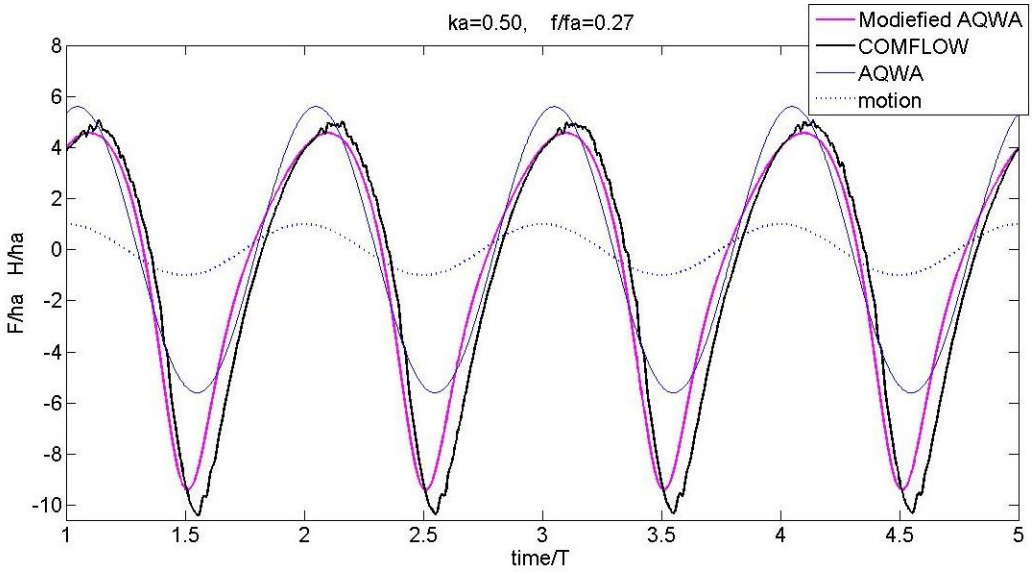

Figure 47: Comparison of Modiefied AQWA Force and COMFLOW force, Case 8

It can be observed from above plot that resemblance between the modified AQWA dynamic force and COMFLOW dynamic force is good. Slight disagreement can be found while the cylinder is moving up. We had observed in section 4.1.1 and in figure 36, 37 that during upward motion of cylinder, when water flows from outer domain to gap domain, the flow is not exactly uniform across the vertical section, but basic premise for deriving dynamic force (equation 17) was that flow is uniform inside the gap domain. Discrepancy between modified AQWA force and COMFLOW can be related to that. An insignificant difference in peak may be due to fact that boundary layer was not modeled while deriving equation 17, while in COMFLOW, numerical scheme applies a boundary layer (even though free stream is inviscid), so actual area available for flow will be slightly smaller, leading to slightly higher inertia and lift forces, but effect will be very small.

A comparison of modified AQWA force with force measured by COMFLOW for all nine cases has been shown in appendix III.

4.6 Significance of Two Nonlinear Inertia and Lift Terms

It would be useful to see the relative significance of two non-linear terms corresponding to h_{tt} and h_t^2 squared in equation 21. It can be used to understand which part is important under what conditions. Also it can be useful to know the effect of frequency and oscillation amplitude on dynamic force. Down below the derivations are aimed to find out the relative significance of two terms and frequency and amplitude effect on non-linear force.

Substituting h_t from equation 1 into equation 21, Non-linear force becomes

$$F_{non-linear} = \left(\frac{1}{8\pi}\right)\rho A^2\omega^2 k_a^2\left[\frac{Cos^2(\omega t)}{(1 + k_a Cos(\omega t))}\right] + \left(\frac{1}{16\pi}\right)\rho A^2\omega^2 k_a^2\left[\frac{Sin^2(\omega t)}{(1 + k_a Cos(\omega t))^2}\right]$$

Writing $\frac{Cos^2(\omega t)}{(1 + k_a Cos(\omega t))} = f_1(t)$ and $\frac{Sin^2(\omega t)}{(1 + k_a Cos(\omega t))^2} = f_2(t)$

Non-linear force can be written as

$$F_{non-linear} = \left(\frac{1}{8\pi}\right)\rho A^2\omega^2 k_a^2\left[f_1(t) + \frac{1}{2}f_2(t)\right] \quad \text{.....(23)}$$

Frequency Dependence: Characteristic of two time dependent terms f1(t) and f2(t) over the time period are independent of frequency. If we plot f1(t) or f2(t) with varying t/T, different plots will overlap. Changing frequency will just have a modulation effect. We can see from equation 23 that oscillation frequency will not affect the spread nonlinear force over the

time period. Magnitude of the non-linear force will be proportional to frequency squared term.

$$F_{non-linear} \propto \omega^2$$

A plot of nonlinear dynamic force (divided by ω^2) obtained from COMFLOW is shown below for Ka=0.75.

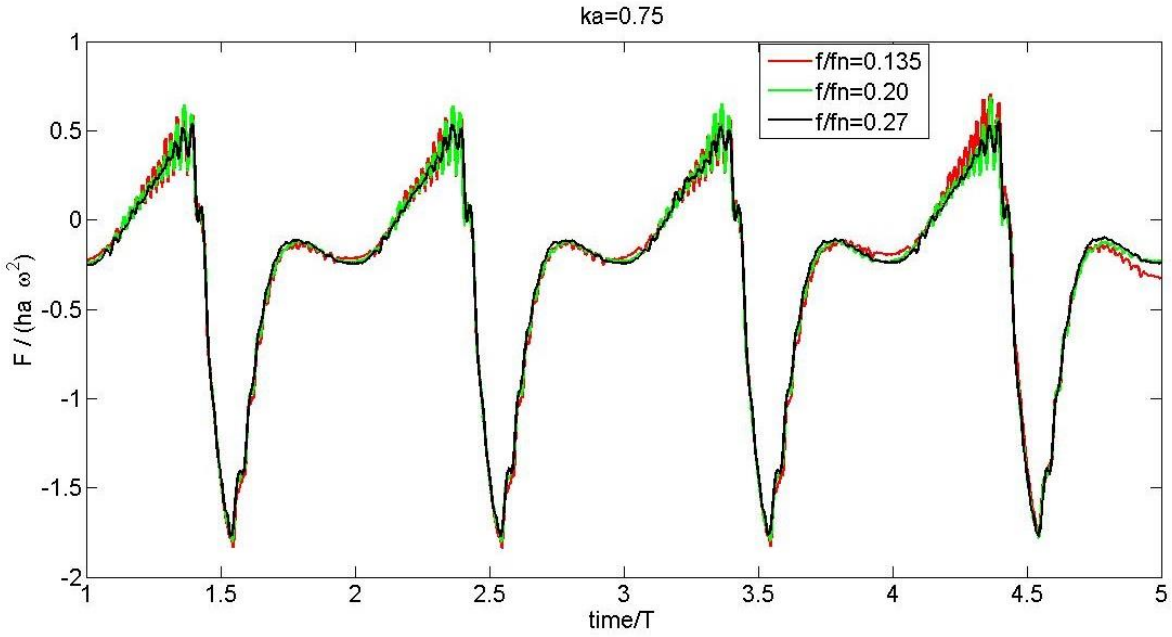

Figure 48: Frequency Dependence of Nonlinear Dynamic Force in COMFLOW

Plot above shows indeed nonlinear dynamic force are proportional to frequency squared for cases studied.

Amplitude Dependence: While first part of the equation 23 is proportional to the squared of amplitude ratio, the dependence of second part which is related to f1(t) and f2(t) is not clear as denominator of the terms f1(t) and f2(t) is not independent of oscillation ratio Ka (except in case when Ka is very small, but in that case whole non-linear dynamic term will be negligible compared to linear part as we have seen in section 3.5 that non-linear effects almost vanish in simulation at ka=0.0625 and 0.125, Appendix I).

Only conclusion on amplitude dependence can be drawn is that, it increases with increasing oscillation amplitude by a factor bigger than Ka squared, which is logical as peak values in time plot of f1(t) and f2(t) will increase when Ka is larger, as it will assume small values for denominator of f1(t) and f2(t). In the plot below Non-linear force in simulation (normalized by amplitude squared) has been plotted for three cases with differing oscillation amplitude but same frequency.

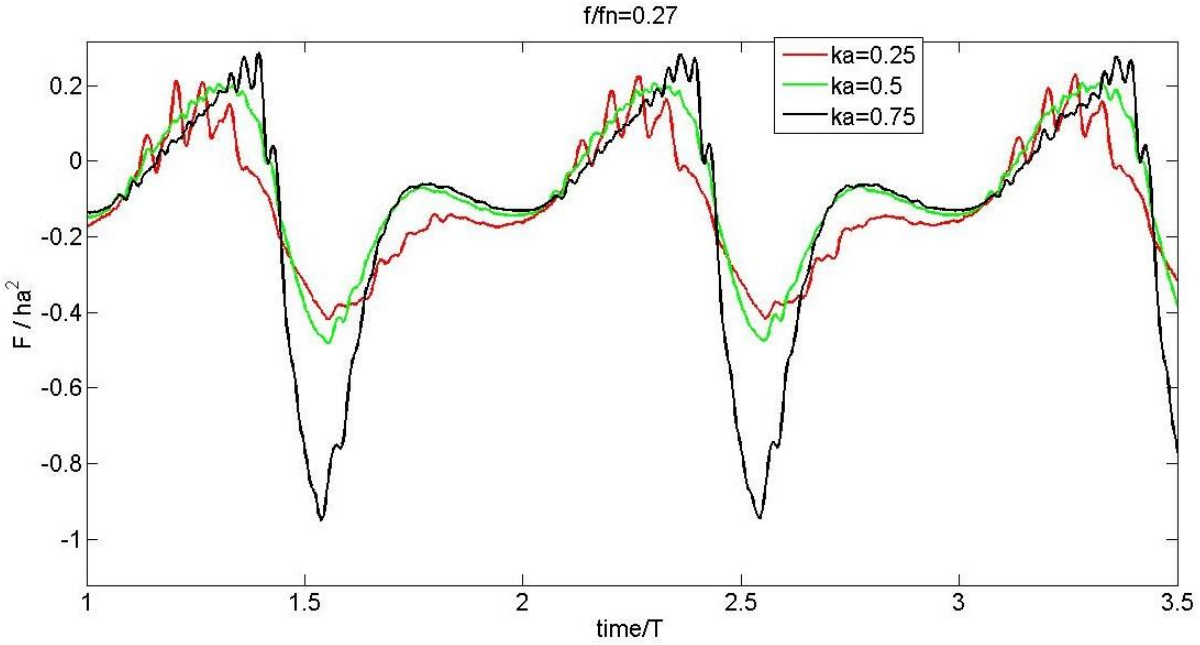

Figure 49: Amplitude Dependence of Non-linear Dynamic Force in COMFLOW

It can be seen from plot above that an increase in oscillation amplitude leads to much greater variation in dynamic forces than factor of amplitude squared. Hence increase in amplitude will normally lead to much higher increase in non-linear forces than compared to increase in frequency.

Relative Contribution of Non-linear Inertia and Lift Terms

In general the relative contribution of both terms will depend upon frequency and amplitude, however it is difficult to come up with a time invariant ratio of two terms. For that reason only relative contribution for the cases 1-9 has been studied for qualitative understanding.

Contribution of two force terms (i.e. inertia term and lift term) has been plotted below for the case 7 (Ka=0.25) and case 9 (Ka=0.75).

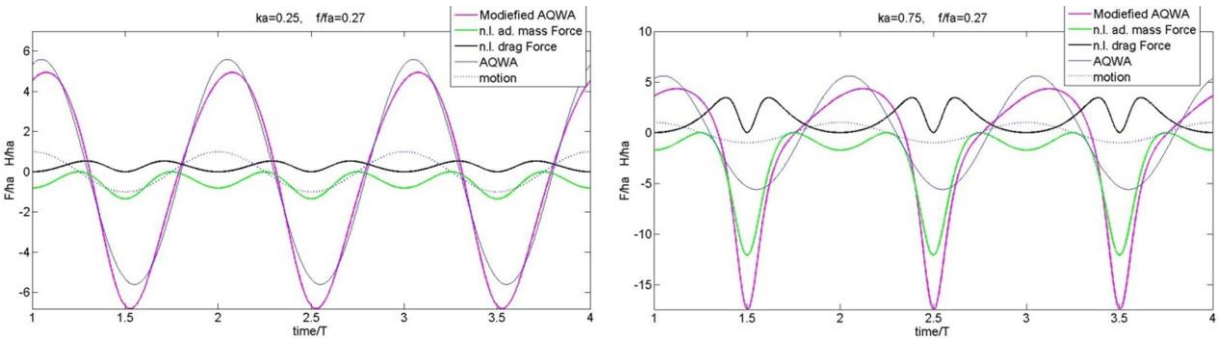

Figure 50: Relative Contribution of Non-linear Terms and Linear Term to Dynamic Force

In above plots, it can be seen that for the particular case, effect of inertia term is much more significant compared to lift term. The contribution of two terms for nine cases has been given in Appendix IV.

Weather these term add to or subtract from the the linear dynamic force calculated by AQWA will depend upon the phase of f1(t) and f2(t).

4.7 Free Surface Effect

If we move the model set up deeper and deeper then calculated dynamic forces will alter in both COMFLOW and AQWA. But from equation 21, we would expect theoretically that non-linear part should not be affected by draft. However, it has been found that free surface affects the flow inside the gap, mostly during inward flow. A comparison of COMFLOW results with increasing draft (while keeping oscillation amplitude and frequency constant) has been plotted below. In the plot draft has been normalized with gap height.

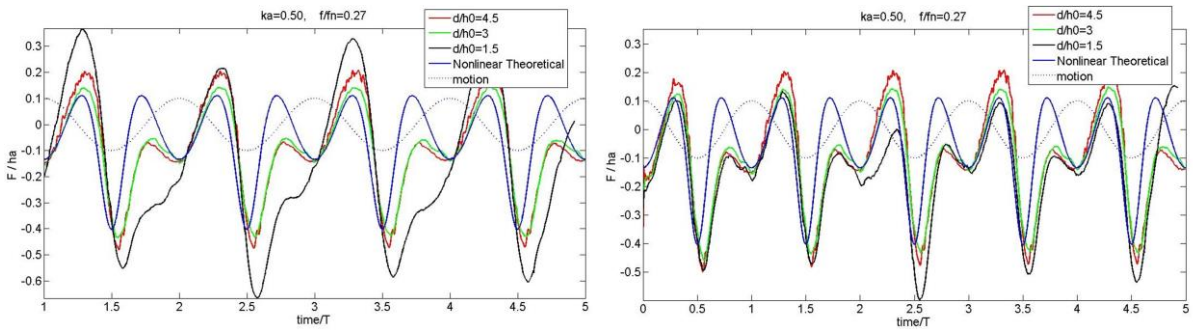

Figure 51: Free Surface Effect on Non-linear Dynamic Forces

In the first plot above it can be seen that with increase in water depth, heave force changes more during inward flow compared to outward flow. Also as water depth increases shape of the plot gets more close to symmetric result from equation 21 (asymmetry results from different flow patterns during inwards and outward flow).

In the second plot it can be seen that during oscillations very close to surface (d/h0=1.5) radiation waves (which will result from oscillation) start having influence on pressure inside gap, on a large scale, hence large oscillations in the pressure and simulated force occurs.

A comparison of velocity and pressure fields have shown that flow velocity and pressure are more closer to theoretical pressure at higher water depths.

A curve fit for simulation at d/h0 ratio of 4.5 and 3 has been found to be much more close to simulation results compared to original modified AQWA equation 22.

$$F\ (\text{Curve Fit AQWA}) = F_{AQWA} + \left(\frac{1}{8\pi}\right)\rho A^2\left(\frac{1}{h_0} - \frac{1}{h}\right)h_{tt} - \left(\frac{1}{16\pi}\right)\frac{\rho A^2}{h^2}\left|h_t\right| h_t \quad \text{.....(24)}$$

In the equation above the second nonlinear term has same value as in equation 22 during downward motion but it alters in sign during upward motion. It may be assumed that it takes care of changed flow model during inward flow.

This curve fit has been found to give very accurate result for all nine cases in table 2.

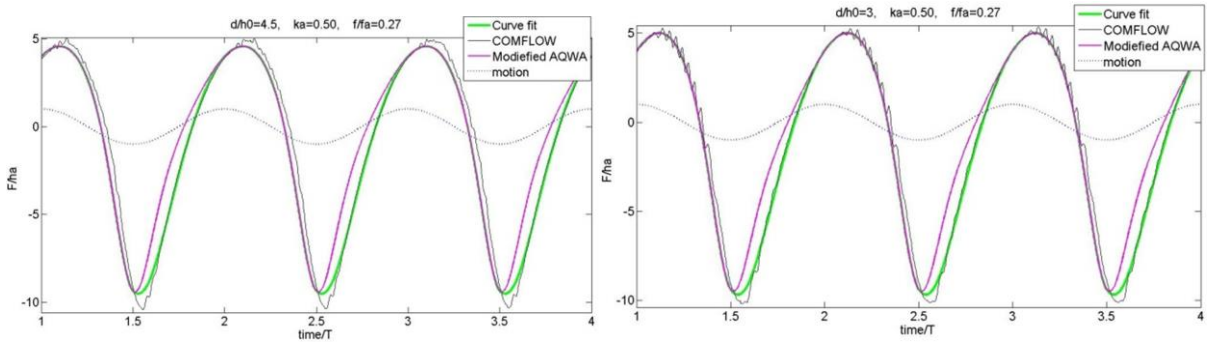

Figure 52: Comparison Curve fit with Modified AQWA

For the sake of brevity, results for other cases have not been shown in appendix, but a similar very accurate result was found for all nine experiment cases. Author has not found any logical reason to explain the fit given in equation 24.

4.8 Analytical Solution for a Long Barge

In this section we consider another simple example, for which flow can be easily modeled. A rectangular bottom barge floating with gap size h between its bottom and seabed, draft d, width 2a, and length L, further we suppose L>>a so that squeezed water comes out from sides of barge, it is assumed that there is no flow along length. For barge assume y-axis along the length, x axis along the width and z axis vertically upward. Velocity of fluid inside gap along x, y and z axis is u, v and w.

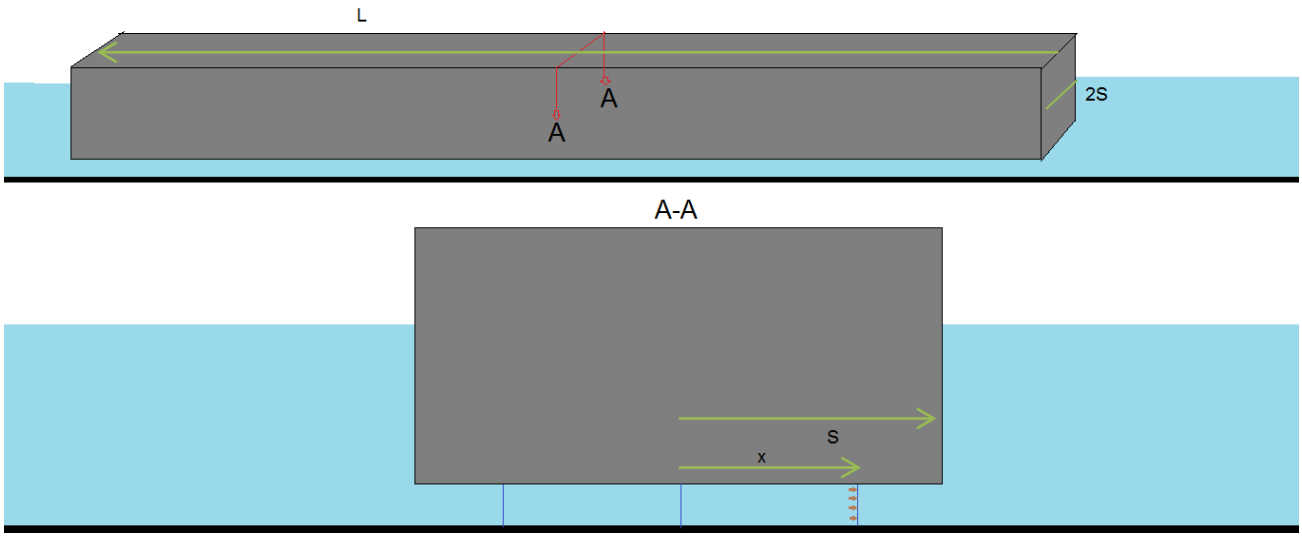

Figure 53: Long Barge Analytical Model

Applying mass conservation along the section length will give following equation for velocities along x and z direction.

$$u = -\frac{x}{h} h_t \text{.....(25)}$$

$$w = \frac{z}{h} h_t \text{.....(26)}$$

2D continuity equation in Cartesian coordinate can be written as

$$\frac{\partial u}{\partial x} + \frac{\partial w}{\partial z} = 0 \text{.....(27)}$$

The values of u and w as given in equation 25 and 26, when substituted satisfies equation 27. Hence these solutions can be substituted in Navier Stokes momentum equation for uniform flow to solve for pressure term p at each point within gap domain.

$$\rho\left(\frac{\partial u}{\partial t} + u\frac{\partial u}{\partial x} + w\frac{\partial u}{\partial z}\right) = -\frac{\partial p}{\partial x} \text{.....(28)}$$

$$\rho\left(\frac{\partial u}{\partial t} + u\frac{\partial w}{\partial x} + w\frac{\partial w}{\partial z}\right) = -\frac{\partial p}{\partial z} + \rho g \text{.....(29)}$$

Substituting u and w from equation 25 and 26 into equation 28 and 29 gives

$$\frac{\partial p}{\partial x} = -\rho\left(-\frac{x}{h} h_{tt} + \frac{x}{h^2} h_t^2\right)$$

$$\frac{\partial p}{\partial z} = -\rho\left(-\frac{z}{h}h_{tt} + \frac{z}{h^2}h_t^2 - g\right)$$

Since p is a function of z and x,

$$dp = \frac{\partial p}{\partial x}dx + \frac{\partial p}{\partial z}dz$$

$$dp = -\rho\left(-\frac{h_{tt}}{h} + \frac{x}{h^2}h_t^2\right)dx - \rho\left(-\frac{h_{tt}}{h} + \frac{z}{h^2}h_t^2 - g\right)dz \quad \text{.....(30)}$$

If we denote pressure at edge at height h as $p_{e,a,h}$ and pressure at height z and distance x from center as $p_{x,z}$. Then integrating above equation from distance a to x from center and height h to z will give following

$$\int_{p_{e,a,h}}^{p_{x,z}} dp = -\rho\left(-\frac{h_{tt}}{h} + \frac{h_t^2}{h^2}\right)\int_a^x xdx - \rho\left(-\frac{h_{tt}}{h} + \frac{h_t^2}{h^2}\right)\int_h^z zdz + \rho g\int_h^z dz$$

$$p_{x,z} = p_{e,a,h} - \rho\left(-\frac{h_{tt}}{h} + \frac{h_t^2}{h^2}\right)\left(\frac{x^2 - a^2}{2}\right) - \rho\left(-\frac{h_{tt}}{h} + \frac{h_t^2}{h^2}\right)\left(\frac{z^2 - h^2}{2}\right) + \rho g(z - h)$$

I II III IV

In above equation, first and fourth term on right hand side are hydrostatic pressure terms, while second and third term contribute to dynamic pressure. If $h << a$, then relative effect of third term on total pressure will be insignificant in comparison to second and fourth term and can be disregarded.

$$\rho\left(-\frac{h_{tt}}{h} + \frac{h_t^2}{h^2}\right)\left(\frac{x^2 - a^2}{2}\right) >> \rho\left(-\frac{h_{tt}}{h} + \frac{h_t^2}{h^2}\right)\left(\frac{z^2 - h^2}{2}\right)$$

Change in pressure in fluid with varying z (0<z<h), can be neglected. Now onwards pressure variation will be assumed hydrostatic between two vertical points.

$$p_{x,z} = \left[p_{e,a,h} + \rho g(z - h)\right] - \rho\left(-\frac{h_{tt}}{h} + \frac{h_t^2}{h^2}\right)\left(\frac{x^2 - a^2}{2}\right)$$

We need pressure at z=h, in order to find force acting on barge bottom.

$$p_{x,h} = p_{e,a,h} - \rho\left(-\frac{h_{tt}}{h} + \frac{h_t^2}{h^2}\right)\left(\frac{x^2 - a^2}{2}\right)$$

For sake of reducing write up henceforth $p_{x,h}$ will be referred as p and $p_{e,a,h}$ will be referred as p_e in this section,

$$p = p_e - \rho\left(-\frac{h_{tt}}{h} + \frac{h_t^2}{h^2}\right)\left(\frac{x^2 - a^2}{2}\right) \quad \text{.....(31)}$$

Above equation has same format as pressure equation for 2D flat plate derived by Brenen [2].

Integrating above equation will give expression for the force on bottom of barge.

$$F = 2\,p_e aL - \frac{2\rho a^3 L}{3h}\,h_{tt} + \frac{4\rho a^3 L}{3h^2}\left(h_t\right)^2$$

$$F = p_e A - \left(\frac{A}{12\,L^2}\right)\frac{\rho A^2}{h}\,h_{tt} + \frac{\rho A^2}{h^2}\left(\frac{A}{6L^2}\right)h_t^2 \quad \text{.....(32)}$$

Total dynamic force after removing static force and statically varying force from above expression can be written as

$$F(\text{total dynamic}) = (p_e - \rho gd + \rho gH)A - \left(\frac{A}{12\,L^2}\right)\frac{\rho A^2}{h}\,h_{tt} + \frac{\rho A^2}{h^2}\left(\frac{A}{6L^2}\right)h_t^2 \quad \text{.....(33)}$$

Here $\frac{A}{L^2}$ is dimensionless quantity, depending on length to width ratio of barge.

4.9 Comparison of Barge Force Derivation with COMFLOW

A comparison of dynamic force calculated on long barge using equation 33, with COMFLOW simulation, was done for the Length (L) to width (2a) ratio of 2,5 and 10.
In equation 33, pressure P_e was taken from COMFLOW simulation. Results shown in figure 54 shows that, equation 33 accurately predicts the dynamic forces due to flow inside gap.

In similar approach as in case of cylinder, dynamic force on Barge can be determined by by modifying AQWA results using following expression below.

$$F(\text{modf AQWA}) = F_{AQWA} - \left(\frac{A}{12\,L^2}\right)\rho A^2\left(\frac{1}{h_0} - \frac{1}{h}\right)h_{tt} + \left(\frac{A}{6L^2}\right)\frac{\rho A^2}{h^2}\,h_t^2 \quad \text{.....(34)}$$

Plot below is shows a comparison between COMFLOW and equation 34, for case with length to width ratio of 5.

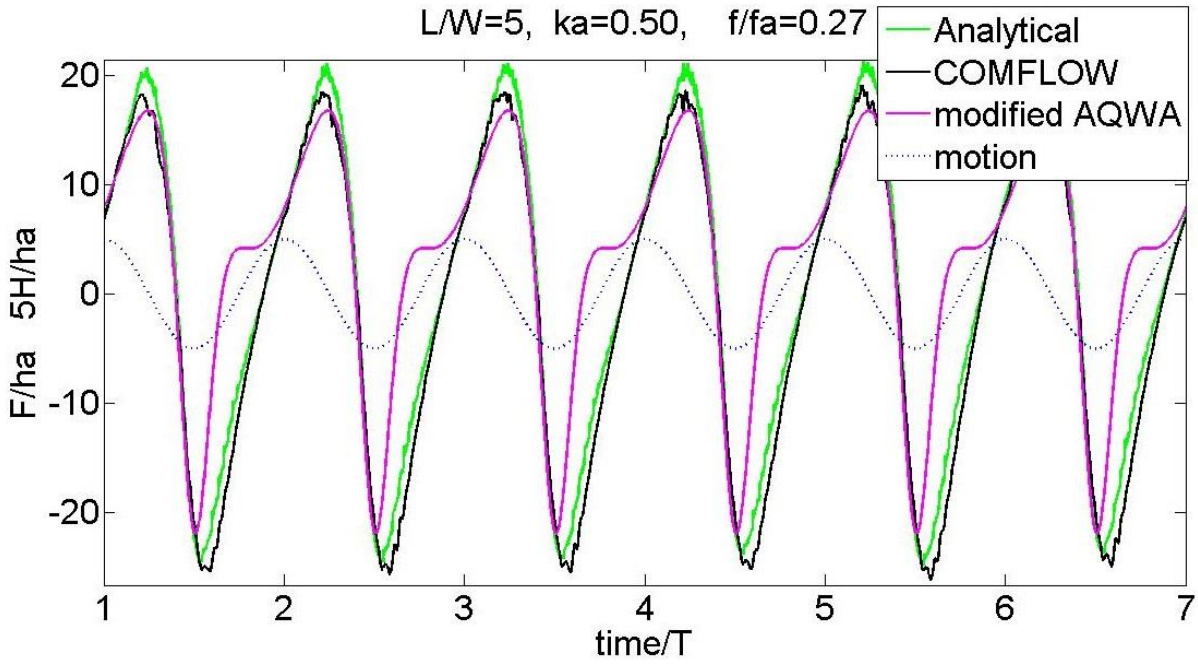

Figure 54: Barge Analytical Force Comparison with COMFLOW Force

In above figure we can see some difference in shape between analytical force represented by equation 33 and modified AQWA force in equation 34 (peaks don't differ much), reason being that analytical force in equation 33 takes into account the non-linear force due to flow inside the gap domain and outer domain both (Ap_e has nonlinear part as it is obtained from COMFLOW), while in modified AQWA only non-linear dynamic force due to gap has been accounted.

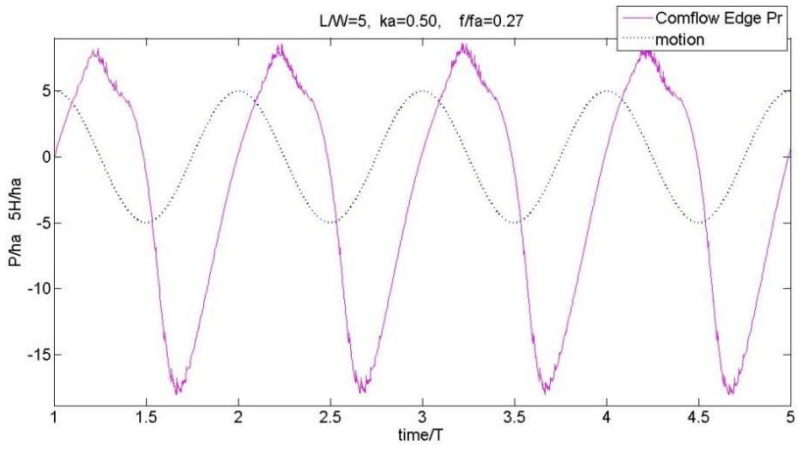

Figure 55: Non-linear Edge pressure at Barge Bottom Edge

It can be seen from plot in figure 55 that, unlike case of cylinder the term Ap_e is not linear, as edge pressure has not been found to be linear. However, it is possible to find a curve fit in the same form as given in equation 24, in case of cylinder before.

$$F(\text{Curve fit AQWA}) = F_{AQWA} - \left(\frac{A}{12\,L^2}\right)\rho A^2\left(\frac{1}{h_0} - \frac{1}{h}\right)h_{tt} - \left(\frac{A}{6L^2}\right)\frac{\rho A^2}{h^2}\left|h_t\right|h_t \quad \text{.....(35)}$$

A comparison of above curve fit equation with COMFLOW force and modified AQWA force (equation 34) has been shown in plot below.

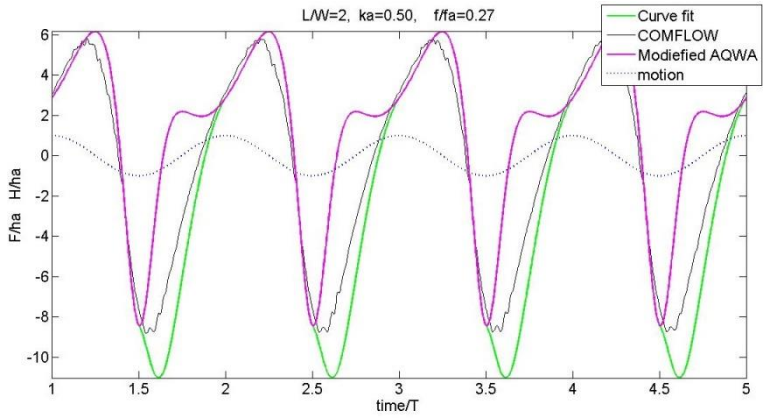

Figure 56: Comparison Curve fit with original modified AQWA, for Barge

Figure above shows that curve fit equation 35 gives a better estimate of the dynamic forces simulated.

A comparison for various L/W ratios has been shown appendix V. It seems that equation 35 above is able to account for non-linear dynamic forces due to flow in outer domain (in vicinity of gap) and different flow pattern inside the gap during upward motion.

5 General Solution and Applicability

We saw in previous chapter that by considering uniform flow in the gap, non-linear dynamic force due to gap can be modeled in the same form of equation for the cylinder and barge. From previous sections 4.5 and 4.8 (equation 22 and 33 respectively), it can be seen that dynamic force on cylindrical and rectangular barge have same form of coefficients of term h_{tt} and term h_t^2. That inspires us to seek total non-linear force for a random bottom surface model in the same form as equations for dynamic force on cylinder and barge have.

To model the dynamic force on a model with a general flat bottom area profile (square, triangle etc.), with area A, lateral dimension L, oscillating close to seabed about gap height h_0, (h_0 <<L), equation for total dynamic force can be written in the following form

$$F = F_{AQWA} - s_1 \rho A^2 \left(\frac{1}{h_0} - \frac{1}{h} \right) h_{tt} + s_2 \frac{\rho A^2}{h^2} h_t^2 \quad \text{.....(36)}$$

Here s_1 and s_2 are shape factors dependent on the shape of model bottom (i.e. rectangular, triangular etc). In case of cylindrical model substitution gives s_1 = 0.039, s_2 = 0.02.

To verify if equation 36 holds for an arbitrary bottom area profile, COMFLOW simulation was conducted with models of triangular and square bottom profile with same area as that of cylinder, oscillating at frequencies and amplitude ratios given in table 2. And coefficients were found using least square method curve fit.

5.1 Square model

In order to check applicability of equation 36 with square model, model of same area as cylinder was simulated in COMFLOW. For curve fit to find s_1 and s_2 the six cases with Ka=0.5, 0.75 and frequency ratios 0.135, 0.20, 0.27 were taken. Reason behind avoiding Ka=0.25 is that, at small oscillation amplitudes non-linear part dynamic forces are very small compared to linear part, it might lead to inaccuracy in estimation. When the dynamic force obtained from simulation was fitted on equation 36, following plot below was obtained for values of s1 and s2 for six cases.

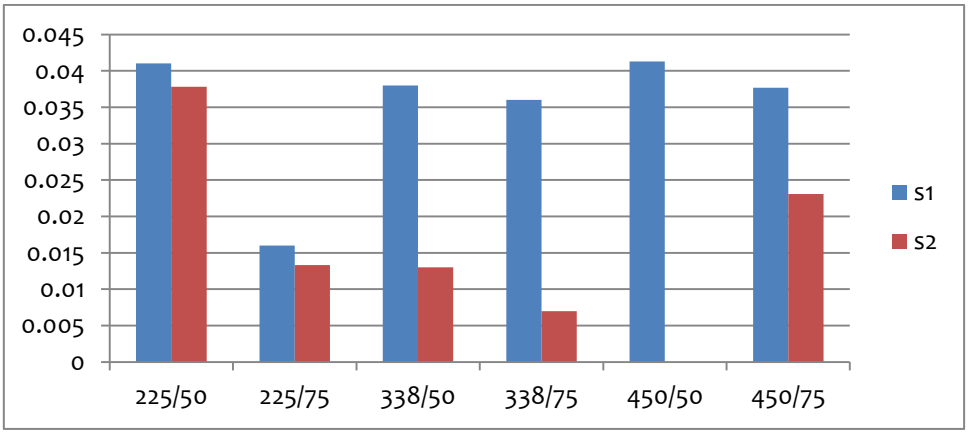

Figure 57: s1 and s2, Square Shape Factors Obtained by Curve Fitting of Simulation Results

In above plot, the mean value of s1 is 0.035, and that of s2 is 0.016. A large variance in s2 results from low significance of lift term in this case.

Expression for modifying AQWA results to include non-linear effect for vertical force on a model with square bottom area can be written as

$$F = F_{AQWA} - 0.035\,\rho A^2\left(\frac{1}{h_0} - \frac{1}{h}\right)h_{tt} + 0.016\,\frac{\rho A^2}{h^2}\,h_t^2 \qquad \text{.....(37)}$$

A comparison between modified AQWA result and COMFLOW result for square for case 8 has been shown below.

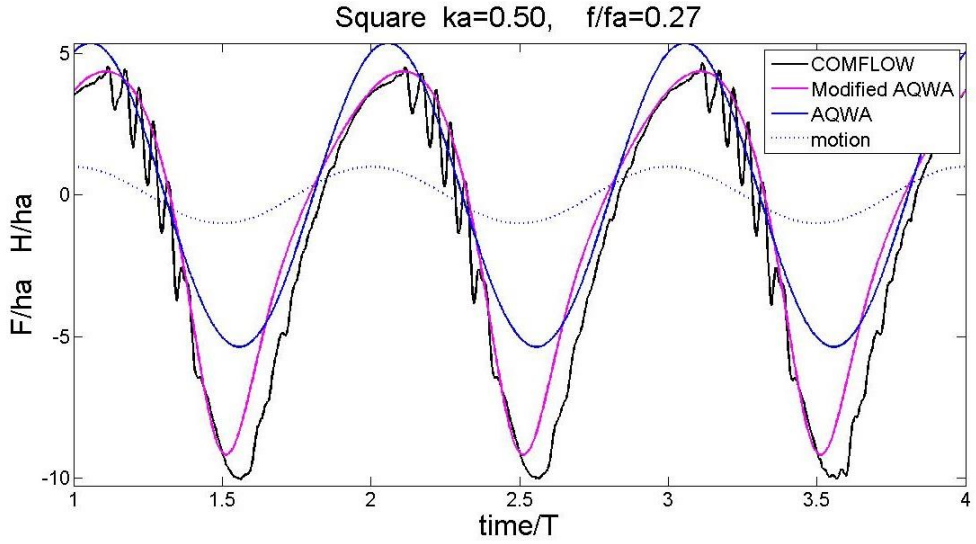

Figure 58: Comparison of Modified AQWA Expression Found by Curve fit With COMFLOW

A comparison of dynamic forces obtained from equation 37 and those from simulation for nine cases has been given in Appendix VI. Overall results show equation 37 holds good for all nine cases presented.

5.2 Triangular Model

In order to check applicability of equation 33 with triangular bottom model, model of same area as cylinder was simulated in COMFLOW, for the six cases with Ka=0.5, 0.75 and frequency ratios 0.135, 0.20, 0.27. Plot below shows the values of s1 and s2 obtained.

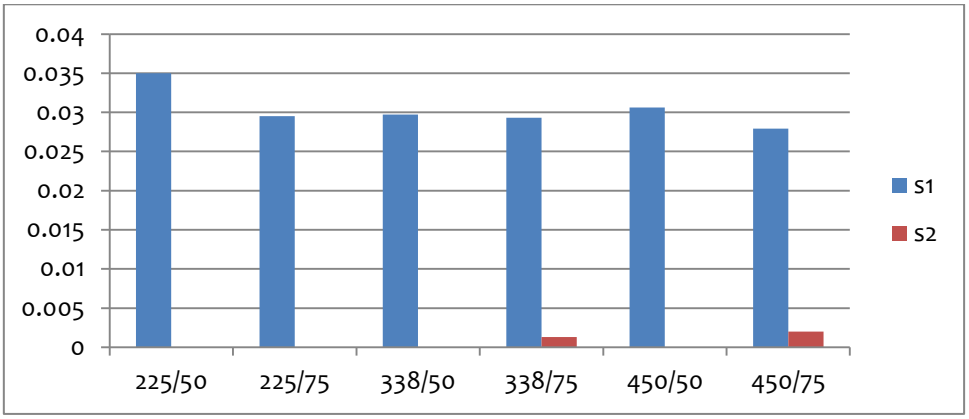

Figure 59: s1 and s2, Triangle Shape Factors Obtained by Curve Fitting of Simulation Results

In above plot, the mean value of s1 is 0.03, and that of s2 is 0.001. The very small value of s2 is due to the fact that for a triangular model, all parts in the gap domain will be much closer to the edges, so small velocities develop before water flows out of the gap, hence relatively smaller dynamic effects will incur due to velocity squared term.

Expression for modifying AQWA results to include non-linear effect for vertical force on a model with bottom area profile of equilateral triangle can be written as

$$F = F_{Aqwa} - 0.03 \frac{\rho A^2}{h} h_{tt} + 0.001 \frac{\rho A^2}{h^2} h_t^2 \quad \text{.....(38)}$$

A comparison between modified AQWA result and COMFLOW result for triangle for case 8 has been shown below.

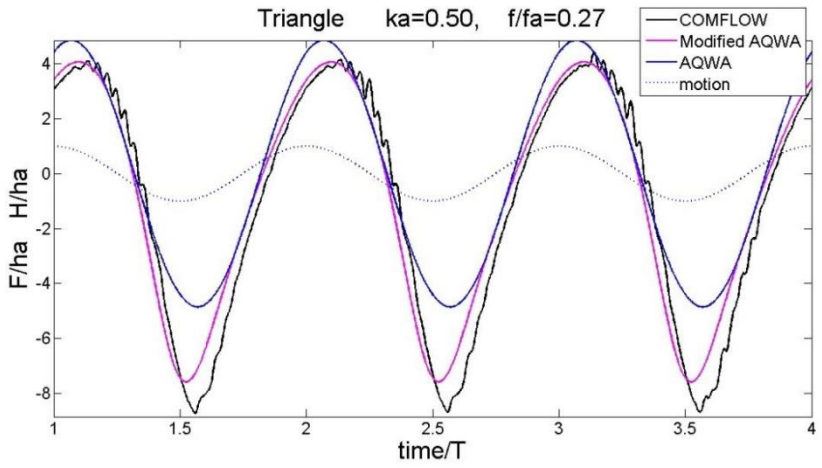

Figure 60: Comparison of Modiefied AQWA Expression Found by Curve fit With COMFLOW

We can see from the plot above that equation 38 gives good estimate for total dynamic forces on triangular bottom model.

A comparison of dynamic forces obtained from equation 38 and those from simulation for nine cases in table 2, has been given in Appendix VII. Overall results show equation 38 holds good for all nine cases presented.

5.3 Applicability of modified AQWA Dynamic Force Equations

Using COMFLOW simulations, it was found that modified AQWA expression derived for cylinder also gives good result with increasing gap sizes, decreasing area of bottom, decreasing oscillation amplitudes as can be seen in plots for Ka=0.125 and 0.625 also. When the gap size is increased, coefficients of terms h_{tt} and h_t^2, get closer to zero as they are inversely proportional to h and h squared respectively. Hence non-linear part of equation 22 tends to become negligible.

While deriving equation for modified AQWA in previous chapter for cylinder and barge, no wave was considered. Equation 32 can be applied to conditions in which waves are present and simulated by AQWA, if surface waves don't influence much the flow inside the gap.

Modified AQWA models are based on the uniform flow inside the gap; hence it may not be valid at very high Reynolds number when flow becomes turbulent inside the gap or the cases in which effect of boundary layer becomes important. It needs to be noted that all the verification with pressure and force equations in present work was done with Euler simulations in COMFLOW (inviscid flow) and turbulence modelling was switched off (it had very small effect for cases studied).

5.4 Why AQWA fails?

It was explained in Chapter 4 that non-linear force have inertia and lift parts. Inertia part of non-linear force results from very high accelerations in the gap, when body is oscillating close to seabed and relative movement of cylinder bottom wrt gap size (variable h in denominator in equation 16 and 22) is high.

Potential software assumes very small movement of source panels relative to distance from seabed, which are considered being far away. To linearize equations, time variation of source strength is neglected. Because of this software is not able to calculate nonlinear part of inertia force when body oscillates close to seabed. ‘

$$\Phi(x, y, z, t) = \phi(x, y, z)\, e^{-i\omega t}$$

$$\phi(x, y, z, t) = \frac{1}{4\pi} \iint_{S_0} \sigma_3(\hat{x}, \hat{y}, \hat{z}).\, G(x, y, z, \hat{x}, \hat{y}, \hat{z})\, dS_0$$

Lift nonlinear forces can’t be calculated if potential software doesn’t account for force induced by velocity. Potential software assumes that velocity terms in the equation below are negligible.

$$p = -\frac{d\phi}{dt} + \rho(u^2 + v^2 + w^2) - \rho\, gh$$

But when the body is oscillating close to seabed, the horizontal velocity is appreciably high, so assumption of negligible velocity effect is not true.

A comparison of Molin result and result obtained in present work is ill advised, as Molins result were derived for a circular disk not cylinder and dynamic effects due to flow in outer domain was not considered in derivation (in Molin derivation $\Delta\phi = 0$ for outer domain).

6 Summary

To optimize float-on/off operation from Dockwise Vanguard, knowledge of vertical hydrodynamic force during separation (when bottom of cargo is very close to deck of Vanguard) is necessary. To check whether linear potential software can be used to determine dynamic forces during separation, Dockwise conducted experiment on a simplified problem of a cylindrical model oscillating close to seabed. Results have shown that the vertical hydrodynamic force acting on bottom have non-linear components which are not captured by linear potential software.

To understand the flow behaviour inside gap and outer domain, model in experiment was simulated in COMFLOW. COMFLOW results have been found to be very close to experiment results. Since experiment result has been available only for limited cases and since it was suspected that experiment results might have some higher frequency components due set up vibrations, for the further analysis, COMFLOW results were used.

A comparison of COMFLOW results with AQWA results have shown that it can calculate linear part of the force observed, not the non-linear part. COMFLOW simulations have shown that viscosity has little effect on the simulated forces. It was observed that flow inside the gap domain in outward direction is close to uniform flow. While inward flow differs from outward flow and is less uniform across the vertical. From observation of vorticity colour maps in COMFLOW it was found that flow separation occurs at the inlet of gap domain when flow is inward direction and there is formation vortices at the entrance which seem to obstruct the inward flow.

Non-linearity in dynamic force can be due to flow inside the gap domain and flow outside outer domain both. The flow in outer domain contributes to dynamic forces on the bottom of cylinder through the boundary between gap domain and outer domain. For the case of cylinder it was found that edge pressures at the boundary between two domains are almost linear and flow outside domain doesn't contribute to non-linear part of dynamic force.

Non-linear part of dynamic force due to flow inside gap between cylinder bottom and seabed can be modelled by considering uniform flow inside the gap, which when added to linear force obtained from AQWA, gives a good approximation of total dynamic forces.

Applying mass and momentum conservation for uniform flow inside gap, a general equation for pressure in gap domain of cylinder can be written as

$$p = p_e + \left[\frac{\rho}{2h} h_{tt} - \frac{\rho}{4h^2} h_t^2\right]\left(\frac{r^2 - R^2}{2}\right)$$

A general equation for vertical dynamic force on cylinder bottom can be written as

$$F = F_{AQWA} + \left(\frac{1}{8\pi}\right)\rho A^2 \left(\frac{1}{h_0} - \frac{1}{h}\right) h_{tt} + \left(\frac{1}{16\pi}\right)\frac{\rho A^2}{h^2} h_t^2$$

When compared with COMFLOW force, above modiefied AQWA expression gives very good estimate of dynamic forces.

Second term on right hand side in above force equation with h_{tt} tells that small gap size leads to non-linear inertia forces and third term is lift force acting on cylinder bottom due to high velocities which develop when cylinder oscillates close to gap, this force acts always in upwards dircetion. Inertia term has same phase as motion and hence assumes highest value when model is closest to seabed. It has been found that contribution of inertia term is much higher than lift term for the cases studied.

Similar to dynamic force expression for cylinder an expression for pressure and dynamic force due to flow inside gap can be analytically found for a barge model with rectangular bottom oscillating close to seabed.

$$p = p_e - \rho\left(-\frac{h_{tt}}{h} + \frac{h_t^2}{h^2}\right)\left(\frac{x^2 - a^2}{2}\right)$$

$$F(\text{modf AQWA}) = F_{AQWA} - \left(\frac{A}{12L^2}\right)\rho A^2 \left(\frac{1}{h_0} - \frac{1}{h}\right) h_{tt} + \left(\frac{A}{6L^2}\right)\frac{\rho A^2}{h^2} h_t^2$$

However in case of barge, it is observed from COMFLOW simulation that pressure at the boundary are not linear. Pressure equation above tells that flow inside gap doesnot contribute to non-linearity in pressure at the gap (x=a), so any non-linearity must come from flow in the outer domain.

A modified (essentially a curve fit) expression for vertical dynamic forces given below has been found to be a better fit.

$$F(\text{Curve fit AQWA}) = F_{AQWA} - \left(\frac{A}{12L^2}\right)\rho A^2 \left(\frac{1}{h_0} - \frac{1}{h}\right) h_{tt} - \left(\frac{A}{6L^2}\right)\frac{\rho A^2}{h^2} |h_t| h_t$$

For a random bottom area profile of a model, it is difficult to derive equations, we can assume that flow patterns inside gap will be similar to that in case with cylinder and barge. This inspires to seek vertical force on a cylinder in following form

$$F = F_{AQWA} - s_1 \rho A^2 \left(\frac{1}{h_0} - \frac{1}{h} \right) h_{tt} + s_2 \frac{\rho A^2}{h^2} h_t^2$$

Where s1 and s2 are shape factors. A curve fit of above equation for triangle and square with vertical forces obtained from COMFLOW simulation has given following curve fit.

$$F(\text{Square}) = F_{AQWA} - 0.035 \rho A^2 \left(\frac{1}{h_0} - \frac{1}{h} \right) h_{tt} + 0.016 \frac{\rho A^2}{h^2} h_t^2$$

$$F(\text{Triangle}) = F_{Aqwa} - 0.03 \frac{\rho A^2}{h} h_{tt} + 0.001 \frac{\rho A^2}{h^2} h_t^2$$

Non-linear forces acting on a model in the vicinity of seabed result (1) from increased inertia inside gap domain and inside outer domain in the vicinity of gap domain; (2) Increased velocities inside gap domain and inside outer domain in the vicinity of gap domain. Non-linear forces can be calculated by numerical scheme which takes into account the time variation of source panel strength and lift force due to velocities developed.

Objective of present work was to find a method to adapt linear potential software results to obtain vertical dynamic forces acting on a flat bottom model oscillating close to seabed, and this objective has been achieved.

7 Recommendation and Future Investigation

Recommendation for HMT Industry

The derivation for vertical dynamic force on a flat bottom of a model has been found to be showing satisfactory result for simple cases like triangular and square shape bottom models in ideal conditions when boundary of the domain was kept far away. To extend it for industrial use, following effects will need to be investigated.

Applicability for an irregular and non-flat bottom Structure

Real structure will not have a regular bottom profile like the models studied in present work. To determine vertical dynamic forces on a real structure, it should be verified that to what extent the expressions for modifying AQWA results can be used.

HTV Cargo Interaction

During float on-off operation there will be motion of HTV and cargo both, but equation were derived in present work only for flat bottom model oscillating close to static seabed and boundary of domain was far away. It needs to be checked if it can be extended to real float-on/off operation situations in which Cargo structure and HTV both will be moving and there will be several boundaries and flow domains in vicinity of gap. Motion in real situation will not be sinusoidal vertical; there will be a degree of roll pitch and other motions.

Effect of Waves

Effect of waves was not considered during derivations, in real operation there will be waves affecting the physical environment and cargo HTV interaction. To check effect of waves, model tests or CFD simulations can be conducted on a two body model (modelling HTV and Cargo) under different wave conditions and it can be checked whether modified AQWA results can still be used.

Some Topics for Future Work

Using edge pressures to predict vertical forces on a random bottom area model oscillating close to seabed:

One way of deriving vertical dynamic forces on a flat bottom structure is to calculate force due to outer domain in the form of edge pressure integrated over area and add dynamic force due to gap (both linear and nonlinear) which can be modelled considering uniform flow inside the gap.

Method has worked for cylinder and barge models but can be investigated further, so as to seek force on flat bottom of a body in following form below.

$$F = Ap_e - s_1 \frac{\rho A^2}{h} h_{tt} + s_2 \frac{\rho A^2}{h^2} h_t^2$$

It is difficult to define edge pressure for an irregular flat bottom profile as pressures will be different at various points along the edge in that case. Pressure Pe should be obtainable from linear potential software.

Investigating model for horizontal fluid boundary interaction:

The main difference between vertical force due to vicinity with a horizontal boundary and horizontal dynamic force on a vertical wall is expected to be effect of gravity on flow inside gap and free surface effect.

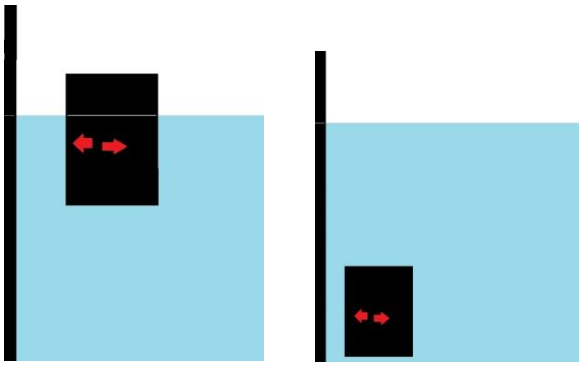

The problem of horizontal boundary has similarity with several applications in shipping and offshore industry, for example in predicting interactive forces between FPSO and shuttle tanker during side by side loading, forces on a vessel in a narrow channel.

Appendix I: Cylinder Dynamic Forces

In the plots below show a comparison of dynamic force in (1) experiment (2) COMFLOW and (3) AQWA.

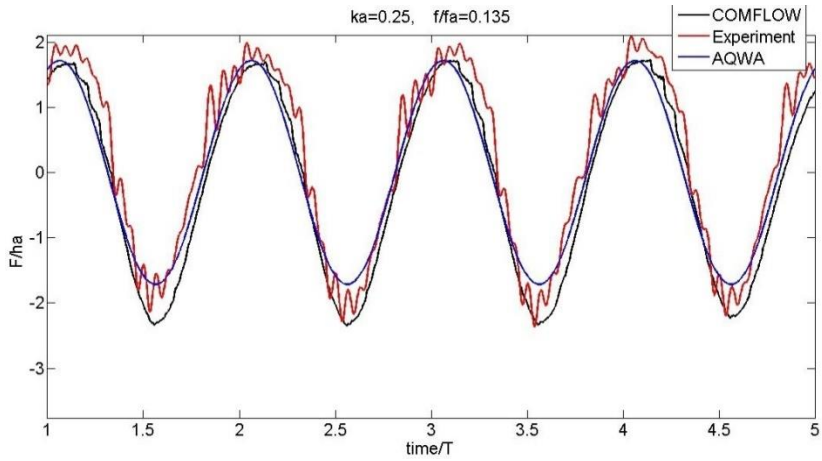

Figure 61: Case 1, Cylinder

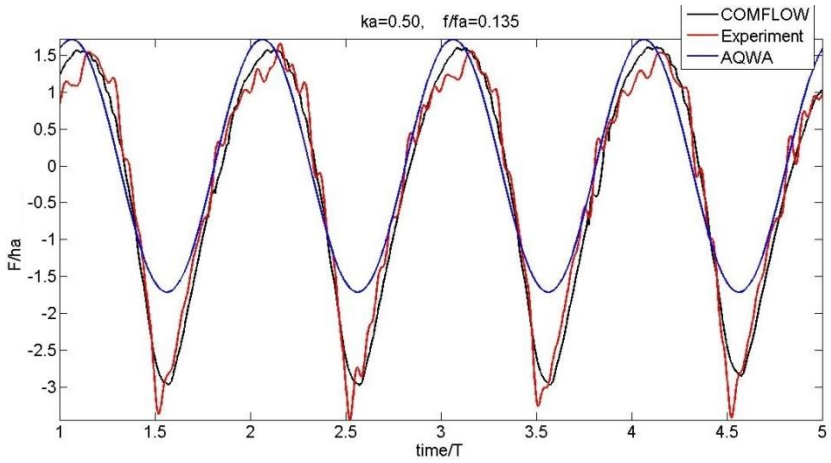

Figure 62: Case 2, Cylinder

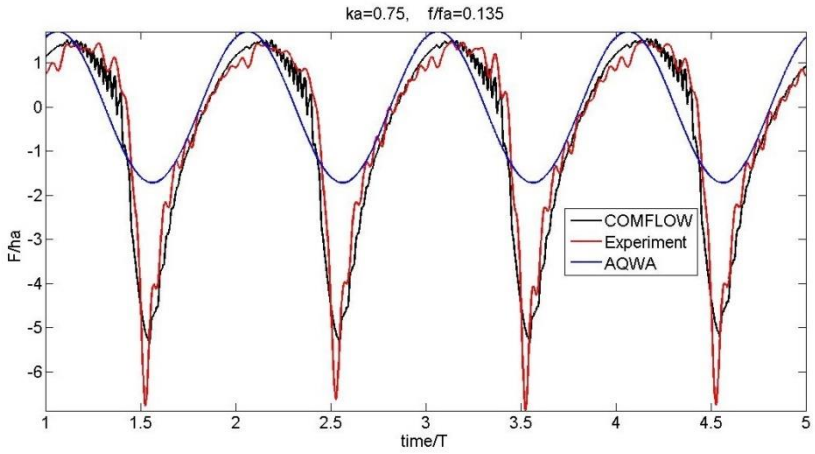

Figure 63: Case 3, Cylinder

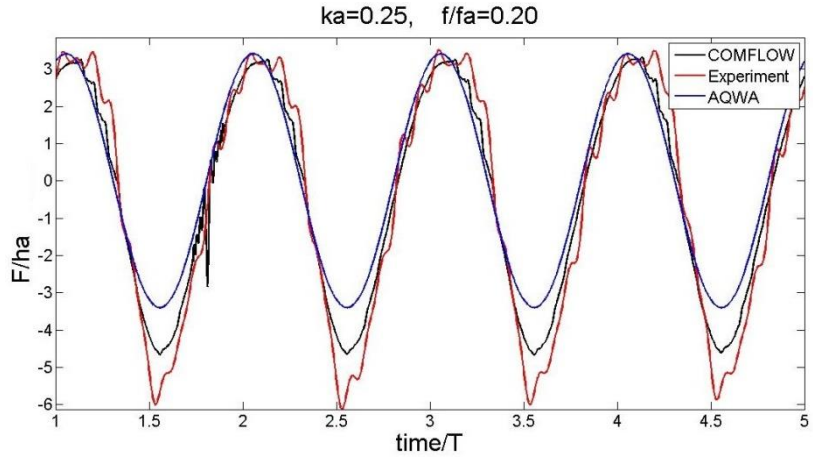

Figure 64: Case 4, Cylinder

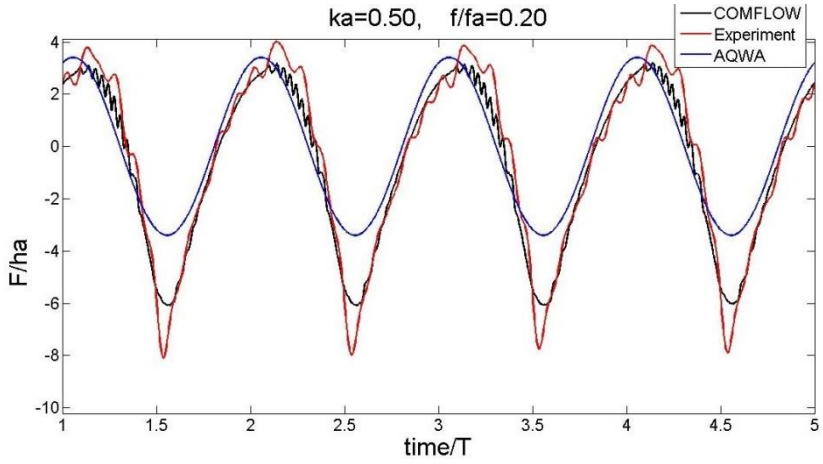

Figure 65: Case 5, Cylinder

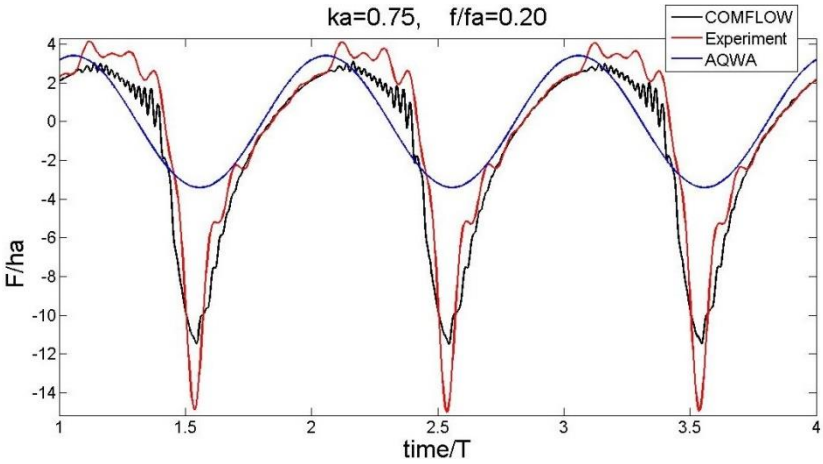

Figure 66: Case 6, Cylinder

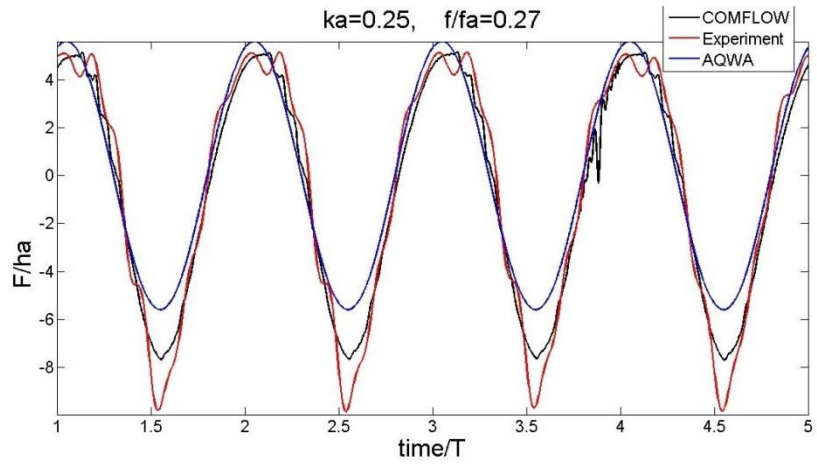

Figure 67: Case 7, Cylinder

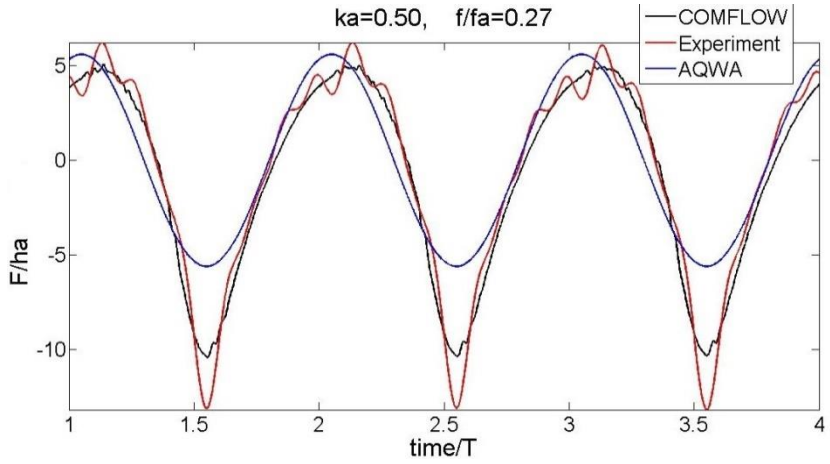

Figure 68: Case 8, Cylinder

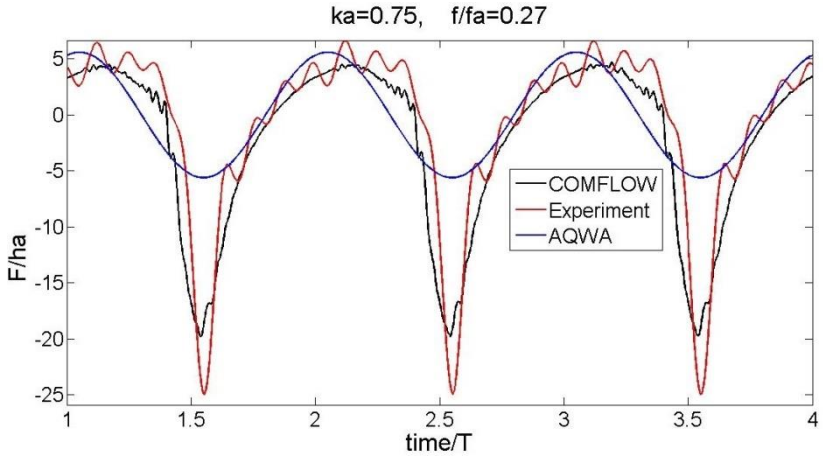

Figure 69: Case 9, Cylinder

At very small oscillation amplitude 1/8 and 1/16 of gap size, five cases were simulated to verify that non-linear dynamic force is not important at small oscillation amplitudes.

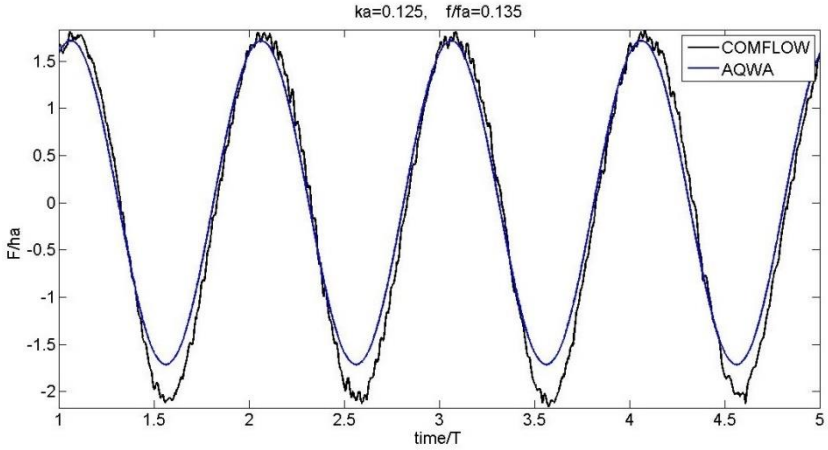

Figure 70: Comparison AQWA and COMFLOW at Small Amplitude

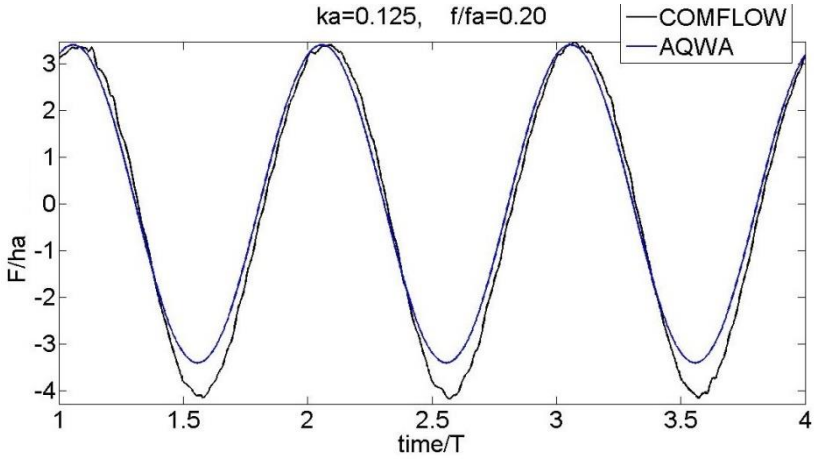

Figure 71: Comparison AQWA and COMFLOW at Small Amplitude

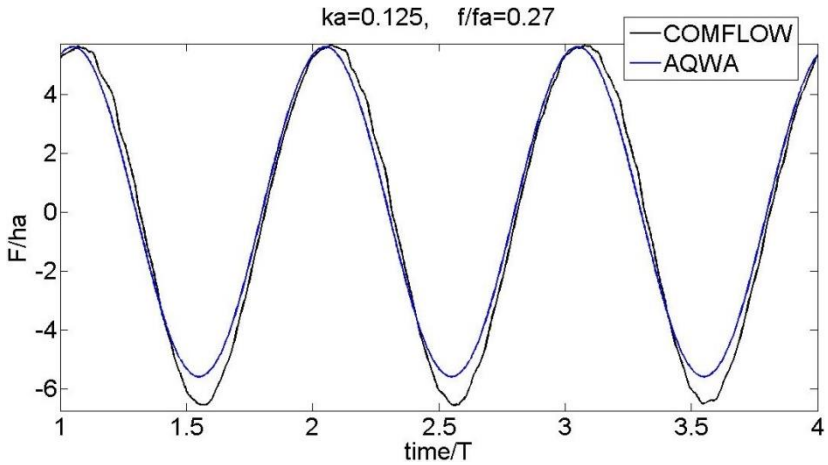

Figure 72: Comparison AQWA and COMFLOW at Small Amplitude

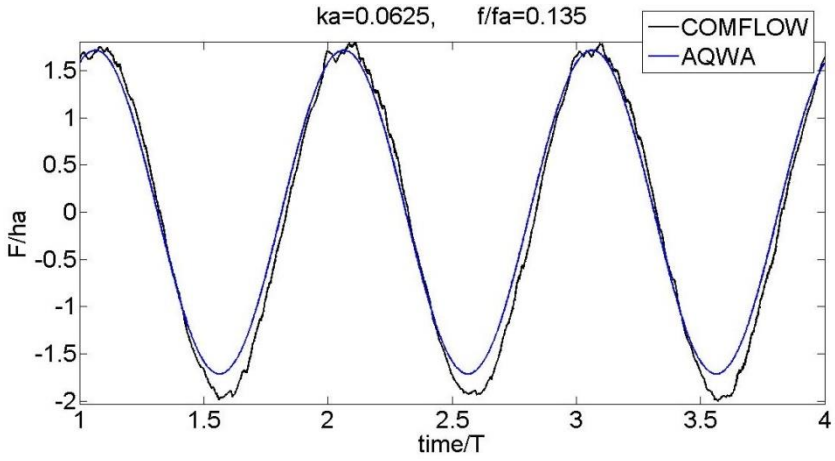

Figure 73: Comparison AQWA and COMFLOW at Small Amplitude

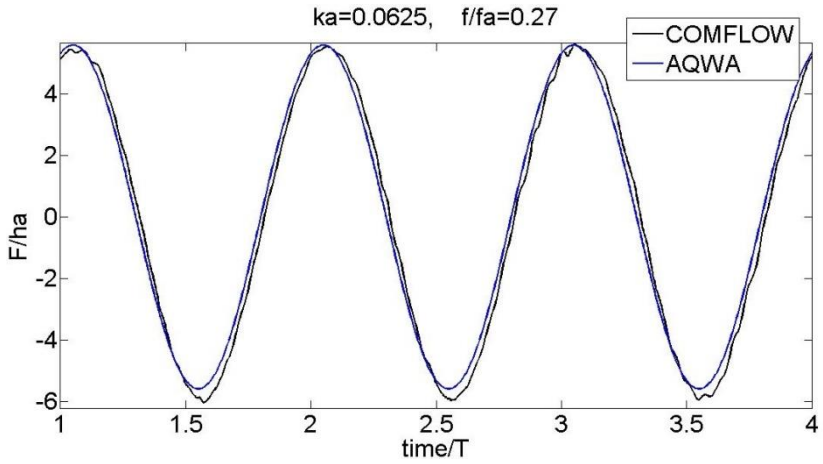

Figure 74: Comparison AQWA and COMFLOW at Small Amplitude

Appendix II: COMFLOW Input

COMFLOW inputs for case 8 described in section 3.2.

```
------------------------------------------------------------------------
-
slosh   movbdy  twph  nproc
1       2       0     4
------------------------------------------------------------------------
-
-- domain definition ---------------------------------------------------
-
xmin    xmax   ymin    ymax    zmin    zmax
0       10     0       10     -0.11     0.05
------------------------------------------------------------------------
-
-- green water parameters ----------------------------------------------
-
grnwtr
0
------------------------------------------------------------------------
-
high    low     length
0.0     0.0     0.0
------------------------------------------------------------------------
-
width   a       b
0.0     0.0     0.0
------------------------------------------------------------------------
-
-- definition initial liquid configuration -----------------------------
-
liqcnf lqxmin  lqxmax  lqymin  lqymax  lqzmin  lqzmax
2      -20    20     -20    20     -0.19     0.0
------------------------------------------------------------------------
-
-- definition of incoming wave -----------------------------------------
-
wave  wvstart  period   wheight  xcrest  waterd  ramp*  order  curr
beta
0     0        0    0       0.0     10.0    0      10     0.0  0.0
ramp  val1  val2
0     1     0.0
------------------------------------------------------------------------
-
-- definition of in- and outflow boundaries ----------------------------
-
nrio
4
i/o     plane   xmin    xmax    ymin    ymax    zmin    zmax
26       1       0       0       0      10      -0.11     0.05
26       2       0       10      0      0       -0.11     0.05
11       1       10      10      0      10      -0.11     0.05
11       2       0       10      10    10      -0.11     0.05
------------------------------------------------------------------------
-
```

```
-- partial slip ------------------------------------------------------
-
pscnf psl
0     0
----------------------------------------------------------------------
-
-- absorbing boundary condition --------------------------------------
-
bcl bcr  gabc a0     a1     b1    kh1    kh2   alfa1 alfa2
1   1    1    1.05  0.12   0.31   7.614  5.0   45.0   45.0
----------------------------------------------------------------------
-
-- definition of numerical beach in positive x-direction -------------
-
numbch  dampto* slope   bstart
0       0       0.0     0.0
----------------------------------------------------------------------
-
-- physical parameters -----------------------------------------------
-
rho1    rho2    mu1     mu2     sigma   theta  patm   gamma
1.0e3 1.0     1.0e-3  1.7e-5  0.0     90.0   1.01325e5  1.4
----------------------------------------------------------------------
-
-- viscous effects ---------------------------------------------------
-
turbles limiter wallmodel diffusion~
0       0       0         0
----------------------------------------------------------------------
-
-- grid parameters ---------------------------------------------------
-
griddef
0
imax    jmax    kmax    xc      yc      zc      sx      sy      sz
0     0    0   0.0    0.0       0.0      1.0      1.0  1.0
----------------------------------------------------------------------
-
-- numerical parameters ----------------------------------------------
-
eps     omega*  itmax   alpha   feab0  feab1  feab2   nrintp  linext
1.0E-6  1.0001  10000    1.0     0.0    1.0    0.0    30      1
----------------------------------------------------------------------
-
-- additional numerical parameters -----------------------------------
--
imilu extrap restol imptol upwind imprel irhoav itscr droptol~
droptolbc~
5     0      1.0E-8 1.0E-3 1      1.0    1      0     1e-2     1e-6
----------------------------------------------------------------------
-
-- time parameters/cfl number ----------------------------------------
-
dt      tmax    dtmax   cfl     cflmin  cflmax  divl
0.005    45    0.5     1       0.2     0.5     0
```

```
-------------------------------------------------------------------------
-
-- free surface methods -----------------------------------------------
-
vofmth vofcor divl
1      2      0
-------------------------------------------------------------------------
-
-- gravitation --------------------------------------------------------
-
gravx   gravy   gravz   ginrt   finrt
0.0     0.0     -9.81   0       0
-------------------------------------------------------------------------
-
-- motion of coordinate system ----------------------------------------
-
motionframe
0
amplx   freqx   amply   freqy   amplz   freqz
0.0     0.0   0.0      0.0     0.0     0.0
-------------------------------------------------------------------------
-
omex    omey    omez    x0      y0      z0
0.0     0.0     0.0     0.0     0.0     0.0
-------------------------------------------------------------------------
-
-- autosave -----------------------------------------------------------
-
load    nsave
0       0
-------------------------------------------------------------------------
-
-- post-processing: snapshots/screen print/center of mass -------------
-
npm2d   npm3d   compr   nprnt   ntcom
0       150      0       1000     0
-------------------------------------------------------------------------
-
npmslic nyz     nxz     nxy
0       0       0       0
planeyz
planexz
planexy
-------------------------------------------------------------------------
-
-- directory name for snapshots ---------------------------------------
-
pathname snapshot data:
data/
-------------------------------------------------------------------------
-
-- fill boxes, force boxes and flux boxes------------------------------
-
nfillb  ntfill
0       10000
xl      xr      yl      yr      zl      zr
```

```
------------------------------------------------------------------------
-
nfrcb  ntfrc
1      10000
xl     xr      yl      yr      zl      zr         mvb  frcmethod
0      0.4     0       0.4     -0.084   -0.076     1   1
------------------------------------------------------------------------
-
nfluxb  ntflux
0       10000
xl      xr      yl      yr      zl      zr
------------------------------------------------------------------------
-
nrelwh  ntrelwh
0       10000
xl      xr      yl      yr      zl      zr
------------------------------------------------------------------------
-
-- stream line/particle path ---------------------------------------
-
npartp  npartl  npartc  ntpart
8       0       0       10000
xpt     ypt     zpt     tstrt                           <- points
0       0      -0.102         0
0.2     0.2    -0.102         0
--------
xl      xr      yl      yr      zl      zr      tstrt   <- lines
xc      yc      zc      radius  orient  tstrt           <- circles
------------------------------------------------------------------------
-
-- monitor points --------------------------------------------------
-
nmntrp  nmntrl  nmntrc  ntmntr
11      0       0       10000
xpt     ypt     zpt           mvp                       <- points
0       0      -0.102         0
0.2     0.2    -0.102         0
0.38    0.38   -0.102         0
--------
xl      xr      yl      yr      zl      zr              <- lines
xc      yc      zc      radius  orient                  <- circles
------------------------------------------------------------------------
-
-- special boxes ---------------------------------------------------
-
nrboxes sb_tmin sb_uvw
0       0.0    0
xmin    xmax    ymin    ymax    zmin    zmax  tmin  tmax
```

Appendix III: Modified AQWA results comparison with COMFLOW

In the plots below give a comparison of (1) Analytical expression for dynamic force (equation 17), (2) Modified AQWA expression for dynamic force (equation 22), (3) Dynamic force obtained from COMFLOW, (4) AQWA dynamic force.

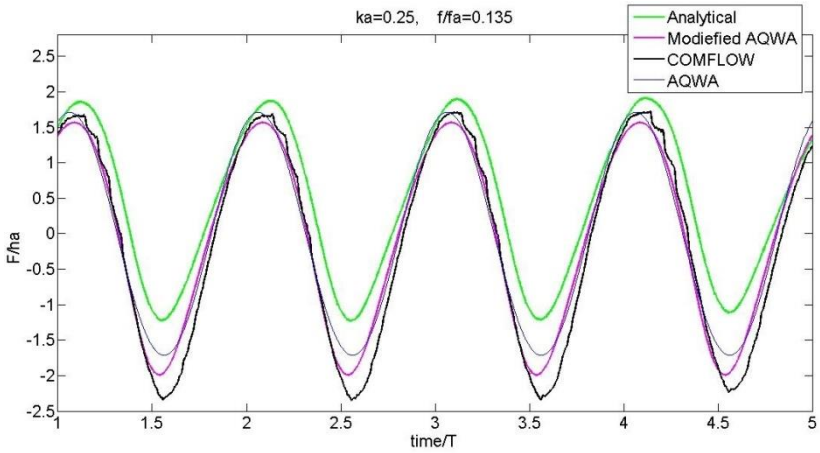

Figure 75: Case 1: Cylinder

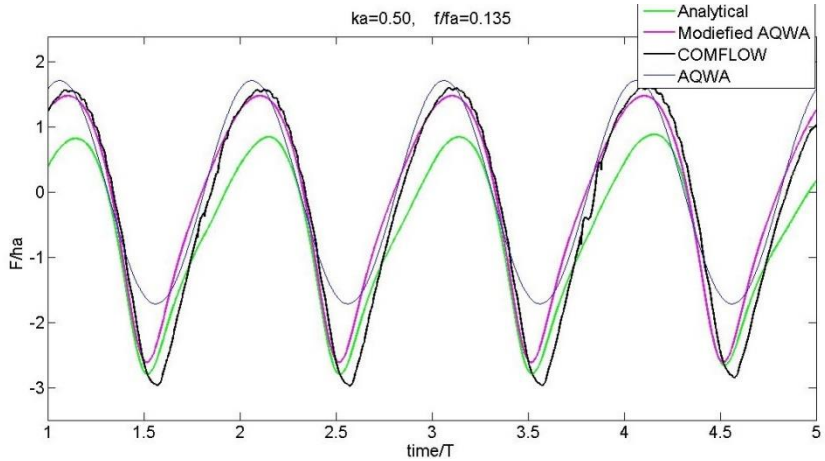

Figure 76: Case 2: Cylinder

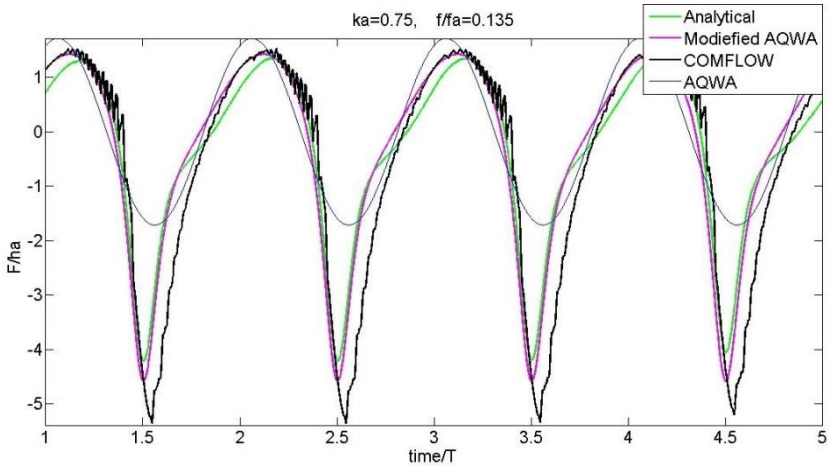

Figure 77: Case 3: Cylinder

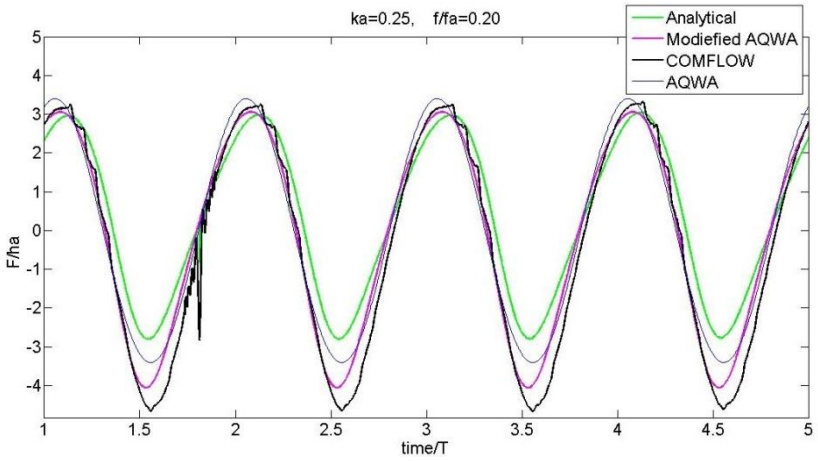

Figure 78: Case 4 Cylinder

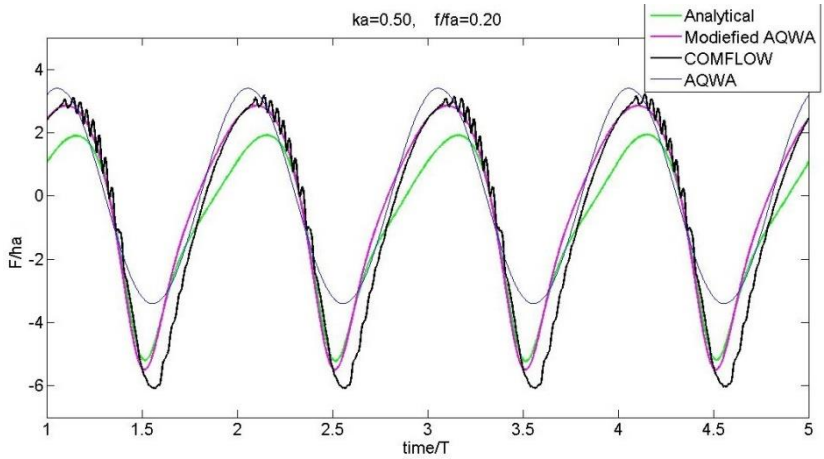

Figure 79: Case 5 Cylinder

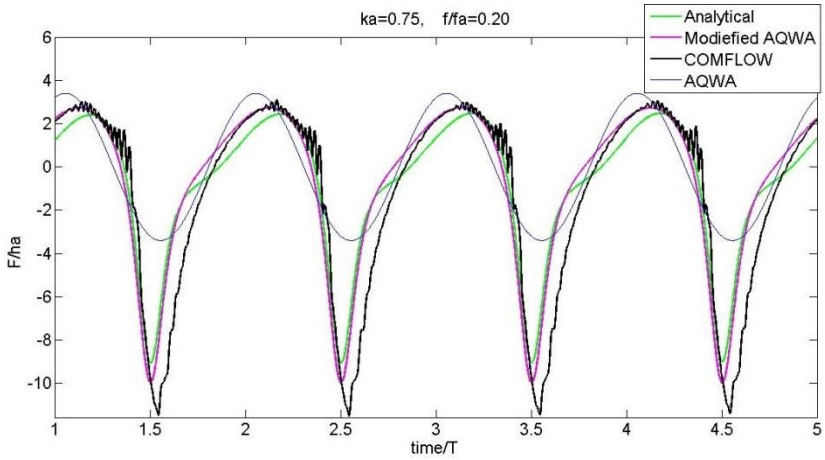

Figure 80: Case 6 Cylinder

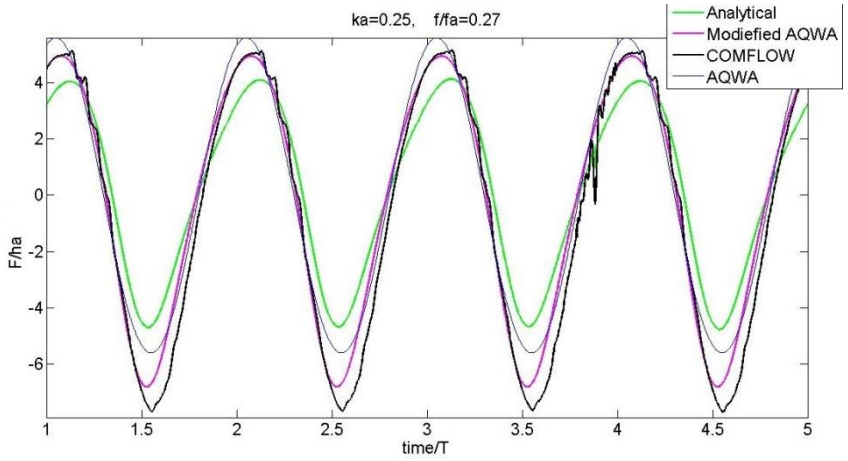

Figure 81: Case 7 Cylinder

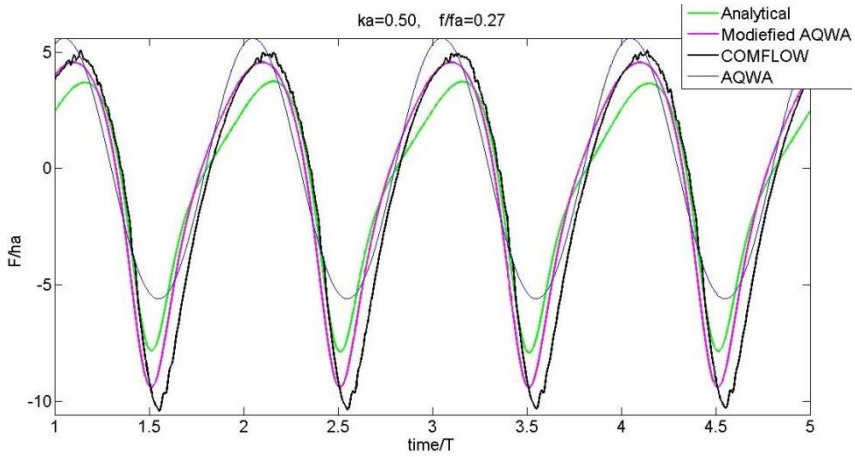

Figure 82: Case 8 Cylinder

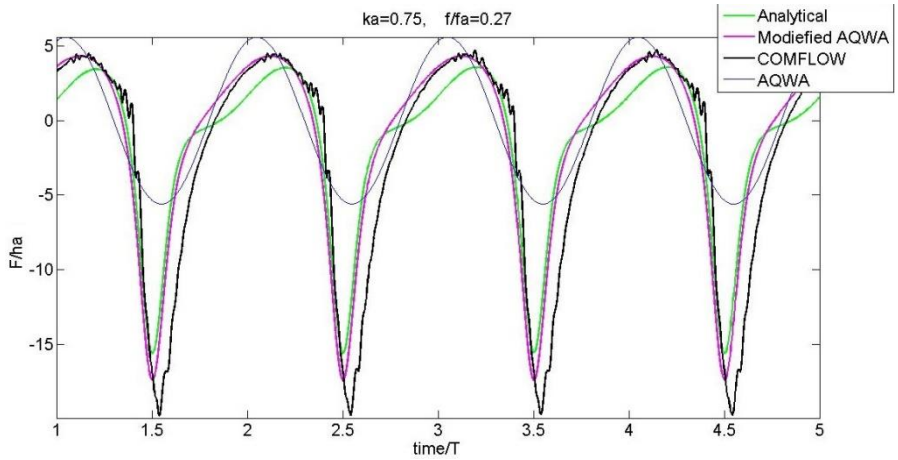

Figure 83: Case 9 Cylinder

Appendix IV: Contribution of Nonlinear Added Mass and Lift terms

In the plots below contribution of different components in modified AQWA expression (equation 22) has been given. Following has been plotted: (1) Total dynamic force using modified AQWA expression; (2) Contribution of nonlinear inertia force term; (3) Contribution of non-linear lift force term; (3) Contribution of linear dynamic force calculated by AQWA.

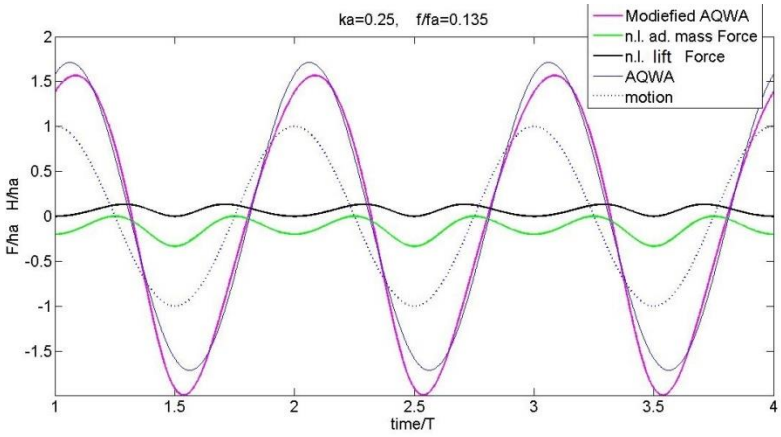

Figure 84: Contribution of Inertia and Lift Non-linear Terms, Case 1

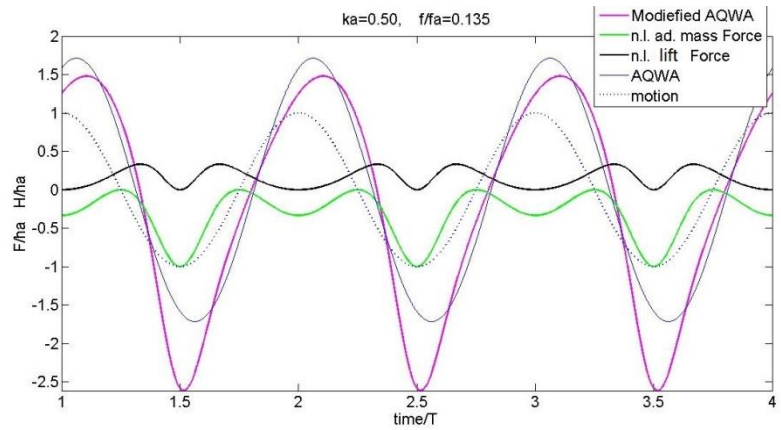

Figure 85: Contribution of Inertia and Lift Non-linear Terms Case 2, Cylinder

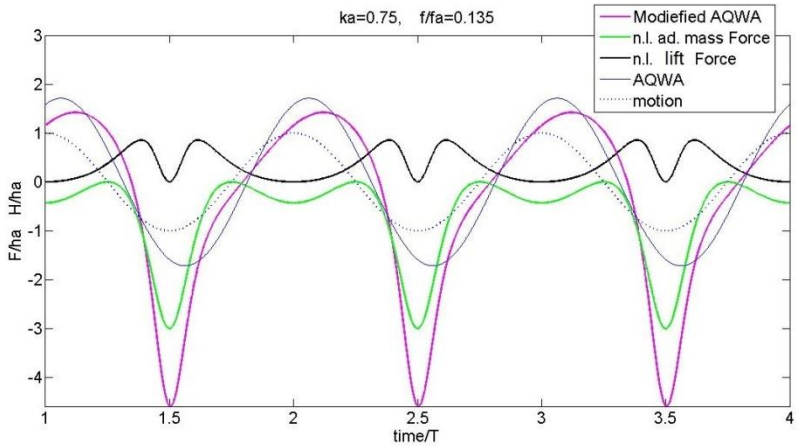

Figure 86: Contribution of Inertia and Lift Non-linear Terms Case 3 Cylinder

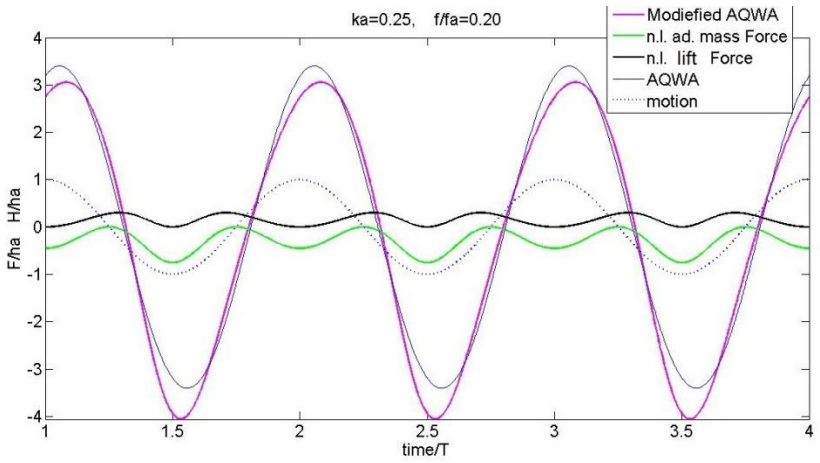

Figure 87: Contribution of Inertia and Lift Non-linear Terms, Case 4 Cylinder

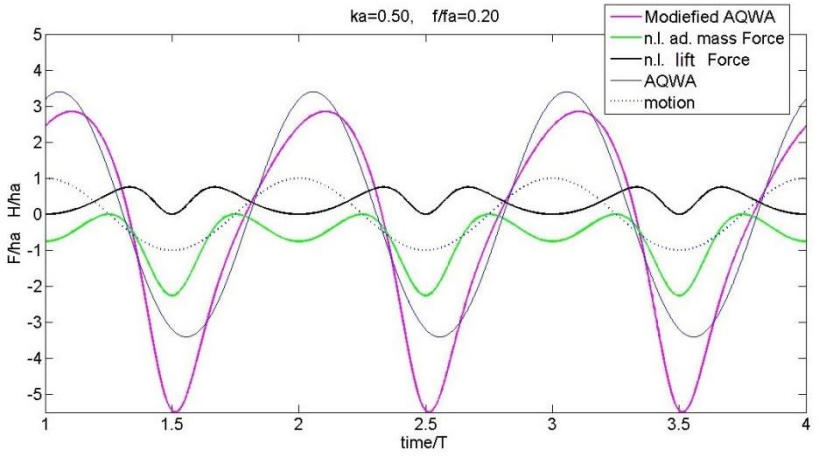

Figure 88: Contribution of Inertia and Lift Non-linear Terms, Case 5 Cylinder

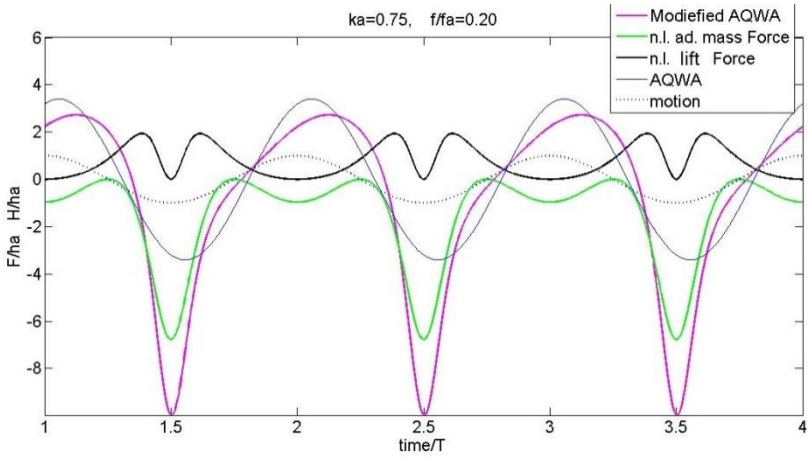

Figure 89: Contribution of Inertia and Lift Non-linear Terms Case 6 Cylinder

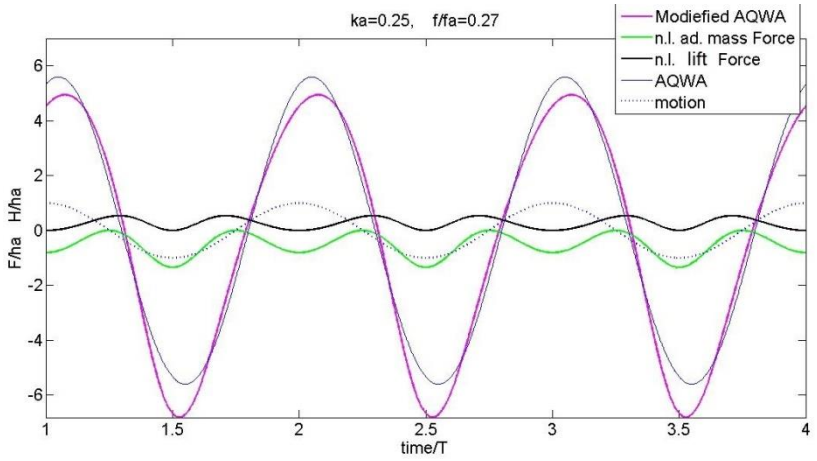

Figure 90: Contribution of Inertia and Lift Non-linear Terms, Case 7 Cylinder

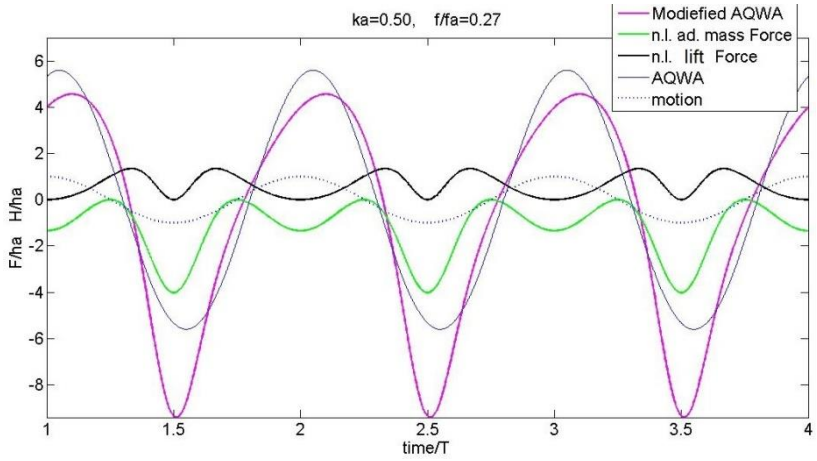

Figure 91: Contribution of Added Mass and Lift Non-linear Terms, Case 8 Cylinder

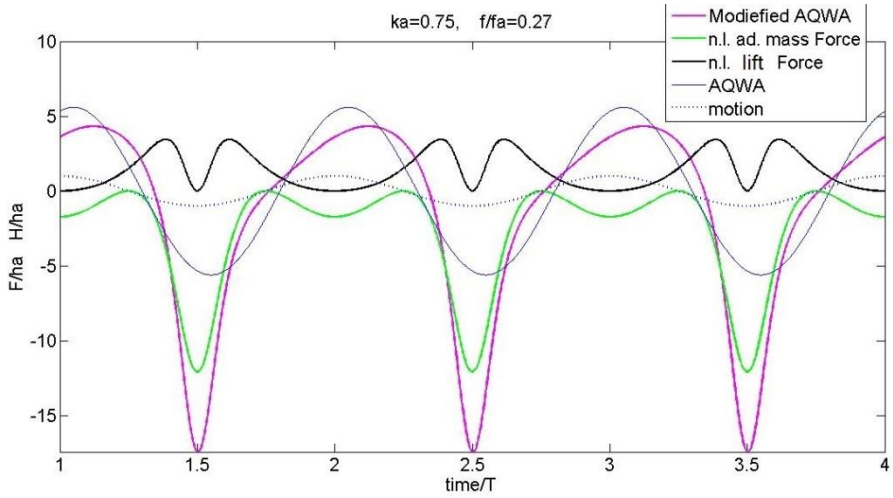

Figure 92: Contribution of Added Mass and Lift Non-linear Terms, Case 9 Cylinder

Appendix V: Barge Dynamic Forces

In the plot below dynamic force on barge calculated from (1) modified AQWA expression (equation 32); (2) COMFLOW dynamic force; (3) modified curve fit expression for barge has been compared for different length to width ratios (L/W =2,5,10).

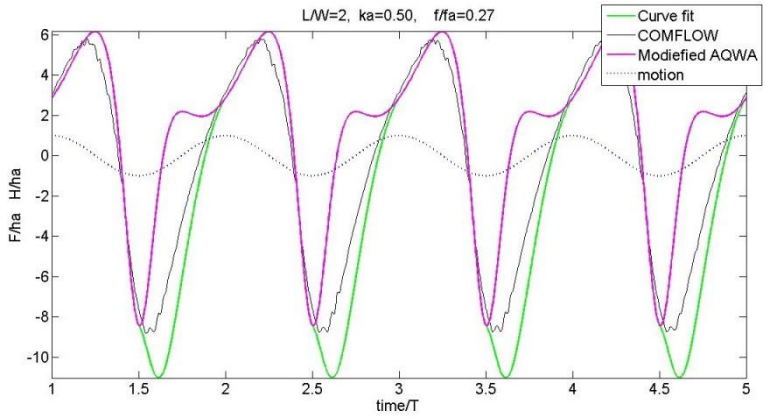

Figure 93: Dynamic Force, Barge L/W=2

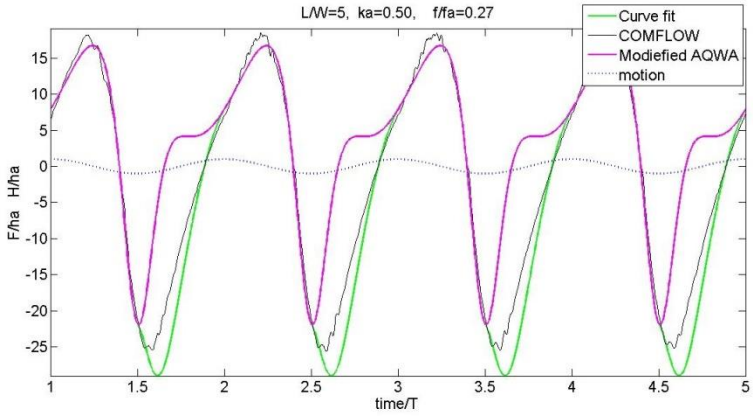

Figure 94: Dynamic Force, Barge L/W=5

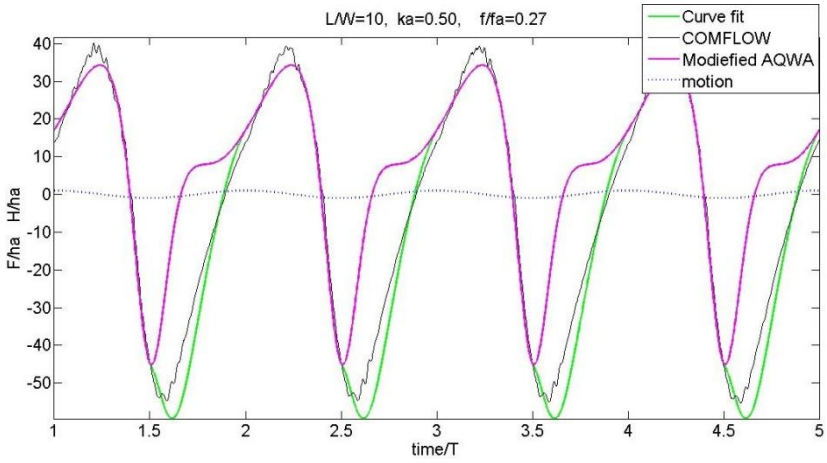

Figure 95: Dynamic Force, Barge L/W=10

Appendix VI: Square Model Dynamic Forces

In the plot below, dynamic force on the on square model with same surface area as cylinder, has been plotted as obtained from (1) COMFLOW simulation; (2) Modified AQWA expression.

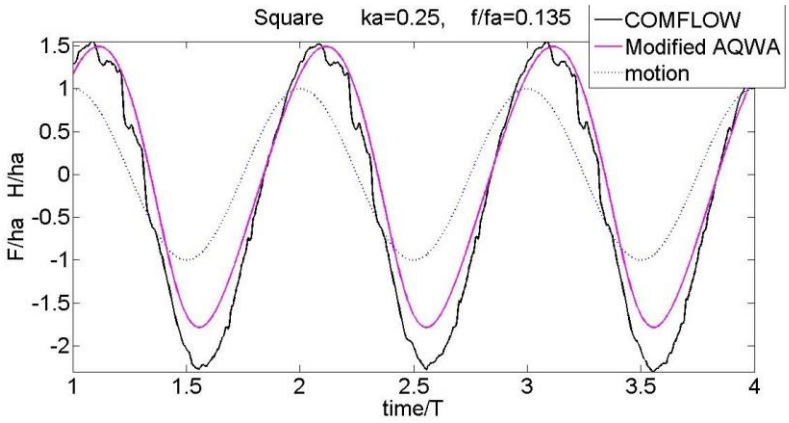

Figure 96: Dynamic Force, Case 1 Square

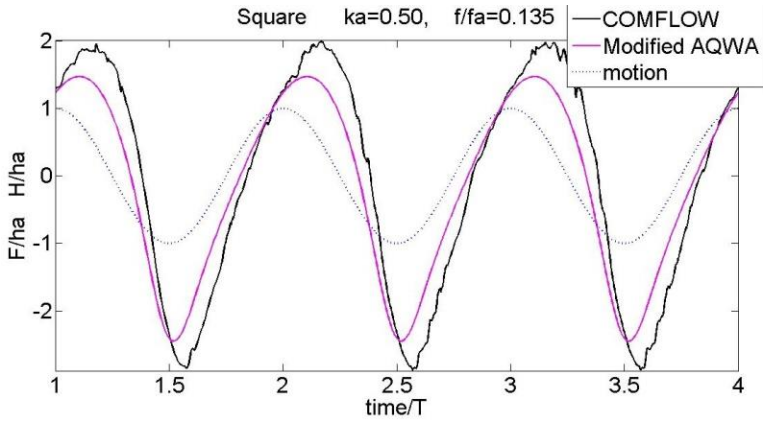

Figure 97: Dynamic Force, Case 2 Square

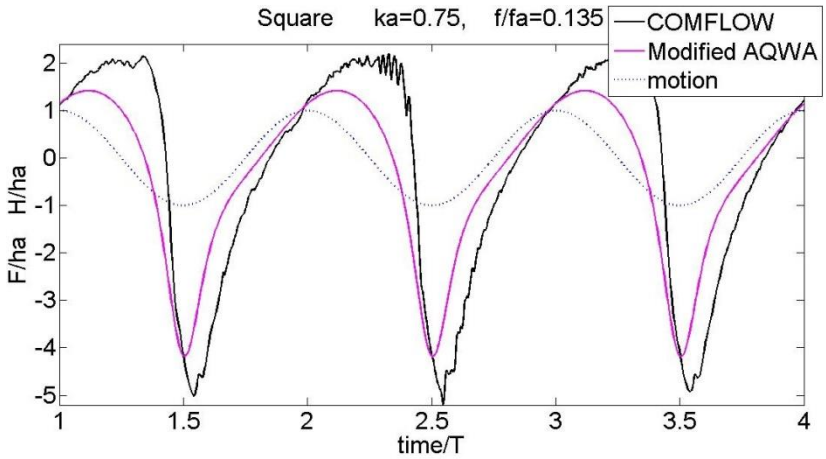

Figure 98: Dynamic Force, Case 3 Square

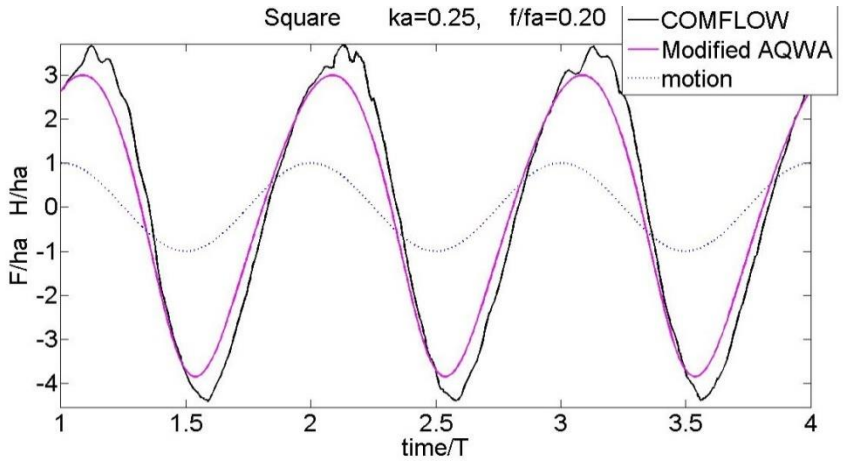

Figure 99: Dynamic Force, Case 4: Saquare

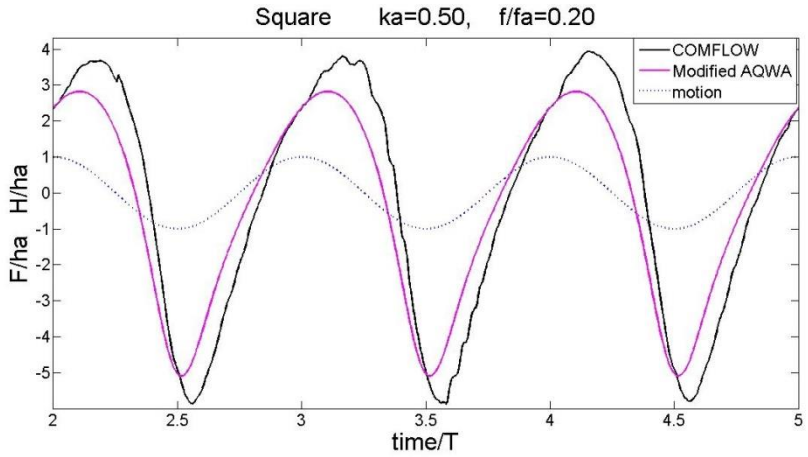

Figure 100: Dynamic Force, Case 5 Square

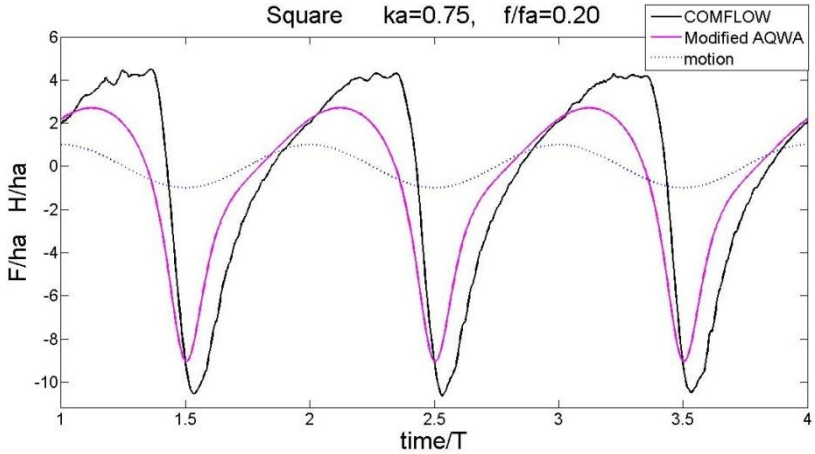

Figure 101: Dynamic Force, Case 6 Square

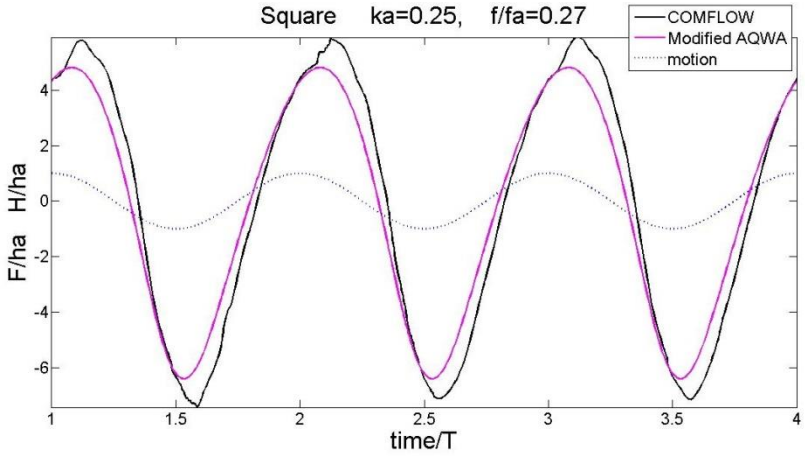

Figure 102: Dynamic Force, Case 7 Square

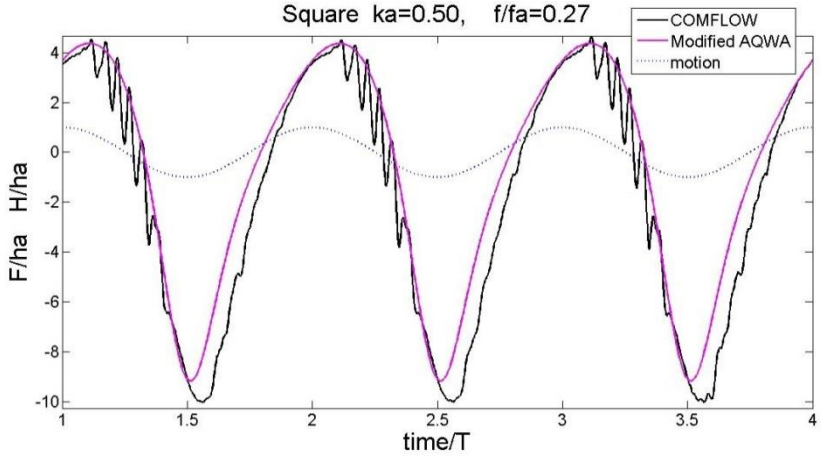

Figure 103: Dynamic Force, Case 8 Square

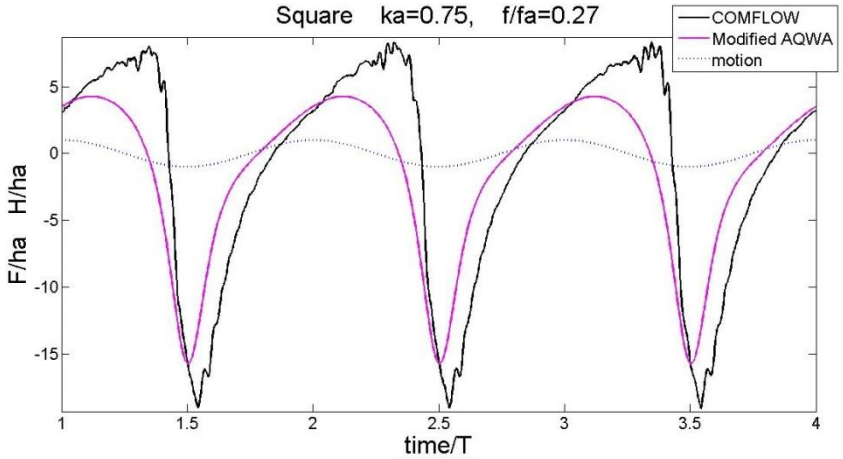

Figure 104: Dynamic Force, Case 9 Square

Appendix VII: Triangular Model Dynamic Forces

In the plot below, dynamic force on the on Triangular bottom model with same surface area as cylinder, has been plotted as obtained from (1) COMFLOW simulation; (2) Modified AQWA expression.

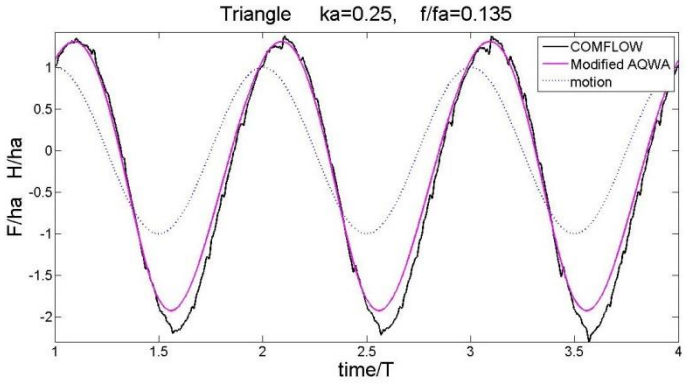

Figure 105: Dynamic Force, Case 1 Triangle

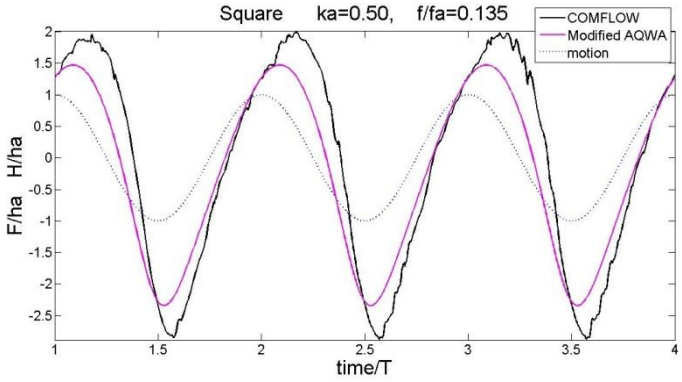

Figure 106: Dynamic Force, Case 2 Triangle

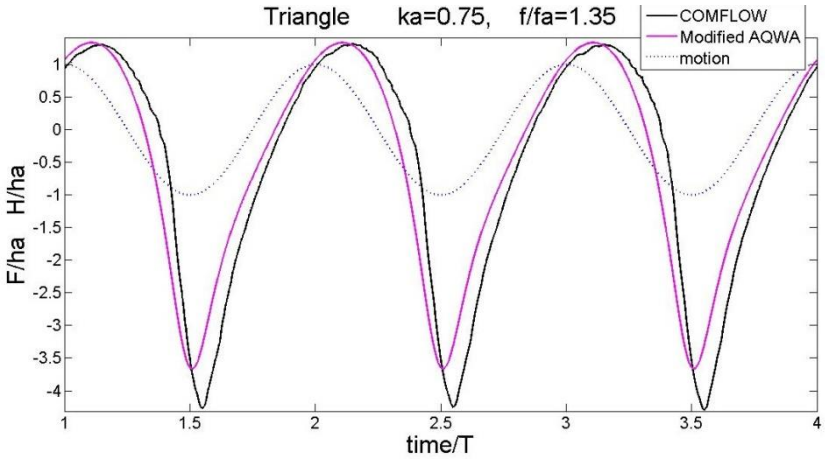

Figure 107: Dynamic Force, Case 3 Triangle

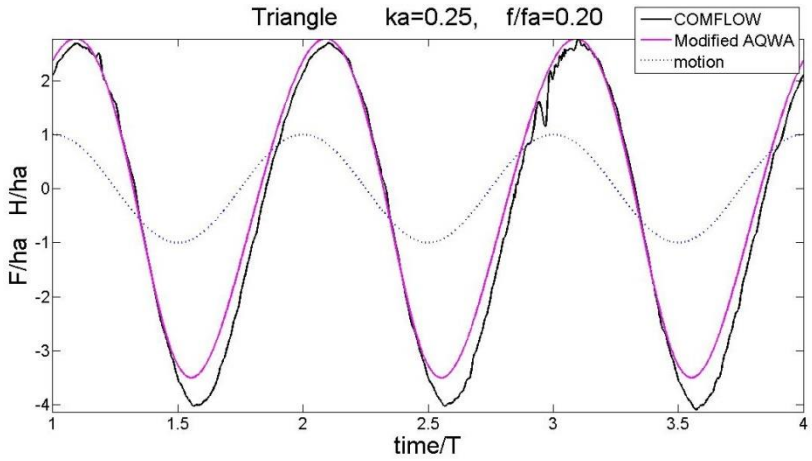

Figure 108: Dynamic Force, Case 4 Triangle

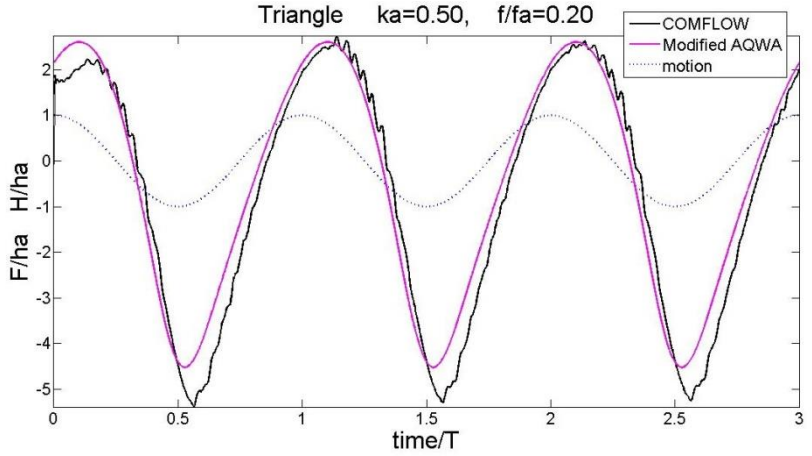

Figure 109: Dynamic Force, Case 5 Triangle

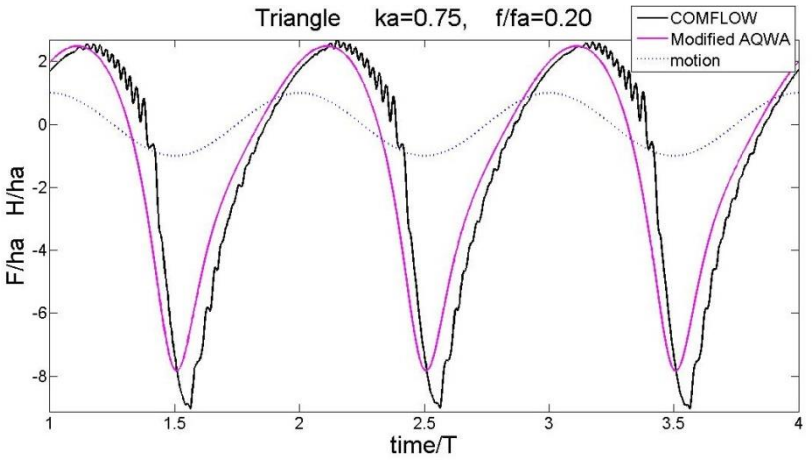

Figure 110: Dynamic Force, Case 6 Triangle

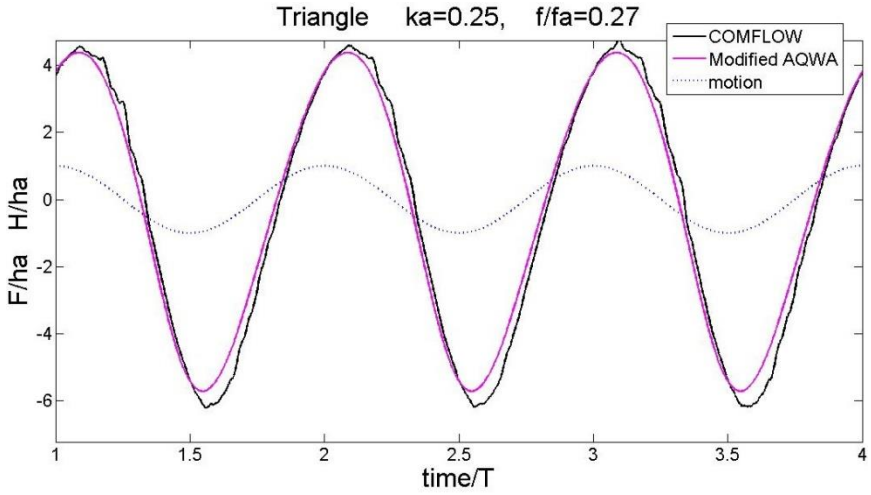

Figure 111: Dynamic Force, Case 7 Triangle

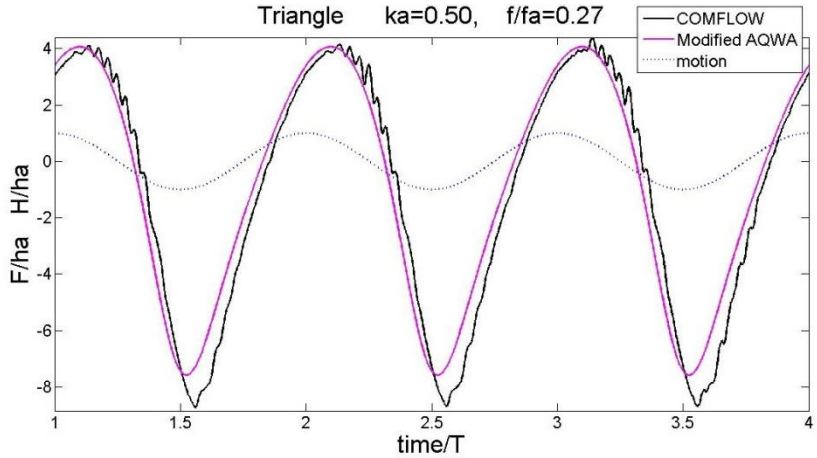

Figure 112: Dynamic Force, Case 8 Triangle

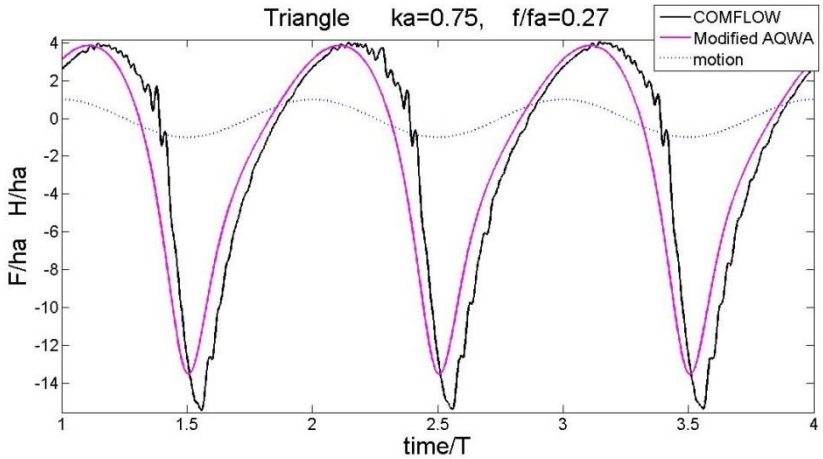

Figure 113: Dynamic Force, Case 9 Triangle

Bibiliography

1. Molin, B., et al. "ETUDE THEORIQUE ET EXPERIMENTALE DES EFFORTS HYDRODYNAMIQUES SUR UNE EMBASE PLANE A L'APPROCHE DU FOND MARIN."
2. Brennen, C. E. "A review of added mass and fluid inertial forces." (1982).
3. Terpstra, T., E. A. Hellinga, and H. C. Leerdam. "Offshore dry-docking of FPSOs; a response to industry needs." (2013).
4. de Jonge, J. B., O. A. J. Peters, and R. H. M. Huijsmans. "A Hydrodynamic Analysis Method for Offshore Discharge Operations." ASME 2008 27th International Conference on Offshore Mechanics and Arctic Engineering. American Society of Mechanical Engineers, 2008.
5. Peters, Onno, Rene HM Huijsmans, and Michel Seij. "Hydrodynamic Behavior during Offshore Loading and Discharge." *Offshore Technology Conference*. Offshore Technology Conference, 2012.
6. Peters, O. A. J., and R. H. M. Huijsmans. "Assessing Hydrodynamic Behavior during Offshore Loading and Discharge in the Heavy Marine Transport." *ASME 2011 30th International Conference on Ocean, Offshore and Arctic Engineering*. American Society of Mechanical Engineers, 2011.
7. Drobyshevski, Y. "Hydrodynamic coefficients of a floating, truncated vertical cylinder in shallow water." Ocean engineering 31.3 (2004): 269-304.
8. Vreeburg, A. C. M. *ShoreTension as cargo handling system: Controlling the relative horizontal motions between the HTV and the cargo during offshore loading and discharge*. Diss. TU Delft, Delft University of Technology, 2015.